FLUORINATED AND FLUOROCARBON COATING OF TiO_2 BY PULSED PLASMA PROCESSING: IMPROVED PHOTOCATALYTIC OXIDATION OF GASEOUS M-XYLENE AND MERCURY

by

SULAK SUMITSAWAN

Presented to the Faculty of the Graduate School of

The University of Texas at Arlington in Partial Fulfillment

of the Requirements

for the Degree of

DOCTOR OF PHILOSOPHY

THE UNIVERSITY OF TEXAS AT ARLINGTON

December 2011

ACKNOWLEDGEMENTS

This is a great opportunity for me to express my respect to the persons who have gratefully helped and supported me during my doctoral study.

This dissertation would not have been possible without Dr. Richard B. Timmons and Dr. Melanie L. Sattler whose are my dissertation co-advisors. I have been fortunate to work with Dr. Timmons since he is a greatest scientist and mentor. He always gives me support, guidance and encouragement for both of my academic and personal aspects. I would like to thank Dr. Sattler for the support, suggestion and advice she has given me. She is the person who brought me to the field of air quality. I would like to acknowledge Drs. Andrew P. Kruzic, Stephen P. Mattingly and Hyeok Choi to be members of my committee and contributed several suggestions. I would also like to thank you Dr. Jai Cho for the exploring fluorine plasma application on the environmental studies, Dr. Rajendra Deshmukh for being a good companion and taught me sense of humor.

Last but not least, I am very fortunate to receive unconditional love and strong support from my parents, my wife, family and friends. They are the reason I can overcome all hurdles and tough times throughout my study.

August 3, 2011

ABSTRACT

FLUORINATED AND FLUOROCARBON COATING OF TiO_2 BY

PULSED PLASMA PROCESSING: IMPROVED

PHOTOCATALYTIC OF GASEOUS

M-XYLENE AND MERCURY

Sulak Sumitsawan, PhD.

The University of Texas at Arlington, 2011

Supervising Professors: Richard Timmons and Melanie Sattler

Titanium dioxide (TiO_2) is a preferred catalyst for photocatalytic oxidation of many air pollutants. In an effort to enhance its photocatalytic activity, TiO_2 was modified by pulsed plasma treatment. In this work, TiO_2 nanoparticles, coated on a glass plate, were treated with a plasma discharge of hexafluoropropylene oxide (HFPO) gas. By appropriate adjustment of discharge conditions, it was discovered that the TiO_2 particles can be either directly fluorinated (Ti-F) or coated with thin perfluorocarbon films (C-F).

Specifically, under relatively high power input, the plasma deposition process favored direct surface fluorination. The extent of Ti-F formation increased with increasing power input. In contrast, at lower average power inputs, perfluorocarbon films are deposited on the surface of the TiO_2 particles.

The plasma surface modified TiO_2 nanoparticles were subsequently employed as catalysts in the photocatalytic oxidation of m-xylene, as carried out inside a closed loop batch reactor. Both types of modified TiO_2 were significantly more catalytically active than that of the unmodified particles. For example, the rate constant of m-xylene degradation was increased from 0.012 min^{-1} with untreated TiO_2 to 0.074 min^{-1} with fluorinated TiO_2. The plasma treatment converts the TiO_2 particles from hydrophilic to hydrophobic. The more hydrophobic TiO_2 surfaces will more readily adsorb non-polar compounds, such as m-xylene, while simultaneously minimizing the competitive adsorption of water molecules. Additionally, it is believed that the presence of surface fluorine atoms can contribute to decreased electron-hole recombinations, thus further increasing TiO_2 photocatalytic activity. Similarly, the promotional effect was also found in elemental mercury, another non-polar compound, where the removal rate of elemental mercury obtained from fluorinated TiO_2 was 1.6 times greater than that of the untreated TiO_2. In contrast, fluorinated TiO_2 showed less reactivity than that of the untreated TiO_2 in degrading acetaldehyde, a polar compound.

The study of the effect of relative humidity on m-xylene degradation revealed that the optimum relative humidity for m-xylene removal was 10% for the untreated TiO_2. The removal efficiency was observed to decrease progressively as the relative humidity

was raised above the 10% level. When fluorinated TiO_2 was used as the catalyst, the impact of relative humidity range from 0 to 40% was minimal. The inhibition effect of water vapor was not observed until the relative humidity was raised to 60% and 80%.

The photocatalytic reactivity of catalyst used in successive runs was lower than that obtained with fresh TiO_2. The catalytic deactivation observed apparently results from deposition of carbonaceous species deposited on the surface of the TiO_2 particles after repeated use. However, it was discovered that subjection of the used catalysts to an oxygen plasma for 10 minutes was successful in regenerating catalyst activity to 96% of its original activity.

TABLE OF CONTENTS

LIST OF ILLUSTRATIONS

Figure Page

LIST OF TABLES

CHAPTER 1

INTRODUCTION

1.1 General

Air is one of the most abundant natural resources on Earth and clean air is essential for human and all living creatures. However, air quality has become an environmental issue of serious concern; larger populations, increased transportation, expansion of industries and many other activities contribute increasing quantities of contaminants into the air. Unfortunately, human do not have the luxury to select only clean air to breathe. As a result, many researchers are trying to find solutions to control emissions and to improve air quality.

Despite the fact that more environmentally friendly alternative energy sources, such as wind, solar, or nuclear are increasingly available, the fact remains that industry,, electric power plants, vehicles and households still rely on fossil fuel as their primary energy source. Fossil fuel combustion emits gaseous pollutants, including carbon monoxide, carbon dioxide, nitrogen oxides and volatile organic compounds (VOCs) to the atmosphere. The burning of biofuel and biomass, the primary sources of energy in some countries, also add VOCs to the environment. These air pollutants cause many threats to human health, ecosystems and economic systems worldwide. VOCs released from anthropogenic sources are estimated as 186 Tg/yr. VOCs have been defined by US Environmental Protection Agency (EPA) as any carbon compounds that take part in

photochemical reactions in the atmosphere excluding carbon monoxide, carbon dioxide, carbonic acid, metallic carbides or carbonates, and ammonium carbonate (U.S. EPA, 2009).

VOCs are common pollutants in the atmosphere that are present in both indoor and outdoor air. They cause adverse effects on human health such as fatigue, sensory irritation, nervous system disorders, asthma and cancer (Zhou et al., 2011). Benzene and 1,3-butadiene are identified by the EPA as known carcinogens (EPA, 2009). Major sources of VOCs include activities and industries based on fossil fuel production and consumption, which includes power plants, petrochemical industries, motor vehicles, and sources that use biomass fuels (Koppman, 2007). VOCs are also released in significant quantities from indoor sources such as paint, cleaning products, building materials, and even cooking activities.

A major concern with respect to atmospheric emissions of VOCs is that these compounds are intimately involved in secondary atmospheric reactions which, in many cases, lead to production of even more noxious compounds. In a complex series of reactions, which occur in the presence of sunlight, VOCs plus nitrogen oxides (NO_x) lead to ground-level ozone formation. Exposure to tropospheric ozone can cause chest pain and respiratory disorders, as well as limit lung function; the effects can be more serious in elderly and children. Ground-level ozone can also damage vegetation and ecosystems. It has been estimated that each year in the United States ozone costs $500 million in lost crop production (U.S. EPA, 2011). For example, xylenes and trimethylbenzenes are highly reactive VOCs in forming ground-level ozone (Kwok et al., 1997). Additionally,

VOCs are also implicated in the atmospheric formation of highly oxidized and exceptionally hazardous compounds, such as peroxyacetyl nitrate (PAN).

In recognition of the atmospheric problems created by VOCs, several control technologies have been employed in attempts to reduce emission of VOCs into the atmosphere. The technologies evaluated for this purpose include absorption, adsorption, incineration, condensation, biofiltration and photocatalytic oxidation (PCO) (A&WMA, 2000). The ultimate goal is to minimize or lower VOCs emissions below threshold levels which are not harmful to human health and welfare. In general, the main mechanisms of these control strategies include separating pollutants from the gas stream, capturing pollutants, or converting them into other forms that are less or non-toxic.

A promising air pollution control technology, which have been developed, is photocatalytic destruction and/or conversion of VOCs. Research in this field began with the discovery of ultraviolet light-induced water cleavage by Fujishima and Honda (1972), as achieved using semiconductor catalysts. Since then, many studies involving photocatalytic oxidation of environmental pollutants by semiconductors have been conducted. The most commonly used photocatalyst for this purpose is titanium dioxide (TiO_2) due to its ready availability, stability, environmental acceptability, and efficiency (Kaneko and Okura, 2002). A photocatalyst, such as TiO_2, can oxidize VOCs leading to ultimate formation of carbon dioxide and water, under extended reaction conditions. In addition to the VOCs, the photocatalytic semiconductors can convert elementary mercury into an oxidized form which is easily captured by wet scrubber/absorption systems (Li

and Wu, 2007), and they have also been shown to be able to reduce nitrogen oxides to molecular nitrogen (Maggos et al., 2007).

The present study centers on examination of the possibility of employing a plasma based surface modification technology to enhance the photocatalytic activity of TiO_2 in helping to improve remediation of VOC and Hg emissions to the atmosphere. Meta-xylene has been selected as a model VOC compound for this purpose. Xylene is a major VOC, typically found in industrial areas. Xylene is emitted mainly from coating facilities, gasoline, and combustion sources. In addition, xylene is not an easily degradable compound due to the stability of aromatic rings against oxidation and reduction processes. Thus, it is felt that this molecule represents a viable challenge in terms of improving the photocatalytic activity of the TiO_2, and that success with this compound would likely translate to success with other important VOC compounds. Additionally, the present investigation also includes examination of the effectiveness of employing the surface modified TiO_2 in achieving more efficient oxidation of elementary mercury emissions.

Plasma deposition is a distinctive and widely used technique to modify surface chemistry of a solid substrate (Timmons and Griggs, 2004). In most cases, the plasma discharge has been employed to deposit thin polymeric films on targeted substrates. The properties of these plasma generated films depend on several operational parameters, for example, type of monomer, applied power monomer flow rate and working pressure. The surface properties can be controlled by suitable adjustment of these parameters in the deposition process. The controllability of surface chemistry is a key factor that makes

plasma deposition superior to other techniques. In particular, variable duty cycle pulsed plasmas have been shown to provide exceptionally high levels of film chemistry control and demonstrated in applications involving biomedical, environmental, electrical devices, and material science (Cho et al., 2006, Timmons and Griggs, 2004). In addition to polymer film depositions, plasma processing can also be effectively employed to achieve surface modifications which involve atomic doping of the substrates. Typically, such doping is carried out under high power input conditions in which partial substrate ablation is accompanied by atom surface depositions. For example, it has been shown that F-, C- and N- atom doping of TiO_2 can be achieved via this route under appropriate plasma conditions (Cheng et al., 2007, Cho, 2005, Liu et al., 2006).

1.2 Research Objectives

The primary objective of this research is to investigate the photocatalytic activity of plasma surface modified TiO_2 for use in oxidation of atmospheric pollutants. Specifically, the use of F-doped and perfluorocarbon coated TiO_2 has been investigated for this purpose. The effectiveness of the surface-modified TiO_2 is compared with standard untreated TiO_2 (Degussa P-25) in terms of oxidizing gas-phase m-xylene, acetaldehyde and elemental mercury.

A second objective is to investigate the impact of plasma treatment on TiO_2 photocatalytic activity under differing conditions of relative humidity. In this study, the photocatalytic activity of directly fluorinated TiO_2 will be measured as a function of relative humidity, and compared with that of untreated TiO_2.

A third objective is to investigate the long term stability of the TiO_2. As in all heterogeneous catalytic studies, one is faced with inevitable catalytic deactivation with time on stream. In particular, the potential of employing a relatively short oxygen plasma treatment to regenerate the deactivated photocatalyst has been examined.

CHAPTER 2

THEORY AND LITERATURE

2.1 Volatile Organic Compounds and Meta-Xylene

2.1.1 Studies of Volatile Organic Compounds and Meta-Xylene

Volatile organic compounds (VOCs) are major air pollutants generally present in urban and industrial regions. Anthropogenic VOC sources produce alkanes, alkenes and aromatic hydrocarbons, as well as a variety of halogenated and oxygenated compounds, (Koppman, 2007). VOCs are defined by United States Environmental Protection Agency (EPA) as any organic compound that participates in atmospheric photochemical reactions except those designated by EPA as having negligible photochemical reactivity. Photochemical oxidant species in the air affect human health, primarily in the respiratory system. The common pathway of getting these pollutants into human body is by inhalation. Methane is typically excluded from the category of VOCs because it is less reactive in forming ozone. In addition to forming photochemical oxidants, VOCs are believed to cause abnormal growth of embryos, including mutations (Alberici and Jardim, 1997), hematological problems, and cancers (Kampa and Castanas, 2008). Many VOCs are thus listed by the Clean Air Act as hazardous air pollutants.

Xylenes are aromatic hydrocarbons (C_8H_{10}) which exist in three isomeric forms, namely ortho-, meta-, and para-, as shown in Figure 2.1. Of these three isomers, m-xylene is clearly the predominant compound used commercially, accounting for 60-70% of total

xylene production. In light of the extensive commercial use of this compound, it was selected as a representative VOC pollutant for this study. Meta-xylene is widely employed as a solvent, particularly in the paint, print ink, rubber and leather industries (World Health Organization, 1997). Such widespread use of this compound provides ample opportunities for its release into the atmosphere.

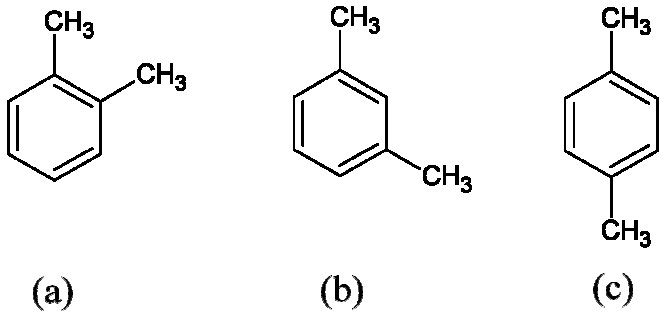

Figure 2.1 Chemical Structure of (a) Ortho-Xylene (b) Meta-Xylene (c) Para-Xylene

In recognition of this problem, a number of prior studies have focused on reduction of m-xylene release to the atmosphere. These studies employed a variety of techniques to achieve this goal, including adsorption (Jo and Yang, 2009), biofiltration (Rene et al., 2010) and photocatalytic oxidation (Boulamanti et al., 2008, D'Hennezel et al., 1998, Tseng et al., 2009). Jo and Yang (2009) studied xylene removal from simulated air streams by activated carbon adsorption, which is a traditional pollution control method. The tested concentration of m-xylene was as low as 0.1 ppm, and the observed removal efficiency was 90%. The removal efficiencies observed using adsorption techniques are typically reduced with increasing pollutant concentrations, thus

a larger adsorption bed is needed which simultaneously increases the costs. Furthermore, the pollutant is not converted into a less toxic form; it is merely transferred from gas phase to solid phase, which then requires additional waste management or regeneration of the used adsorbent.

A study of m-xylene removal using compost inoculated with culture extracted from a municipal sewage treatment plant as biofilter was conducted by Rene et al. (2010). Removal efficiency, when the initial m-xylene concentration was 0.38 g/m^3 (81.4 ppm), was 80%. However, when the inlet concentration was increased to 1.3 g/m^3 (279 ppm), the removal efficiency dropped to 72%. Moreover, the removal efficiency dropped further to slightly over 60% during the spike loading of 1.5 g/m^3 (321 ppm). This indicates high sensitivity of biofiltration to inlet concentration fluctuation, due to the apparent adjustment period required by the microbes to respond to shock loading.

Nickel-doped TiO_2 was prepared by Tseng et al. (2009) via the polyol method, with samples maintained at temperatures between 90 - 135°C for 0 – 60 minutes and then calcined at 400°C in air for 4 hours. Photocatalytic activity tests were conducted at atmospheric pressure. An air stream, with initial m-xylene concentration of 70 ppm, flowed through the photooxidation reactor. Either untreated TiO_2 or Ni/TiO_2 coated on granular silicate glass was used as a photocatalyst. Gas circulation was maintained until adsorption equilibrium was reached. The removal efficiencies were measured at 54 seconds after the UV light was turned on. The results showed that Ni doped TiO_2 could improve photocatalytic activity of standard P25 TiO_2, with the m-xylene removal efficiency increased from 33% to 60%. However, it should be noted that TiO_2 crystalline

size was decreased from 20.3 to 14.6 nm during the heat treatment. Therefore, the higher removal efficiency could be partly explained by particle size reduction.

Boulamanti et al. (2008) studied photocatalytic oxidation of VOCs, including m-xylene, using P25 TiO_2 powder coated on the inside of an annular reactor wall. The surface TiO_2 concentration was 3.5 mg/cm^2. The overall process employed was identified as a continuous stirring tank reactor with recycle ratio maintained at 6 over the entire tests. The effective reactor volume was 20 mL, with the UV lamp located just 8.25 mm away from the photocatalyst. This experiment was conducted using a relatively low m-xylene concentration of 10.2 ppm. A maximum conversion of 92% was achieved after a 60 seconds reaction time. Boulamanti reported that ethylbenzene was detected by a gas chromatography-mass spectroscopy technique as a by-product of xylene degradation.

D'Hennezel and Ollis (1997) studied photocatalytic oxidation of m-xylene using P25 TiO_2. Inlet m-xylene of 50 mg/m^3 (12 ppm) was introduced at a flow rate of 0.83 cm^3/s, using a 12.6 cm^3 continuous flow reactor. They reported a maximum conversion of 72%, with no intermediate detected.

2.1.2 Degradation Pathway of m-Xylene

There are two degradation pathways of m-xylene when reacting with $OH^{\bullet}$, namely H-atom abstraction and $OH^{\bullet}$ addition, as shown in Figure 2.2 (Kwok et al., 1997, Zhao et al., 2005). Zhao et al. (2005) studied the oxidation mechanisms for $OH^{\bullet}$ initiated m-xylene oxidation by using ion drift-chemical ionization mass spectrometry. The temperature was controlled at 298 K under a 80% N_2 and 20% O_2 environment. The initial concentrations of $OH^{\bullet}$ and m-xylene were 20 – 70 ppb and 0.3 – 1.5 ppm,

respectively. These workers report that the H-atom abstraction is a minor pathway which accounts for 10% of the overall reaction at ambient temperature and forms methylbenzyl radicals. The subsequent reactions of the methylbenzyl radicals in the presence of O_2 lead to the formation of tolualdehydes, as illustrated in reaction pathway (a) shown below.

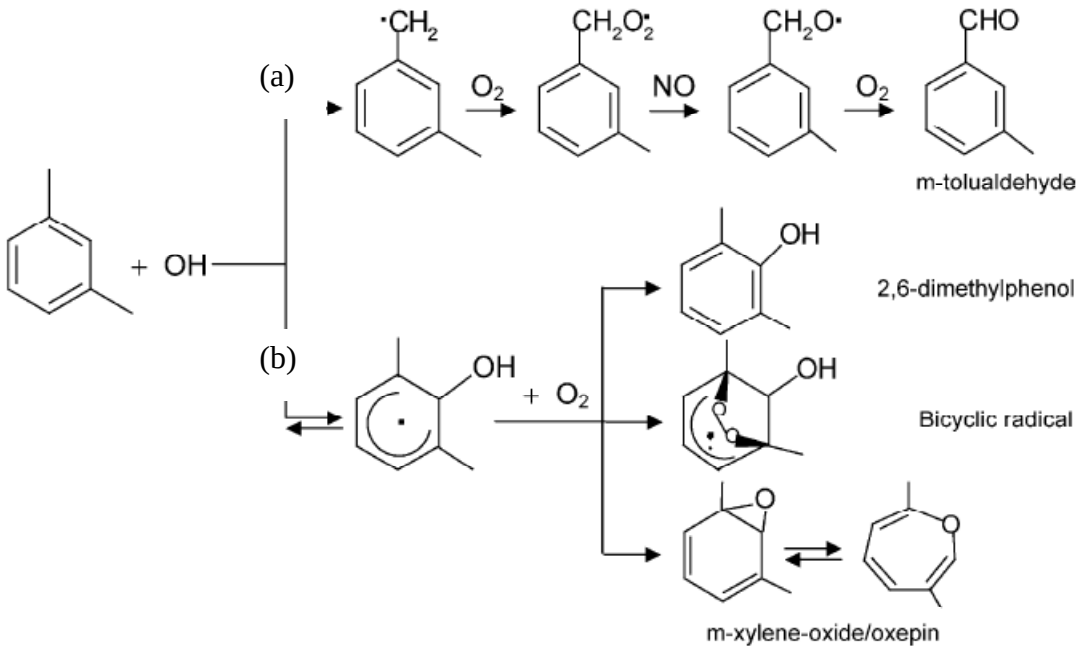

Figure 2.2 Degradation pathway of m-xylene (a) H-atom abstraction (b) OH addition (Zhao et al., 2005)

The major m-xylene degradation pathway was determined to be OH addition to the aromatic ring to form hydroxycyclohexadienyl radical, which subsequently reacts with O_2 to form dimethylphenol, bicyclic radical and m-xylene-oxide/oxepin, as shown in pathway (b) in Figure 2.2. The bicyclic route is the main ring opening product

pathway that ultimately leads to the formation of glyoxal or methylglyoxal as the final products of the oxidation, as shown in Figure 2.3.

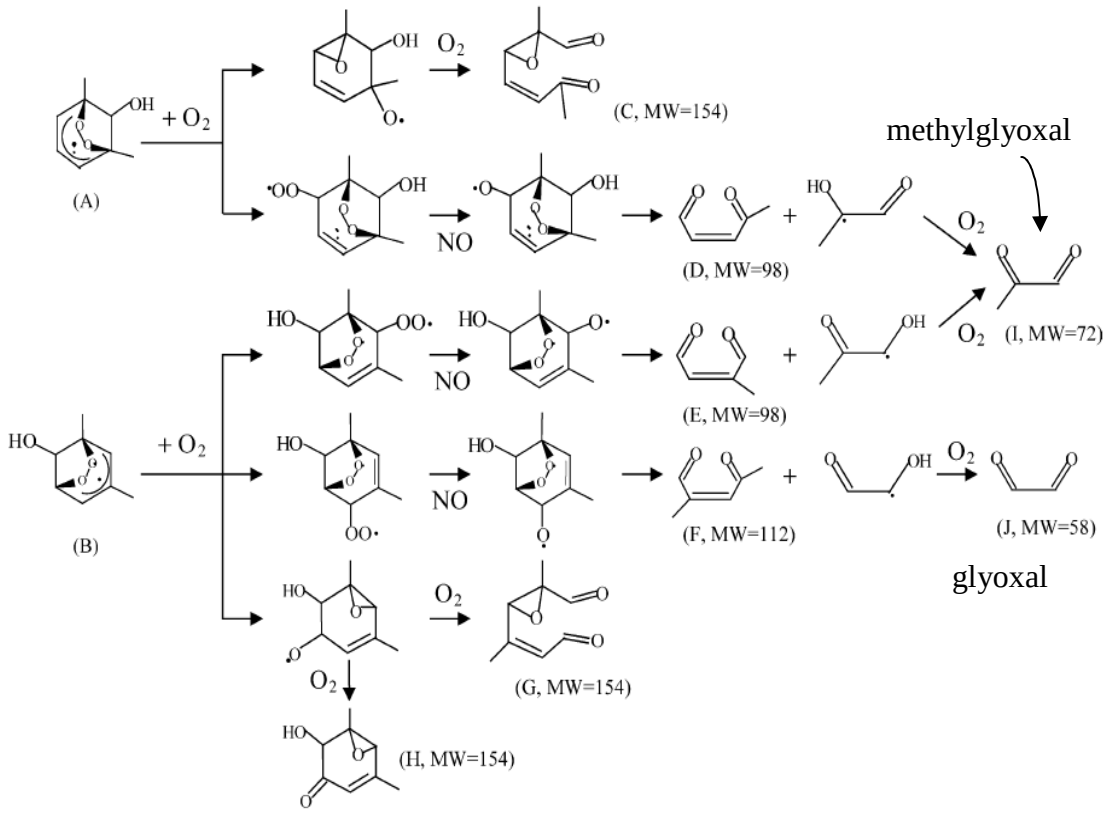

Figure 2.3 Mechanistic diagram of the bicyclic pathway from $OH^{\bullet}$ initiated oxidation of m-xylene (Zhao et al., 2005)

The subsequent reactions involved in the m-xylene-oxide/oxepin pathway are shown in Figure 2.4. The addition of $OH^{\bullet}$ to m-xylene 1,2-oxide leads to ring cleavages which are followed by H-abstraction by O_2 to produce 2-methyl-6-oxo-2,4-heptadienal (M) or 4-methyl-6-oxo-2,4-hexadienal (N), are illustrated in Figure 2.4.

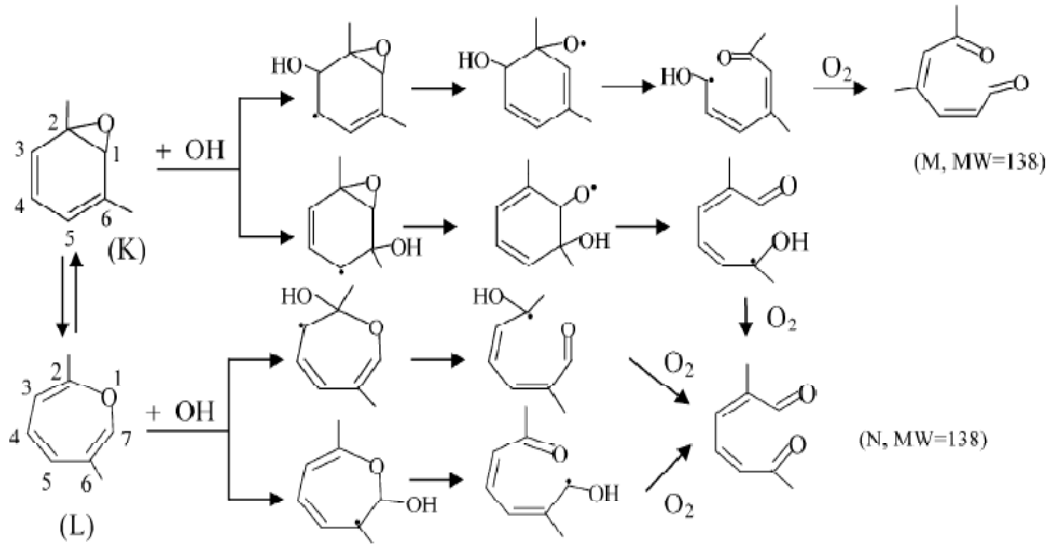

Figure 2.4 Mechanism pathways of m-xylene-oxide/oxepin from $OH^{\bullet}$ initiated m-xylene oxidation (Zhao et al., 2005)

2.2 Photocatalytic Oxidation

2.2.1 Background of Photocatalytic Oxidation

Photocatalytic oxidation is gaining attention from researchers as a promising technique to degrade air pollutants, especially VOCs (Tomasic et al., 2008). Photocatalytic oxidation reactions can effectively degrade hydrocarbon gas pollutants, at atmospheric temperature, to carbon dioxide and water after sufficiently long reaction times. Furthermore, a common and effective photocatalyst is TiO_2, which is a relatively safe material, as it is widely used as white pigment in paint or even as a component in toothpaste. The ultimate source of oxygen in this oxidation process is molecular oxygen, which is far less harmful than other strong oxidants, such as hydrogen peroxide or ozone (Mo et al., 2009).

Photocatalytic systems have the potential to oxidize, as well as reduce, a variety of air pollutants, rendering them less toxic or non-toxic. Examples of such reactions by photocatalysis include oxidation of volatile organic compounds (VOCs) (Geng and Chen, 2011), malodorous compounds (Portela et al., 2010), and mercury (Li et al., 2011). An important example of a potential beneficial reduction process is that involving conversion of carbon dioxide to useful hydrocarbon compounds (Abou Asi et al., 2011). Additionally, it might be noted that photocatalysts have also shown promise for degrading various inorganic and metal ion wastes, and even biological pathogens such as bacteria and viruses (Cho et al., 2001, Zhang et al., 2001, Zhang et al., 2000). Photocatalytic systems, via absorption of ultraviolet light, provide mechanisms whereby pollutants can be reduced or oxidized by electrons and so-called positive holes, respectively, as generated by photon absorption by the catalysts.

2.2.2 Mechanism of Photocatalytic Oxidation

Photocatalysis, as the name implies, are materials which accelerate a reaction in the presence of a suitable photon source. Semiconductors are typically employed as catalysts in photocatalytic reactions due to their ability to produce conduction band electrons (e^-_{cb}) and valence band holes (h^+_{vb}) by absorption of light of appropriate wavelength. When a semiconductor absorbs photons, an electron is excited from the highest occupied orbital to the lowest unoccupied orbital, leaving an electron vacancy in the valence band, called a hole with a positive charge. The excited electron in the conduction band and positive hole in the valence band are called an electron-hole pair. The photocatalysts must absorb photons having energy which is at least equal or greater

than the band gap energy between the conduction and valence band in order to produce e^-_{cb} and h^+_{vb}. In the case of the semiconductor TiO_2, the generation of e^-_{cb} and h^+_{vb} can be represented simply by the following reaction:

$$TiO_2 + h\nu \rightarrow h^+_{vb} + e^-_{cb} \qquad (2.1)$$

The e^-_{cb} and h^+_{vb}, so produced, can migrate to the surface of the TiO_2 and induce reduction and oxidation reactions with electron acceptor or donor species, respectively, adsorbed on the surface of semiconductor. Figure 2.5 illustrates the overall dynamics involved in a typical semiconductor based photocatalytic reaction.

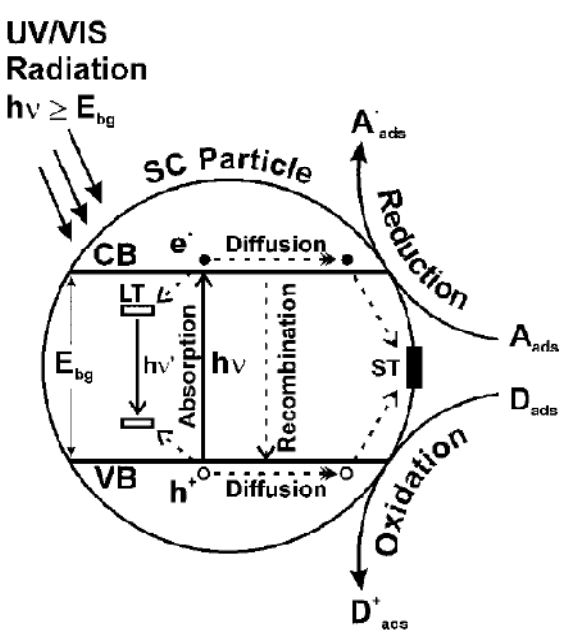

Figure 2.5 Photophysical and photochemical reactions in a semiconductor (Oppenlander, 2003)

In the presence of water, including either adsorbed water molecules or hydroxyl

ions on the surface of the photocatalyst, oxidation by h^+_{vb} may occur as illustrated below, in Equation 2.2. The products of this reaction include hydroxyl radicals ($OH^\bullet$), a very potent oxidizer species. Therefore, water vapor in the air stream can exert an important role in photocatalytic oxidation reactions because it can function as a source of hydroxyl radicals.

$$H_2O + h^+_{vb} \rightarrow OH^\bullet + H^+ \qquad (2.2)$$

Since hydroxyl radicals are extremely reactive species, pollutants adsorbed on the surface of the semiconductor are readily oxidized. The redox potential of hydroxyl radicals of +1.98 V is relatively high (Koppenol and Liebman, 1984). It is just slightly smaller than the reduction potential of ozone, +2.07 V (Oppenlander, 2003), which is known as a strong oxidant. Thus, $OH^\bullet$ provides an effective route in mineralization or degradation of organic compounds. There are several chemical pathways by which hydroxyl radicals can oxidize organic and inorganic substrates, such as electron transfer, hydrogen abstraction or electrophilic addition. These oxidation pathways are shown in Equations 2.3 to 2.5.

$$OH^\bullet + M^n \rightarrow M^{n+1} + (OH^-) \qquad \text{electron transfer} \qquad (2.3)$$

$$OH^\bullet + R\text{-}H \rightarrow R^\cdot + H_2O \qquad \text{hydrogen abstraction} \qquad (2.4)$$

$$OH^\bullet + R_2C{=}CR_2 \rightarrow {\cdot}CR_2{-}C(OH)R_2 \qquad \text{electrophilic addition} \qquad (2.5)$$

The complete photocatalytic oxidation of VOCs will result in formation of carbon dioxide (CO_2) and water (H_2O). The net degradation reaction of a VOC by hydroxyl radical can be expressed as Equation 2.6.

$$OH^{\bullet} + VOC + O_2 \rightarrow nCO_2 + mH_2O \quad (2.6)$$

Photoexcited electrons, as well as e^-_{cb} produced by photon absorption, can react with adsorbed oxygen ($O_{2(ads)}$) to form superoxide radical anions ($O_2^{\bullet -}$), as exemplified in Equation 2.7.

$$O_{2(ads)} + e^-_{cb} \rightarrow O_2^{\cdot -}{}_{(ads)} \quad (2.7)$$

Consequently, the superoxide radicals, which can function as strong reducing agents, also have the potential to react with various VOCs.

The photoreduction can also occur via simple direct electron transfer from excited conduction band electrons to the adsorbed molecules. For example, metal ion, M^{n+} can be reduced by e^-_{cb} to their elemental form, M^0, as exemplified in Equation 2.8.

$$e^-_{cb} + M^{n+} \rightarrow M^0 \quad (2.8)$$

In the absence of any adsorbed species, the photo-promoted conduction band electron simply recombines with the valence band holes, as expressed in Equation 2.9.

$$e^-_{cb} + h^+_{vb} \rightarrow \text{heat} \quad (2.9)$$

In fact, this recombination of e^-_{cb} and h^+_{vb} can occur even in the presence of adsorbed molecules, and this represents an important limitation in terms of the overall catalytic efficiencies which can be achieved. Clearly, the efficiency of pollutant degradation is strongly dependent on the lifetime of e^-_{cb} and h^+_{vb}. In the case of TiO_2, the lifetime of electron/hole pairs is believed to be relatively short. For example, it has been reported that photogenerated electron / hole pairs in TiO_2 particles recombine within 30 ± 15 ns (Moser et al., 1987). Obviously, if the lifetime of e^-_{cb} and h^+_{vb} pairs could be increased, higher rates of photocatalytic activity would be achieved.

In light of the above discussion, an outline of a typical semiconductor based photocatalytic reaction scheme is shown in Figure 2.6.

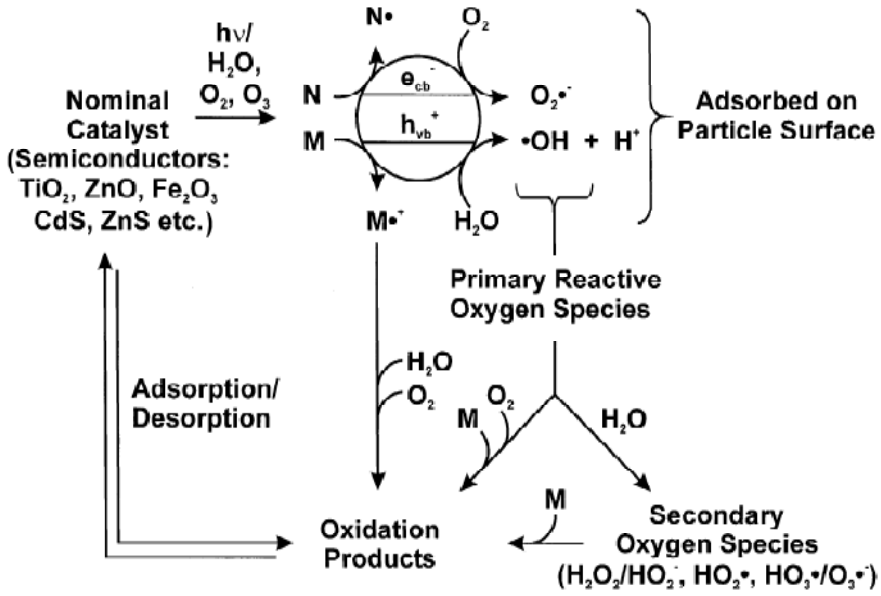

Figure 2.6 Scheme of photocatalytic oxidation reactions; M and N represent substrate molecules with different reduction potentials (Oppenlander, 2003).

2.2.3 Titanium Dioxide as a Photocatalyst

A rather wide variety of semiconductors have been employed as photocatalysts. Typically, photocatalysts are metal oxides or sulfides: for example, CdS, ZnS, Fe_2O_3, ZnO, SnO_2 and TiO_2. However, the most widely used catalyst in photocatalytic oxidation is titanium dioxide (TiO_2) due to its strong oxidative ability, exceptional stability, wide availability and relative low cost (Kaneko and Okura, 2002, Ollis, 2000, Rajeshwar, 1995). TiO_2 exists in three different crystalline structures, namely: anatase, rutile and brookite. Among these structures, anatase and rutile have been employed in numerous photocatalysis studies. However, it is interesting to note that while there have been

relatively few reports involving brookite, this crystalline form appears to be gaining increased interest; it has been reported that brookite is more electrochemically active than anatase (Pan et al., 2009). Redox potentials of h^{+}_{vb} and e^{-}_{cb} of TiO_2, compared to standard hydrogen electrode (SHE) of 0.00V, are +2.53 eV and -0.52 eV, respectively. The band gap energies of anatase, rutile and brookite are reported to be 3.2 eV (Sun et al., 2010), 3.0 eV (Sun et al., 2010) and 3.5 eV (Zallen and Moret, 2006), respectively. These energies correspond to photons having wavelengths shorter than 385 nm. Thus TiO_2, unfortunately, can utilize only a relatively small fraction of the solar spectrum. Figure 2.7 illustrates the energy band gap of TiO_2 and various processes which are energetically possible on the surface of TiO_2 following absorption of photons of appropriate wavelength.

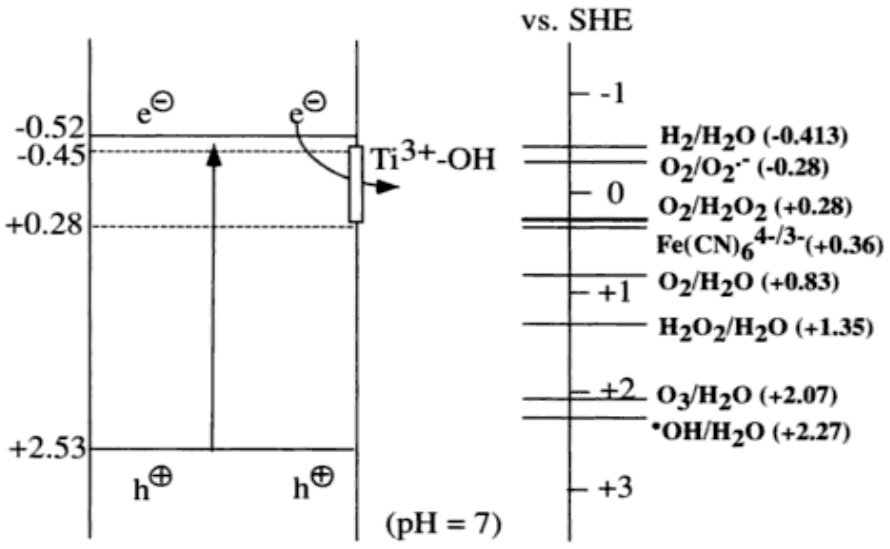

Figure 2.7 Energy band gap of TiO_2 and redox potentials process on the surface of TiO_2 (Kaneko and Okura, 2002).

Thus, one of the main practical drawbacks of using TiO_2 as a photocatalyst is its energy band-gap of 3.0 eV, or higher, which automatically eliminates the major portion of the sunlight photons present in the troposphere. In addition, there are two other important limitations which must be considered in terms of TiO_2 photocatalytic activity. One of these is the inherent, aforementioned, extremely rapid recombination of electron-hole pairs. The other concern is that of catalyst deactivation over time on stream, which can result from the accumulation of adsorbed product intermediates, thus reducing catalyst activity (Mo et al., 2009).

2.2.4 Modification of TiO_2 to Improve Photocatalytic Activity

In light of the above considerations, several studies have been conducted to improve photocatalytic degradation of air pollutants over TiO_2 catalyst. These prior investigations have included doping TiO_2 with transition metals such as Ni (Tseng et al., 2009), Fe (Liu and Chen, 2009), Cu (Xu et al., 2010) or Mn (Chen et al., 2010), in attempts to broaden light absorption into more of the visible region. For example, the study of Di Paola et al. (2001) revealed that impregnating TiO_2 with Co, Cr, Cu, Fe, Mo, or V atoms shifted the bandgap to longer wavelength, thus extending absorption somewhat further into the visible region. However, unfortunately, these workers report that the photocatalytic activities of transition metals doped TiO_2 particles were actually lower than the undoped control materials. The authors believe this decreased photocatalytic activity resulted from an increased recombination rate of electrons and holes, as promoted by the transition metal ions.

TiO_2 has also been doped using a variety of other materials, including carbon (Cheng et al., 2007), nitrogen (Ananpattarachai et al., 2009), sulfur (Yu et al., 2005), fluorine (Chen et al., 2009, Ooka et al., 2004) and tetramethyltin (Cho et al., 2006). Doping of carbon on titania catalyst, achieved using a combustion method, was conducted by Cheng et al. (2007). C-doped titania showed high photocatalytic activity in degradation of 4-chlorophenol under visible light. Nitrogen doping decreased the bandgap of P-25 TiO_2 from 3.20 eV to 2.85 eV and it was active under visible light as shown by the oxidation of 2-chlorophenol (Ananpattarachai et al., 2009). Sulfur-doped TiO_2 was evaluated as a disinfectant and exhibited strong bactericidal activity under visible light irradiation against *Micrococcus lylae* (Yu et al., 2005). Surface fluorination of TiO_2, prepared by a sol-gel method, was reported to enhance the photocatalytic degradatioin of Rhodamine B (Chen et al., 2009). Ooka et al.(2004) increased surface hydrophobicity of TiO_2 by synthesizing TiO_2-pillared clay and observed an improvement in the photocatalytic oxidation of toluene and trichloroethylene removal. Cho et al.(2006), employing a plasma polymerization technique, deposited a thin coating of tetramethyltin on the TiO_2 and this film was subsequently oxidized to tin oxide by calcination. Subsequently, these tin oxide coated TiO_2 nanoparticles exhibited a significantly enhanced oxidation rate of acid orange as measured in aqueous solution.

There have been several attempts to improve TiO_2 photocatalytic activity by using anions, such as PO_4^{3-} and SO_4^{2-}. For example, Yu et al.(2003) reported that phosphate/TiO_2 had a higher activity than commercial P25 for photocatalytic degradation of n-pentane in air. They attribute this enhanced activity to decreased band energy,

accompanied by a higher surface area. Muggli and Ding (2001) examined photocatalytic activity of SO_4^{2-}/TiO_2 for toluene oxidation. They report that the unmodified TiO_2 was more active than sulfated TiO_2 at room temperature, while the SO_4^{2-}/TiO_2 had higher photocatalytic activity at the higher temperature of 373 K. Sulfation on TiO_2 helped prevent the conversion of the anatase phase to rutile, which is known as the less active form due to its high recombination rate of e^-_{cb} and h^+_{vb} and its low ability to photoadsorb oxygen (Augugliaro et al., 2010).

Fluorination is another surface modification that has been employed on TiO_2. It is believed that a surface Ti-F group can strongly bind free electrons, thus reducing the rate of recombination between h^+_{vb} and $_{e^-cb}$ (Park and Choi, 2004a). A study of photocatalytic activity of fluorinated TiO_2 was conducted by Park and Choi (2004b). Fluorinated TiO_2 film was placed next to a stearic acid coated glass, with a space of 30 μm between these two surfaces to avoid direct physical contact between photocatalyst and target pollutant. The result showed that stearic acid was degraded in the case of Ti-F, while no stearic acid degradation was observed in case of standard TiO_2. The authors concluded that fluorinated TiO_2 more readily produced $OH^{\cdot}$ free radicals that could mobilize and react with pollutant that was not adsorbed on the TiO_2 surface. Thus, the photocatalytic oxidation reaction was not limited to the surface of the catalyst. Another fluorinated TiO_2 study, carried out by Yu et al.(2009), involved fluorinated TiO_2 as prepared by hydrothermal treatment of precipitates of tetrabutyl orthotitanate in NH_4HF_2-$H_2OC_2H_5OH$ mixed solution. Photocatalytic activity of fluorinated and untreated TiO_2 were compared using acetone vapor oxidation. The catalyst was immobilized on glass

plates and loaded into a glass chamber where liquid acetone was injected into a chamber to test photocatalytic activity of the catalysts. The results showed that photocatalytic activity of fluorinated samples were clearly higher than that of untreated TiO_2. These authors attributed the increased catalytic activity of the F-doped materials to their ability to more readily create OH radicals. The measurement of $OH^{\bullet}$ was done by a photoluminescence (PL) technique using terephthalic acid as probe molecule. Hydroxyl radical readily reacts with terephthalic acid, producing a highly fluorescence product, 2-hydroxyterephthalic. The intensity of the PL spectra is proportional to the amount of hydroxyl radical generated in water by the photocatalytic reactions. It was reported that fluorinated TiO_2 generated significantly more hydroxyl radicals than untreated TiO_2. They claimed that free hydroxyl radicals ($OH^{\bullet}_{free}$), created in case of fluorinated TiO_2, had good mobility, as they are not tightly bound to the TiO_2 surface. However, Yu et al. assumed that the hydroxyl radicals generated from Ti-F existed in the form of $OH^{\bullet}_{free}$. There was no direct evidence which proved that the hydroxyl radicals created by Ti-F were $OH^{\bullet}_{free}$, not surface adsorbed $OH^{\bullet}$.

The distinction between reactions of $OH^{\bullet}_{free}$ and surface hydroxyl radical are shown in equations 2.10 and 2.11, respectively (Chen et al., 2009, Park and Choi, 2004b, Park and Choi, 2005).

$$\text{Ti-F} + H_2O \text{ (or } OH^-) + h^+_{vb} \rightarrow \text{Ti-F} + OH^{\bullet}_{free} + H^+ \qquad (2.10)$$

$$\text{Ti-OH} + h^+_{vb} \rightarrow \text{Ti-OH}^{\cdot +} \qquad (2.11)$$

Several workers have investigated the band structure of fluorine doped TiO_2 by UV-Visible diffuse spectra analysis. However, controversy remains concerning the effect,

if any, of the F doping on the optical properties of TiO_2. Some researchers reported that doping of fluorine does not change light absorption properties of TiO_2 with respect to bandgap narrowing or creation of a new absorption band (Augugliaro et al., 2010, Chen et al., 2009, Yu et al., 2009). The apparent absence of any effect of F-doping on the TiO_2 bandgap is in agreement with the theoretical work of Yamaki et al. (2003) whose calculations show that F- localized energy levels are located below the valence band of TiO_2 and, as such, should not change the optical properties. On the other hand, Yu et al (2002) have reported that TiO_2 powder, doped by fluorine via a hydrolysis process, exhibited stronger UV-Visible absorbance, which included a shift in the TiO_2 bandgap to longer wavelengths (a so-called red shift).

With respect to the photocatalytic activity of F-doped TiO_2, several workers have reported increased activity with F-doping. For example, according to Li et al. (2005), fluorine doped TiO_2 powder, prepared by a spray pyrolysis technique, exhibited high photocatalytic activity for decomposing acetaldehyde and trichloroethylene. This enhanced activity is attributable to oxygen vacancies (F and F^+ centers), which provide two intermediate energy levels at 0.53 and 0.84 eV below the TiO_2 conduction band, thus shortening the bandgap energy and extending the photoactivity further into the visible region of the spectrum. UV-Vis absorption which was observed in Li et al.'s work is shown in Figure 2.8. A slight red shift observed reflects the fact that T-900 sample contained rutile phase TiO_2.

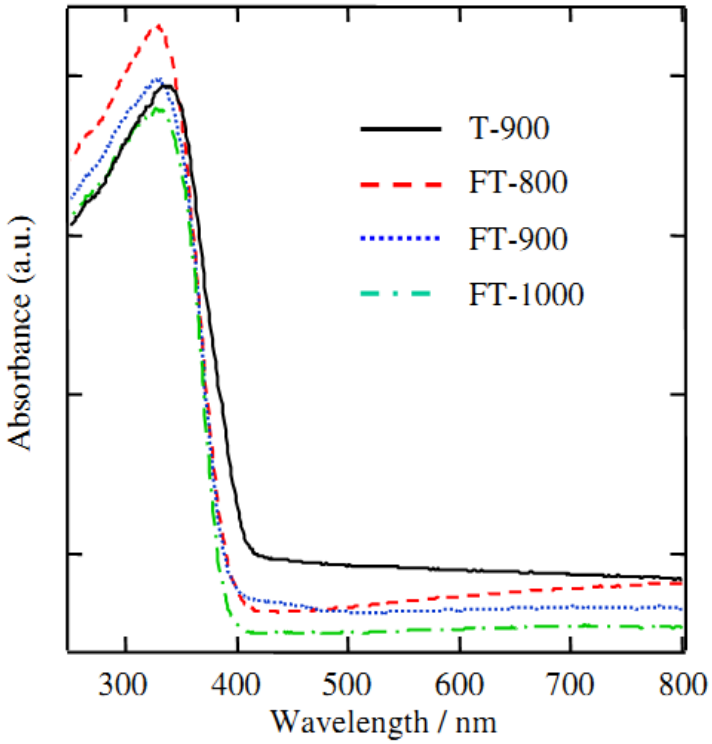

Figure 2.8 UV-Vis absorption spectra of F-doped TiO_2 powder (Li et al., 2005).

One recent study involving surface modification of TiO_2, of particular relevance to the present work, involved co-doping of TiO_2 with carbon and fluorine, as achieved by hydrolysis of TiF_4 and α-D-glucose as a precursor to carbon doping. This co-doping increased photocatalytic activity of styrene destruction under visible light (Lim et al., 2008). The enhanced catalytic activity was attributed to the high electronegativity of fluorine in trapping electrons, thus reducing the electron-hole recombination rates. Additionally, the band gap energies of fluorinated and fluorine/carbon codoped TiO_2 were reduced by 7%. However, it is also important to note that, in contrast to the styrene study, fluorinated TiO_2 has been reported to be non-effective in enhancing the

photocatalytic destruction of toluene and actually inhibited the photocatalytic oxidation of benzene (Lewandowski and Ollis, 2003a).

In summation, although there are obviously conflicting reports on the effect of F-doping of TiO_2 on catalytic activity, the preponderance of studies do indicate that, in general, increased photocatalytic activity is observed. This enhanced activity has been attributed to more efficient creation of free $OH^{\bullet}$ and to reductions in the rate of electron-hole recombinations. With respect to F-doping changes in TiO_2 band gap, the situation is less clear, although the preponderance of evidence would suggest that no measureable changes in band gap are observed.

2.3 Photocatalytic Oxidation of Elemental Mercury

Atmospheric mercury can be present in elemental, oxidized, and particulate bound forms. Many studies have reported that between 97 and 99% of the mercury in air is in the form of elemental mercury (Hg^0) (Granite et al., 2008). Elemental Hg and its compounds are toxic, especially to human neural systems. Exposure to excessive levels of mercury can cause impaired motor and cognitive skills, as well as potential cardiovascular, immune, and reproductive system impacts (U.S. EPA, 1997). Mercury is anthropogenically released into the air when coal, oil, wood, or mercury containing wastes are burned. Airborne mercury can deposit on water bodies or soil via wet or dry deposition. Gaseous mercury has a relatively long atmospheric life-time of 0.5-2 years (Lamborg et al., 2002), which allows this pollutant to travel long distances from its source of origin. In water bodies, biological processes transform Hg^0 to methylmercury

(CH_3Hg^+), an extremely toxic form of mercury which is unfortunately readily bio-accumulated in fish.

At the present time highly effective control strategies to decrease airborne Hg emissions are sorely lacking (Li et al., 2011). Traditional control technologies, such as adsorption by activated carbon, can reduce up to 90% of Hg emissions from bituminous coal, which are mostly present as oxidized mercury (Hg^{2+}). Oxidized mercury is readily adsorbed on the adsorbent and consequently captured by particulate control devices. Hg^{2+} is water soluble and can be easily captured using scrubber technology as another method of removal (Li et al., 2011). However, elemental mercury, the predominant species when sub-bituminous and lignite coal are burned, can only be 60-70% removed by activated carbon adsorption due to its high mass-transfer resistance which permits Hg^0 to slip through the adsorbent bed (McLarnon et al., 2005). As a result, control methods to oxidize Hg^0 to Hg^{2+}, or remove Hg^0 with significantly higher efficiencies, are needed (Alptekin et al., 2003). In order to oxidize Hg^0, strong oxidants are required because Hg^0 is relatively inert material (Granite et al., 2008). Elemental mercury can be oxidized by photolysis of ozone (O_3), which produces an oxygen atom free radical (O). For example, a study by McLarnon et al.(2005) stated that ozone exposure to UV light of wavelength 254 nm oxidized Hg^0 to Hg^{2+}. Li and Wu (2007) reported that SiO_2-TiO_2 had the potential to oxidize Hg^0 from coal combustion flue gas due to the relatively high surface area and more open structure of SiO_2-TiO_2, which can accommodate more Hg^0 molecules. The rate of photocatalytic Hg^0 oxidation increased when the inlet concentration of Hg^0 increased when no water vapor was presented. In case of the absence of water, $OH^\bullet$ could

be formed in another route by the reaction between the h^{+}_{vb} and surface hydroxyl originated from silanol (Si-OH) groups. Silanols were produced in hydrolysis and alcoholysis during photocatalyst preparation process. This study also found that the removal of Hg^0 was inhibited by the presence of water vapor, which is unfortunately abundantly present in flue gases, due to competitive adsorption of water on the TiO_2 surface.

Elemental mercury in air can be photocatalytically oxidized into mercury oxide (HgO) by TiO_2 at ambient temperature (Snider and Ariya, 2010). Under UV irradiation, $OH^{\bullet}$ can be created from oxidization of adsorbed water molecules on the TiO_2 and the $OH^{\bullet}$, in turn, oxidizes Hg^0 into HgO. This oxidative process is expressed as follows (Li and Wu, 2007, Snider and Ariya, 2010):

$$OH^{\bullet} + Hg^0 \rightarrow HgO \qquad (2.12)$$

A recent study (Jeon et al., 2008) of photocatalytic oxidation for Hg^0 using nanotitanosilicate fiber, which had a surface area of 45 m^2/g, was conducted in a continuous flow reactor. The inlet Hg^0 concentration was 400 $\mu g/m^3$ and it was introduced at the flow rate of 50 cm^3/min. A maximum removal efficiency of 78% of Hg^0 in air was observed under UV irradiation. Jeon et al. explained briefly that large moisture content in TiO_2 amorphous attributed to the high Hg^0 conversion. Li et al. (2011) used the high surface area photocatalyst SiO_2-TiO_2-V_2O_5 to photooxidize Hg^0 from simulated flue gas. The surface area of SiO_2-TiO_2-V_2O_5 was 250 m^2/g, compared to 50 m^2/g for standard P25 TiO_2. It was also reported that this catalyst combination removed 80% of the Hg^0 at a

temperature of 135°C when the inlet Hg^0 concentration was 70 $\mu g/m^3$. However, the Hg^0 removal efficiency dropped from 80% to 44% when water vapor was increased from 0% to 8%, respectively. Thus, water vapor in the air stream had a strong inhibitory effect on Hg^0 degradation, presumably due to the competitive adsorption on the active sites.

2.4 Effects of Relative Humidity on Photocatalytic Activity

The influences of water vapor on the photocatalytic activity of TiO_2 have been widely investigated because it impacts the oxidation rates of VOCs. However, as in much of the TiO_2 literature, conflicting results have again been reported with respect to relative humidity effects on oxidation rates. In fact, inhibition, neutral (no effect) and activity promotion effects of humidity on photocatalytic activity of TiO_2 have all been reported, depending on the particular pollutants examined (Raillard et al., 2005). Overall, two potentially conflicting roles of water molecules have been suggested with respect to increasing or decreasing the efficacy of TiO_2 photocatalytic oxidations. On one hand, water may serve as an important source of $OH^{\bullet}$ radicals, generated as shown in Equation 2.2, a species which can function as a strong oxidizing agent to remove pollutants. It has been reported that the amount of $OH^{\bullet}$ produced is proportional to the adsorbed water molecules (Boonstra and Mutsaers, 1975, Lawless et al., 1991). Thus, based on this consideration, a higher amount of water would be predicted to promote increased photocatalytic reactions. However, there is a potential inhibitory role water vapor could play that would reduce the photocatalytic decomposition rate of pollutants. Specifically, when larger amounts of water vapor are present, competitive adsorption for TiO_2 catalytically active sites between water and pollutant molecules could take place. As a

result, decreasing photocatalytic oxidation rates could be observed. The formation of adsorbed water molecules on TiO_2 was recognized by Gregg and Sing (1982), who proposed that water can be both chemisorbed and physisorbed on the surface of TiO_2. Two types of chemisorbed water have been suggested, either as H_2O ligands or as hydroxyl (OH) groups formed by the hydrolysis of H_2O via interaction with the Ti^{+4} and O^{2-} ions. Ligand adsorption is a rapid process. After the layer of chemisorbed water is formed, additional water can be physisorbed on the chemisorbed layer. This physisorption takes place by hydrogen bonds between ligand water molecules and the surface hydroxyl groups.

Pichat (2010) has suggested that oxygenated organic pollutants may form hydrogen bonds with water, thus disorganizing the water network that covers the TiO_2 surface and in this manner assisting access of the organic species to the surface of TiO_2. However, in the case of non-polar organic pollutants, which cannot form hydrogen bonds with water, the adsorbed water would presumably act as a barrier to prevent organic molecules from accessing the TiO_2 surface. The results from several studies appear to support the suggestions of Pichat. Beneficial influences of humidity on the photocatalytic oxidation were observed with methyl ethyl ketone (MEK, butanone) (Raillard et al., 2005), 2-propanol (Vildozo et al., 2010), and acetone (Coronado et al., 2003). These pollutants are oxygenated organic pollutants whose further oxidative decomposition rates were promoted by higher concentrations of water vapor. In contrast, the presence of relatively high concentration of water vapor appeared to function as an inhibitor in the photooxidation of non-oxygenated organic compounds such as chlorobenzene (Zhang et

al., 2007), toluene (Quici et al., 2010), 1-3-butadiene (Obee and Brown, 1995) and cyclohexane (Einaga et al., 2002). Thus, the reports noted above can be considered to be in line with expectations predicted by Pichat. Unfortunately, there have been several studies in which the results did not agree with Pichat's explanations. For example, an improved rate of photooxidation of toluene, benzene and cyclohexene with the increasing of humidity was reported (Einaga et al., 2002). These are three non-polar compounds in which the presence of additional water should have been inhibitory in nature according to Pichat. However, Einaga et al. (2002) suggest formation of additional hydroxyl radical under higher humidity as the reason for the observed acceleration in photooxidation rates. Also to be noted is the inhibitory effect of water on an oxygenated organic compound as reported by Peral and Ollis (1992), who tested photooxidation of acetone under UV light using P25 TiO_2 in a plug-flow reactor. In fact, they reported that the rate of photooxidation of the acetone dropped dramatically by 75% when the relative humidity was increased from 250 to 9000 mg/m^3. Peral and Ollis also investigated the effect of moisture on 1-butanol and m-xylene. They found that water had no influence on the 1-butanol conversion in a range of water concentration of 250 – 4000 mg^3/m^3. The m-xylene removal rate, tested at water concentrations of 0 – 5500 mg/m^3, was promoted when the water concentration was below 1000 mg/m^3 and inhibited above that value.

The effect of moisture on the photocatalytic oxidation of MEK, a highly water soluble compound, was investigated by Railard et al. (2005). The relative humidity was varied between 0% and 30% in a batch reactor that used TiO_2 P25 powder deposited on a glass plate. The rate of photocatalytic oxidation doubled when the relative humidity was

raised from 0% to 30%. However, it should be noted that the Langmuir-Hinshelwood adsorption constant decreased from 0.446 m^3/g to 0.115 m^3/g. These results indicated that more water molecules increased the formation of $OH^{\bullet}$ and improved MEK removal rate, despite the fact the increasing relative humidity led to a sharp decrease in the MEK L-H adsorption constant.

Photocatalytic oxidation of chlorobenzene (CB), a moderately soluble compound in water, was conducted by Zhang (2007) under relative humidity conditions ranging from 12 to 80%. Powdered P25 TiO_2 was slurry coated on the inside wall of the batch reactor, where UV light was irradiated. The initial CB concentration was 740 mg/m^3. A severe inhibition effect of water vapor was observed on CB photo oxidation in that the percent conversion of CB decreased from 98% to less than 50% as the relative humidity varied from 12% to 80%.

A study of the influence of relative humidity on trichloroethylene was conducted by Amama et al. (2004). Relative humidities of 25, 50, 75 and 100% were employed in a batch reactor, using UV light as the energy source. TiO_2 powder was coated on a glass fiber cloth via a sol gel technique and the catalyst density per surface area was 4.8 g/cm^3. The trichloroethylene removal rate increased from 52 to 71% when relative humidity increased from 0 to 25%. However, an inhibition effect of water vapor was observed at relative humidities above 25%.

Geng et al. (2010) examined the effect of RH ranging from 5 to 40%. They found that relative humidity of 20% was the optimum for cyclohexane removal. Their experiment was conducted in a fluidized bed annular reactor, which was expected to

provide higher mass transfer and higher UV emission to the photocatalyst. An initial cyclohexane concentration of 7.5 mg/L was introduced into the reactor. At 5% relative humidity, a removal efficiency of 40% was observed. The peak removal of 52% was observed when the relative humidity was increased to 20%. At relative humidities above 20%, the removal efficiency started to decrease; for example, a removal efficiency of 39% was observed under 40% relative humidity.

Sleiman et al. (2009) investigated toluene photocatalytic oxidation using 100% anatase powder coated on fibrous paper in a plug-flow reactor. The inlet concentration of toluene was 120 ppb at a flow rate of 350 cm^3/min. Relative humidity ranged from 0 – 70%. The optimum relative humidity was in the range 0-20%, where the removal efficiencies were 95%. The removal efficiency dropped gradually as the RH increased reaching a value of 85% when the RH was raised to 70%.

Quici et al. (2010) also studied the effect of moisture, employing RH values of 0, 10, 33 and 66%, in the air stream during photocatalytic oxidation of toluene. The UV light irradiated P25 TiO_2 coated on ring-shaped media called Raschig Rings, having an internal diameter of 4 mm, external diameter of 6 mm and 20 mm length. Placing several Raschig rings inside a tubular flow reactor could increase effective surface area of the catalyst. Quici et al. observed the toluene removal rate was highest at 10% relative humidity, followed by relative humidities of 0%, 33% and 66%, respectively. Quici et al. suggested that dissociated water molecules were the source of active species on the surface of TiO_2. At higher relative humidities, namely 33 and 66%, adsorbed water

molecules created many monolayers, which competed with toluene molecules to adsorb onto the active sites, thus leading to the lower reaction rate.

Thus, taken in combination, these results from various laboratories make it difficult to generalize unequivocally on the effect of relative humidity on the TiO_2 photocatalytic activity. However, many studies have found that there is an optimum relative humidity for VOCs which would be consistent with occurrence of both inhibition and promotion effects of water vapor. Additionally, it appears that the effect of relative humidity on photocatalytic activity is also strongly dependent on the nature of the particular pollutant compounds employed in the various studies. Overall, it does appear that low humidity could be beneficial for photocatalytic oxidation of some VOCs, especially for moderately to low water soluble pollutants. However, excessive amounts of water vapor in the gas stream can apparently retard the pollutant removal by competitive adsorption processes.

2.5 Deactivation and Regeneration of Photocatalysts

Deactivation of catalysts, including photocatalysts, is a significant problem in many catalyzed reactions. The most common reason for this deactivation is the accumulation of by-products on the surface of the catalyst. These by-products inhibit reactants, in the present case pollutants, from accessing the active sites. Tomasic et al. (2008) reported that benzaldehyde and benzoic acid, which are by-products from degradation of toluene, were found as the deposits on the active sites of TiO_2 and they were responsible for catalyst deactivation. The color of the TiO_2 changed from white to yellow during toluene photocatalytic oxidation. A similar observation has been reported

by other researchers (D'Hennezel et al., 1998, Xie et al., 2004, Zhong et al., 2007). Second, the Ti-OH surface hydroxyl group was consumed in the formation of $OH^{\bullet}$ and thus becomes depleted (Zhong et al., 2007). An additional source of catalyst deactivation, suggested by Ollis (2000), is the possible occurrence of photo-polymerization of organic pollutants on the surface and thus blockage of active surface sites, as reported in the degradation of benzene. Finally, it is noted that carbon dioxide, the end product in some of these photooxidation processes, can be trapped on active sites in another form, i.e. as carbonate ions (Ollis, 2000).

Regenerations of deactivated TiO_2 catalysts has been examined in a number of laboratories. Techniques which have been employed include rinsing the deactivated catalyst with solvents, thermal regeneration (Kaewgun and Lee, 2010) ; (Cao et al., 2000), or exposing deactivated catalyst to pure air or humid air under UV irradiation (Lewandowski and Ollis, 2003b).

Kaewgun and Lee (2010) using brookite TiO_2, prepared by a solgel method, also incorperated N-methylpyrrolidene (NMP) in an attempt to shift photon absorption to longer wavelengths. Their catalyst is identified as NMP-200. Oxidation rates of methyl orange in the liquid phase, under UV and visible light irradiation, were determined. After 4 consecutive runs with the NMP-200 catalyst, deactivation was observed and believed to arise from deposition of decomposed methyl orange on active catalytic sites. The initial rate of methyl orange degradation had decreased by more than 47% after NMP-200 had been employed in the fourth run. Solvent washing and recalcination were tested as methods of catalyst regeneration. Methanol, ethanol, isopropanol and acetone were used

in solvent washing; calcination involved heating of deactivated catalyst at 200 and 250°C in air for 4 hours. Washing deactivated NMP-200 by methanol resulted in 80% recovery of the fresh sample's catalytic activity. The other solvents employed partially regenerated the NMP-200, but they were not as efficient as methanol. Recalcination at 200 and 250 °C could not remove carbonaceous deposition from the NMP-200 surface. It was determined, by TGA analysis, that temperatures above 400 °C were required to remove the carbon deposits. However, applying such high temperature decreases surface area by agglomeration of particles. Additionally, the visible light active NMP-200 is destroyed at these high temperatures. Thus sintering of the NMP-200 severely limits regeneration of this photocatalyst.

In the study by Cao et al. (2000), TiO_2 powder, prepared by a solgel technique, was used to study toluene photocatalytic oxidation. Regeneration of deactivated TiO_2 was examined by heating deactivated catalyst at 350 °C and 420 °C for 2 hours in air. Photoreactivity was recovered up to 80% and 100% for TiO_2 subjected to thermal treatment at 350 °C and 420 °C, respectively. However, heating deactivated TiO_2 beyond 420 °C results in phase transformation from anatase to rutile, this latter crystalline form being significantly less photoreactive. Also, as noted above, high temperature also creates undesirable sintering and thus decreases surface area of the catalyst.

D'Hennizel et al. (1998) conducted an experiment on regeneration of P25 TiO_2 impregnated with water and hydrochloric acid after the catalyst had been used in photooxidation of 13 ppm toluene in a flow-through reactor. The regeneration process involved flowing pure air through the catalyst under UV light for 2 hours and 16 hours

after the catalysts had been employed for a single run. After 2 hours of pure air and UV exposure, only 25-30% catalytic activity, compared to the original TiO_2, was observed. The TiO_2 regained 70-75% of its original activity after 16 hours of pure air purging with UV irradiation.

Lewandowski and Ollis (2003b) investigated the regeneration of P25 TiO_2 powder which was deposited on fritted glass in a flow through annular reactor. After 2 hours of toluene photooxidation under UV light, the removal efficiency dropped from 80% to 20%. The exhausted TiO_2 samples were regenerated by passing 7% humidified scientific grade air under UV exposure for 2, 4 and 6 hours. They reported that the catalyst needed 6 hours of regeneration to recover 80% of the initial activity.

Thus, as these various reports indicate, regeneration of used TiO_2 photocatalysts is an important limitation in dealing with photo-oxidation of VOCs. Although a number of regeneration techniques have been employed, e.g. calcination, solvent washing and photooxidations with pure air, complete regeneration of catalytic activity was not achieved, even when extended treatment times were employed.

2.6 Plasma Surface Modification

2.6.1 Background of Plasma Surface Modification

Plasma is a partially ionized gas which includes electrons, positively and negatively charged ions, radicals, neutral atoms and molecules. The applied electric field produces electrons by partial ionization of the gas; these electrons transfer energy to gaseous monomer molecule by elastic and inelastic collisions. Collisions between

electrons and gas molecules lead to dissociation and ionization of the molecules and thus formation of reactive species.

The characteristics and properties of plasma generated coatings depend mainly on reactant monomers and plasma reaction variables employed during the deposition processes. In the present case, pulsed plasmas were employed in addition to the more common continuous wave (CW) operational mode. The controllable plasma variables in this work include plasma duty cycle, power input, monomer flow rate and reaction pressure. A higher level of monomer dissociation is observed as the input power is increased. In general, the increased monomer dissociation results in formation of more highly cross-linked polymers. Variations of monomer flow rates or pressures have much less effect on the polymer compositions formed than power input, with the actual film structures being dependent on the nature of the monomer employed.

In the case of pulsed plasma, duty cycle is an important variable to control film chemistry during plasma polymerizations. This is not surprising, in that the average power input under pulsed conditions varies with changes in the plasma on:off duty cycles employed, as shown in Equation 2.13.

$$\text{Duty Cycle} = \frac{\text{(On Time)}}{\text{(On + Off Time)}} \qquad (2.13)$$

Plasma treatment is a relatively new technique in modifying catalysts, including a few studies involvng photocatalytic oxidation. Under plasma conditions, a thin film of monomer vapor can be deposited directly by polymerization onto a solid substrate;

alternatively, the substrate surface can be modified under high energy input conditions by reactive etching processes. Polymer films deposited by the plasma technique are very uniform in composition and are distributed evenly across the entire surface of the targeted substrate. The thickness of pulsed plasma deposited films can be controlled exactly in that deposition rates vary linearly with deposition times employed. In general, much better film thickness and film compositional control are obtained under pulsed conditions compared to CW operational mode.

2.6.2 Plasma Surface Modification on TiO_2

As reported by Cho (2005), fluoropropylene oxide (HFPO, C_3F_6O) and perfluorohexane (C_6F_{14}) can be employed as gaseous monomer to either directly fluorinate or to deposit a polymerized perfluorocarbon film on the surface of TiO_2, dependent on the plasma conditions employed. At high average power inputs, fluorination of TiO_2 was observed, while polymerization of perfluorocarbon was produced at low average power input. X-ray photoelectron photoscopy (XPS) spectra of fluorinated samples showed that increasing the treatment time increased the amount of fluorine atom on the surface. It was also demonstrated that the crystalline phases of TiO_2 were not changed by plasma treatment, as shown by X-ray diffraction (XRD) results. TiO_2 particles, treated by HFPO plasma, were found to be significantly more hydrophobic than commercial TiO_2. Photocatalytic activity of treated samples was evaluated by reduction of dichromate ($Cr_2O_7^{2-}$) in aqueous solutions. TiO_2 nanoparticles were subjected to plasma fluorination for 15, 30, 60 and 120 minutes. The nanoparticles which were treated for 15, 30 and 60 minutes were significantly more reactive than

untreated TiO_2. Photocatalytic activity of TiO_2 plasma treated for 60 minutes performed better than that treated for only 30 and 15 minutes. However, TiO_2 fluorinated for 120 minutes was significantly less catalytically active than the untreated TiO_2 due to the excessive thickness of the plasma film which essentially eliminated contact between $Cr_2O_7^{2-}$ and the surface of the catalyst.

The use of plasma processing to modify TiO_2 catalytic activity has been reported in several other recent studies. These studies include use of a nitrogen discharge to produce N-doped TiO_2 (Liu et al., 2006), acrylic acid to deposit an amorphous polymer coating on TiO_2 (Wang and Zhang, 2006), and plasma deposition of a tin containing coating on TiO_2 which was subsequently converted to tin oxide by calcinations (Cho et al., 2006). Liu et al. used N_2 in the generation of N doped TiO_2 by plasma deposition. TiO_2 which had been plasma treated for 10 minutes exhibited visible light adsorption which was not observed in the untreated material. Photocatalytic reduction of $Cr_2O_7^{2-}$ was conducted using this N doped catalyst and higher photoreactivity was observed than that of untreated TiO_2. Cho et al. used tetramethyltin as the monomer in the deposition of a tin containing coating which was then converted into tin oxide coating by calcination. Photocatalytic oxidation of acid orange 7 was conducted in liquid phase to investigate the activity of tin oxide coated TiO_2 under UV light. The tin oxide coated TiO_2 removed the acid orange 7 much faster than the untreated material. It was speculated that the coupling effect between the titanium dioxide and the tin oxide coating lead to a decreased rate of electron-hole recombination and thus higher overall catalytic activity.

CHAPTER 3

EXPERIMENTAL METHODS

3.1 Formation of TiO_2 Coating

Standard P25 TiO_2, which has an anatase to rutile ratio of 80:20, was obtained from Aeroxide. The physical properties of TiO_2 nanoparticles, obtained from the manufacturer, are as follows: average surface area of 50 ± 15 m^2/g, primary particle size around 21 nm, and purity above 97% (Evonik Industries, 2011). Adapting a procedure employed by McLintock and Ritchie (1965) and Sattler and Liljestrand (2003) in previous work, P25 TiO_2 was coated onto a 2.5 cm x 30 cm glass plate. In this process, 2.0 grams of the nanoparticles were dispersed in 200 mL of deionized water, and the mixture was stirred using a magnetic stirrer for 30 minutes. After stirring was completed, the slurry was poured into a flat bed container. A glass plate was immersed in the TiO_2 slurry and the water allowed to evaporate to dryness. The TiO_2 coating thickness on each plate was approximately 8 microns, as determined by profilometry. The weight of TiO_2 on each plate was 0.16 grams, or 2.19 x 10^{-3} g/cm^2.

3.2 Plasma Deposition of Hexafluoropropylene Oxide

3.2.1 Plasma Polymerization System

The plasma reactor chamber was a cylindrical reactor with 5 cm inner diameter and 46 cm length. The reactor was made of borosilicate glass (Pyrex). The inlet and outlet were connected to hollow shaft cartridge mount Ferrofluidic feedthroughs

(Ferrotec, Model-HS5 00SLXC), which enabled the plasma reactor to rotate freely and continuously under vacuum. A live electrode was located outside and underneath along the length of the reactor, while the ground electrode was placed on top of the reactor.

The RF system consisted of a 300 W RF amplifier (ENI, Model-A300), a pulse generator (Tetronix, Model-2101), a function generator (Wavetek, Model-166), a frequency counter (Hewlett Packard, Model-5315A) and an in-house made capacitance/inductance matching network. Plasma treatments were conducted at the RF frequency of 13.56 MHz. An exhaust valve controller (MKS, Model 252E-1-VPO) monitored the pressure inside the reactor and controlled a butterfly valve (MKS Model 253B-1-40-1) positioned downstream, which was employed to adjust the pressure inside the reactor. The system was evacuated by a mechanical rotary vacuum pump (Leybold, Model D16B). Typically, background pressure was pumped down to 5 mTorr before the monomer was introduced into the plasma reactor to avoid contamination from other molecules. A liquid nitrogen cold trap was placed after plasma reactor and before the vacuum pump to condense unreacted monomer and products that escaped from plasma reactor thus preventing these molecules from flowing into the vacuum pump. A schematic diagram of the plasma reactor is provided in Figure 3.1.

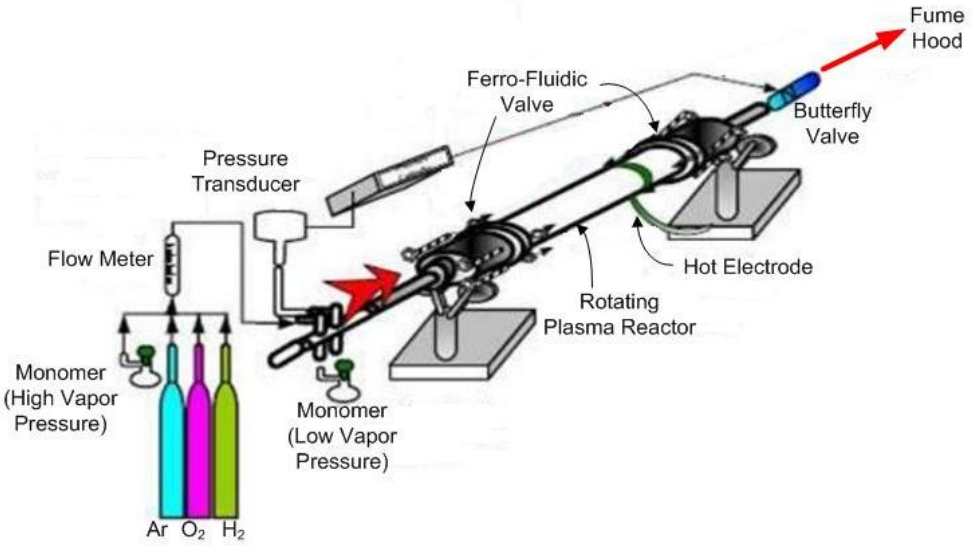

Figure 3.1 Schematic diagram of the plasma reactor system employed for the TiO_2 surface modifcations (Cho, 2005)

.

3.2.2 Plasma Deposition of Hexafluoropropylene Oxide on TiO_2

The plasma deposition technique was applied for either direct fluorination or coating of thin perfluorocarbons film on the TiO_2 particles. The plasma reaction monomer employed in this study was hexafluoropropylene oxide (HFPO, C_3F_6O, 98%, Aldrich). A glass plate, having a layer of TiO_2 nanoparticles, was loaded into the plasma tubular reactor for each treatment process. An oxygen plasma pre-treatment, conducted using a pulsed plasma discharge operated for 10 ms-on/10 ms-off at 150W peak power input, was performed to remove any adventitious carbonaceous material adsorbed on the TiO_2 film. Following evacuation of the oxygen gas, the background pressure was re-adjusted to 5 mTorr. The HFPO was then introduced into the reactor; the HFPO flow rate into the reactor was 50 cm^3/min (STP) and the pressure in the reactor was adjusted to 160 mTorr via use of the butterfly control valve. Based on prior experiments of plasma

treatment of TiO_2 using HPFO monomer from our laboratory (Cho, 2005), direct fluorination of the TiO_2 occurs with high power plasma discharges, whereas perfluorocarbon polymer films are deposited at lower average power inputs. In this research, continuous wave (CW) plasma provided the highest plasma power input employed, while pulsing plasma generated lower average power input. After completion of the plasma deposition, the modified TiO_2 surface was removed from the reactor and subjected to tests for gas-phase photocatalytic activity.

The HFPO plasma deposition conditions employed in this study are summarized in Table 3.1. Prior to all HFPO plasma deposition, TiO_2 samples were subjected to the brief O_2 plasma discharge as noted above.

Table 3.1 Summary of HFPO Plasma Treatment Conditions

Peak Power (Watt)	On-Time/Off-Time (ms/ms)	Pressure (mTorr)	Treatment Time (minutes)
150	Continuous Wave	100	5
150	10/100	160	5
150	10/10	160	5
150	10/10	160	20
150	10/10	160	30
150	10/10	160	60

3.3 Characterization of Plasma Deposited TiO_2

X-ray photoelectron spectroscopy (XPS) was employed to characterize the surface composition of TiO_2 particles as a result of the plasma treatment. XPS spectra were obtained using a Perkin-Elmer PSI 5000 series spectrometer. High resolution spectra of TiO_2 samples, subjected to both high and low power HPFO plasma discharges, were obtained. These included samples exposed to pulsed plasmas of 10/100 and 10/10 ms on/off ratios, as well as continuous wave (CW) discharges, all carried out at peak power input of 150W.

Ultraviolet-visible diffuse reflectance spectra of untreated and modified catalysts were measured by UV-VIS spectrophotometer (Perkin-Elmer, model Lambda 35). Static water contact angles, which provide a good measure of the surface energy of the sample, were measured using a goniometer (Ramé-Hart, model 100-00-115).

3.4 Evaluation of Photocatalytic Activity

3.4.1 Photocatalytic Oxidation Reactor

The photocatalytic activities of the untreated and modified TiO_2 were tested under UV light irradiation at ambient temperature in a batch reactor with closed loop constant gas circulation. A cylindrical glass tube, 2.6 cm inner diameter and 30 cm length, placed horizontally, served as the photocatalytic oxidation reaction chamber. Two 366-nm UV lamps (Osram Black Light Blue, model F15T8BLB, 15 W), located 4.3 cm above the photocatalyst, were used as the UV light source in this study. The UV intensity was 3.72 mW/cm^2, as measured by UV radiometer (UVX Radiometer, model UVX-36) and was maintained constantly throughout the experiments. The intensity was verified before

starting each photocatalytic oxidation (PCO) reaction. A peristaltic pump (Masterflex, L/S Variable-Speed Console Drives with EW-77200-62 pump head) provided gas circulation inside the reactor through a 0.25 inch Viton tube. The air circulation in the reactor was maintained at a flow rate of 200 cm^3/min. The global volume of the reactor was 275 cm^3. The schematic diagram of photocatalytic oxidation reactor is shown in Figure 3.2.

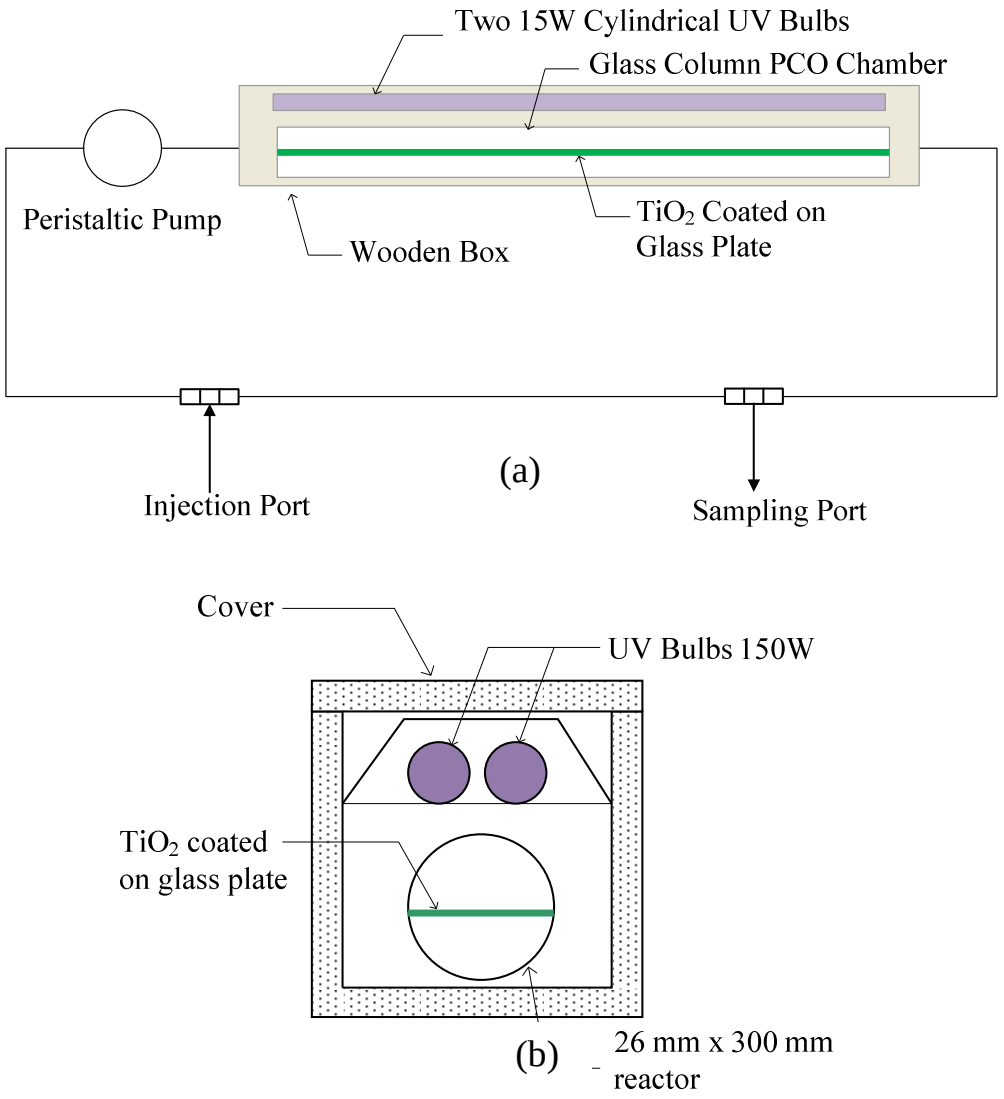

Figure 3.2 Details of photocatalytic oxidation reactor (a) schematic diagram (b) cross-section of the reactor.

3.4.2 Photocatalytic Oxidation of m-Xylene

A mixture of the analyte (m-xylene) in air was cycled continuously over the catalyst and the xylene concentration monitored as a function of reaction time. The coated glass plates, having either untreated or surface modified TiO_2, were placed inside the PCO chamber. Liquid m-xylene (C_8H_{10}, 99+%, Acros Organics) was introduced into

the reactor through an injection port using a microsyringe. The m-xylene was allowed to vaporize and reach equilibrium in the reactor before UV light irradiation. Air was circulated in the loop to stabilize the m-xylene concentration in the dark for 60 minutes before the two UV lamps were turned on to initiate the PCO reaction. All experiments were conducted at ambient temperature of 74±1 °F. It was observed that illumination of the TiO_2 sample resulted in a slight gradual increase in temperature of the catalyst during the reaction which amounted to approximately 7 $^{\circ}$C above room temperature. The slight temperature increase observed was the same for both treated and untreated TiO_2. The relative humidity was maintained essentially constant throughout the course of the experiments, ranging from relative humidity values of 47 to 52%, as monitored with a humidity sensor (Testo Model 605-H2).

The initial concentration of m-xylene employed in each catalytic run was approximately 1000 ppm before initiation of the PCO reaction. Gas samples were periodically withdrawn from the reactor through the sampling port, using a gas-tight syringe, and directly injected into the gas chromatography.

3.4.3 Measurement of m-Xylene Concentration

The concentration of m-xylene in the gas stream was analyzed, as a function of reaction time, using a gas chromatograph (GC) with flame ionization detector (FID) (SRI Instruments, model-8610C), equipped with a capillary column (Restek, RTX-1, 30 m, 0.53 mm i.d.). The GC was set to analyze m-xylene in terms of peak area by the iso-temperature method in which the oven temperature was maintained constant at 70 °C. A calibration curve of FID response as a function of xylene concentration was obtained

using standard known amounts in m-xylene in air. Liquid m-xylene was injected into known volume Tedlar bags to produce different known m-xylene gaseous concentrations. After m-xylene was completely evaporated, the gas samples were injected to the GC to create the calibration curve, which is shown in Figure 3.3. The calibration curve was verified for its accuracy by injecting standard concentration m-xylene gas (200 ppm, Matheson Tri-Gas) into the GC and converting the measured peak area into corresponding concentration; the concentration from the calibration was 208 ppm compared to 200 ppm of standard concentration. This calibration curve was then employed to obtain the amount of m-xylene remaining unreacted as a function of reaction times during the photocatalytic runs.

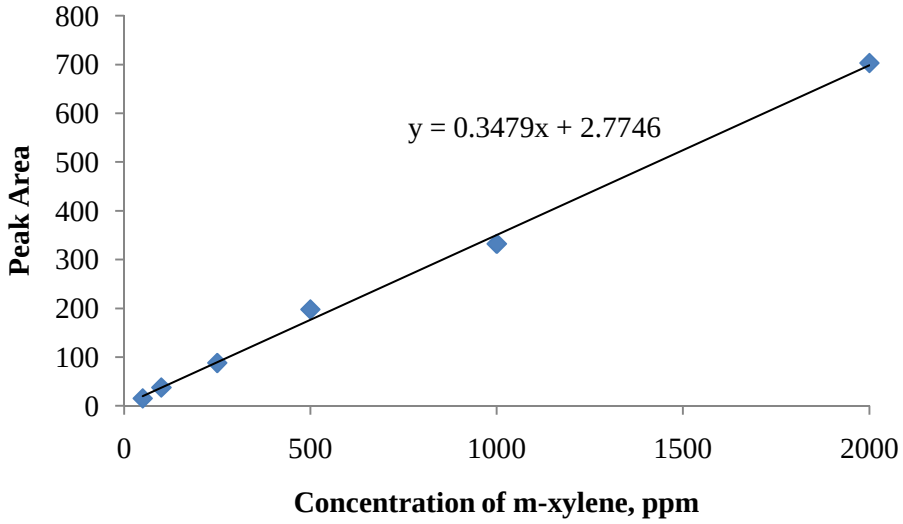

Figure 3.3 Calibration curve of m-xylene concentrations versus peak area

3.4.4 Adsorption of m-Xylene on Plasma Modified TiO_2 Particles

Experiments were carried out to quantify the effect of plasma surface modification on the direct adsorption of m-xylene compared to that on untreated TiO_2. In these experiments, identical amounts of xylene, 1000 ppm, were injected into the catalytic reactor containing identical amounts of either treated or untreated TiO_2. The air/xylene mixture was circulated continuously over the catalytic bed, without any light illumination, with aliquot samples withdrawn every 10 minutes for GC analysis. This process was continued until a steady state value was obtained for the xylene concentration. The time required to reach the steady was approximately 60 minutes. The relative humidity inside the photocatalytic reactor was set constantly at 0% in all runs.

3.4.5 Photocatalytic Oxidation of Acetaldehyde

The evaluation of photocatalytic oxidation of acetaldehyde was conducted in the same procedure as employed in the m-xylene experiments. Liquid acetaldehyde (C_2H_4O, 99.5%+ ACS Reagent, Sigma-Aldrich) was injected through the injection port. The initial concentration of acetaldehyde was 1000 ppm. The acetaldehyde was allowed to vaporize and reach equilibrium in the reactor before UV light was turned on to initiate the reaction. The unreacted acetaldehyde was measured by withdrawing air samples through sampling port using gas-tight syringe and injected to the GC. The concentration of acetaldehyde was monitored as a function of reaction time.

3.4.6 Photocatalytic Oxidation of Elemental Mercury

Figure 3.4 is a schematic diagram of the system employed to study the photocatalytic oxidation of elemental mercury (Hg^0). The cylinder of compressed air

(80% N_2, 20% O_2, Matheson Tri-gas) was divided into two separate lines, with the air flow rates controlled by mass flow controller (Omega Model FMA5518). The total flow rate was kept constant at 2 L/min. One air stream was passed over the surface of liquid elemental mercury (Hg^0, ≥ 99.99% trace metal basis, Sigma-Aldrich) to produce Hg0 saturated air. The vapor pressure of the Hg^0 was maintained constant by placing the liquid Hg^0 in an ice water bath. The second air stream was employed to dilute (adjust) Hg^0 concentration to 500 $\mu g/m^3$. The Hg^0 concentration was measured using an Hg analyzer (Ohio Lumex, Model RA-915+) directly connected to a microprocessor for data logging. The relative humidity inside PCO reactor was kept constantly at 0%. The photocatalyst employed was either untreated or directly fluorinated TiO_2 as prepared using a CW plasma discharge of the HFPO monomer. In each experiment, Hg^0 laden air was circulated through PCO reactor in the dark for 60 minutes to equilibrate Hg^0 concentration. Subsequently, the UV lamps were turned on and Hg^0 concentrations were recorded as a function of UV irradiation time.

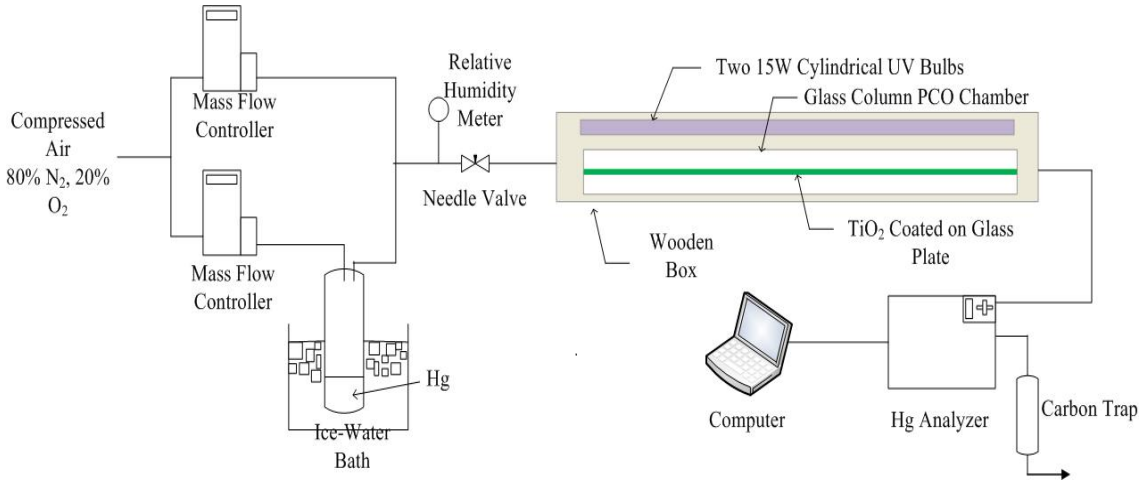

Figure 3.4 Schematic diagram of photocatalytic oxidation of elemental mercury

3.5 Effect of Relative Humidity on Photocatalytic Oxidation of m-Xylene

The investigation of the effects of water vapor on photocatalytic activity of m-xylene was conducted under relative humidities ranging from 0 - 80%. The specific relative humidity values employed were 0, 10, 25, 40, 60 and 80%. The relative humidity experimental set-up is shown in Figure 3.5. One stream of compressed air gas (80% N_2, 20% O_2, Matheson Tri-gas) was passed through a humidifier to produce water saturated air. A second dry air stream served as the balancing air to adjust relative humidity to a desired value. Dry air and humidified air flow rates were controlled by mass flow controllers (Omega Model FMA5518). The relative humidity was monitored using a relative humidity meter (Testo Model 605-H2) inserted into a Viton tube. The adjusted humidity air was purged throughout the system for 60 minutes to ensure that the relative humidity in the system was at the required level. Subsequently, the continuous gas supply was terminated and the PCO reactor was operated in a closed-loop mode. Liquid m-xylene was injected to PCO reactor and circulated in the dark for 60 minutes. Initial m-

xylene concentrations for all experiments were approximately 1000 ppm. Fluorinated TiO_2, treated by CW plasma for 5 minutes, and untreated TiO_2 were used in this study.

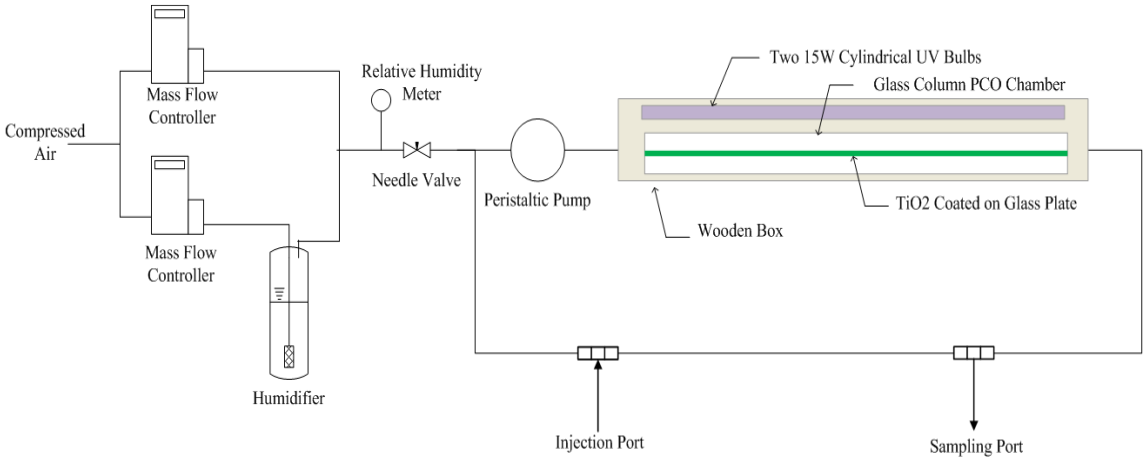

Figure 3.5 Schematic diagram of photocatalytic oxidation reactor to investigate the effects of relative humidity

3.6 Deactivation and Regeneration of HFPO Plasma Treated TiO_2

The deactivation of the photocatalyst was tested on fluorinated TiO_2 which had been treated by HFPO CW plasma for 5 minutes. The sample had been used in photocatalytic oxidation of m-xylene for 4 consecutive runs without any treatment between runs. In each run, the conditions of experiments were identical, and the initial concentration of m-xylene was 1000 ppm. The remaining m-xylene was monitored with reaction time by GC. After the end of the fourth run, the catalyst was treated by oxygen plasma as the regeneration method to recover the photocatalytic reactivity. The oxygen plasma treatment was conducted as 10 ms_on/10 ms_off pulsing at peak power of 150 W and pressure of 160 mTorr. The first oxygen treatment was applied for 3 minutes. After

oxygen treatment, the photocatalyst was employed in photocatalytic oxidation of m-xylene again to examine its reactivity after 3 minutes regeneration. Another regeneration process was done by the same plasma treatment settings but with a longer treatment time of 10 minutes. The regenerated photocatalysts were then tested in m-xylene degradation to determine the recovery of its photoreactivity.

CHAPTER 4

RESULTS AND DISCUSSION

4.1 Characterization of Hexafluoropropylene Oxide Plasma Treated TiO_2

The hexafluoropropylene oxide (HFPO) plasma treated TiO_2 were characterized using profilometry, XPS analysis, UV-Vis absorption and water contact angle measurements.

4.1.1 HFPO Plasma Film Deposition Rate

The deposition rates of the film produced under plasma on/off time (in ms) of 10/10 and 10/100 were determined by the ratio of film thickness to plasma deposition time. The ratios are expressed in Table 4.1.

Table 4.1 HFPO Plasma Film Thicknesses and Deposition Rates

Plasma on/off time, ms	Deposition Time (min)	Film Thickness (Å)	Deposition Rate (Å/min)
10/10	20	40	2
10/100	20	140	70

The plasma deposition by CW mode did not form thin polymer film on the substrate but instead created chemical bonds between F and Ti. As a result, the film thickness and deposition rate are not relevant for those runs.

4.1.2 XPS Characterization of Plasma Treated TiO_2

4.1.2.1 XPS Analysis of Oxygen Plasma Treated TiO_2

Preliminary treatment of the TiO_2 catalyst involved exposure to an oxygen plasma in an attempt to reduce the carbonaceous surface content of the raw material. Results from other laboratories had reported C atom content of 16.7 atom% (Yamashita et al., 2004) and 30.7 atom% (Lenk et al., 1994). The carbon surface contamination is believed to arise from the manufacturing processes and, additionally, by simple adsorption of hydrocarbons from the atmosphere. The oxygen plasma was operated under pulsed conditions of 10 ms on/10 ms off for a period of 10 minutes at a peak power input of 150W. Subsequently, XPS analyses were carried out on both the treated and untreated particles.

XPS survey spectra of untreated and O_2 plasma treated samples are shown in Figure 4.1. In both cases, the survey spectra reveal the presence of titanium, oxygen and carbon atoms. However, a comparison of the untreated and plasma treated TiO_2 reveals a sharp reduction in the C atom surface content from 23.5% to 10.6% The high resolution C(1s) XPS spectrum of the oxygen treated samples reveals the presence of a major component at 284.6 eV and two smaller subpeaks at 286 and 288.1 eV. The assignment of these peaks are graphitic (C-C) or hydrocarbons (C-H) at 284.6 eV, C-O at 286.0 eV and O-C=O at 288.1 eV (Cho, 2005, Yupeng and Chunxu, 2011). The presence of C-O and O-C=O is presumably caused by oxidation of graphitic carbon by oxygen plasma.

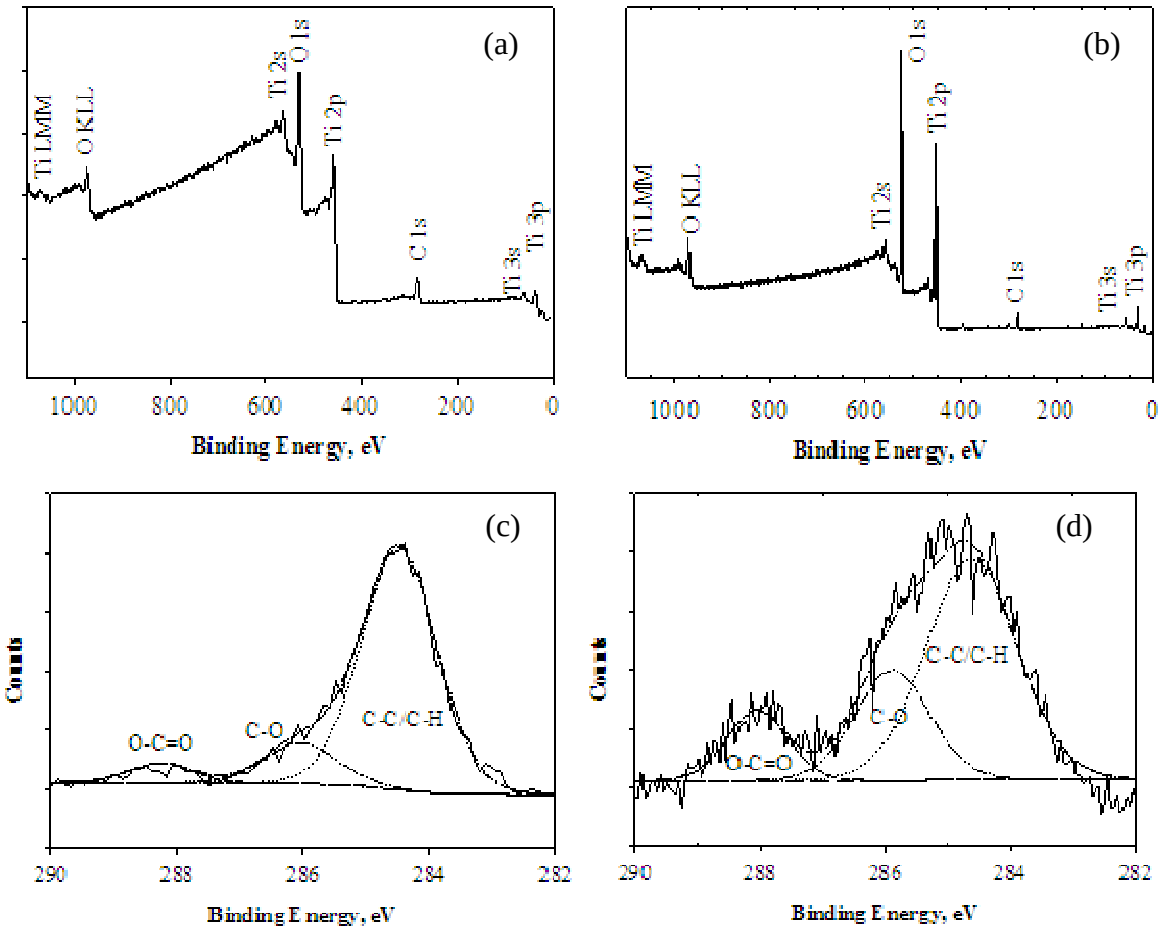

Figure 4.1 XPS spectra of oxygen plasma treated TiO_2 (a) survey scan: raw TiO_2 (b) survey scan: O_2 treated TiO_2 (c) C(1s) high resolution: raw TiO_2 (d) C(1s) high resolution: O_2 treated TiO_2. The treatment was conducted at 10 ms_on/10 ms_off at 150W for 10 minutes

4.1.2.2 XPS Analysis of HFPO Plasma Treated TiO_2

TiO_2 samples, initially treated with oxygen plasma, were subsequently exposed to HFPO plasma discharges. The initial HFPO treatments were conducted using a 10 ms-on/ 10 ms-off duty cycle at a peak power of 150W. To investigate the effect of plasma deposition time, the TiO_2 nanoparticles were treated for periods of 5, 20, 30 and 60

minutes. XPS spectra, shown in Figure 4.2 and Figure 4.3, reveal the dramatic change in TiO_2 surface chemistry following the HFPO plasma exposures. As shown in Figure 4.2, the intensity of the F(1s) and C(1s) peaks, relative to those of O(1s) and Ti(2p) peaks, increase progressively with treatment time. In fact, it is important to note, no photoelectrons are observed from the O and Ti atoms for the sample which was treated for 60 minutes, as shown in Figure 4.2(d). This result clearly indicates that the thickness of the plasma deposited film from this long duration run is sufficiently thick to prevent either the penetration of the X-Rays to the actual TiO_2 surface and/or the subsequent photoelectrons emitted cannot escape from the polymer film.

High resolution C(1s) and F(1s) XPS spectra of TiO_2, as modified with plasma pulsing of 10 ms_on/10 ms_off, after treatment times of 5, 20, 30, and 60 minutes, are arranged from top to bottom in Figure 4.3. The C(1s) spectra reveals fluorocarbon peaks, including CF_3- (294 eV), CF_2- (292 eV), C-F (289 eV) and C-CF_x (287 eV) functional groups (Beamson and Briggs, 1992). In addition, the small peak at 285 eV represents carbons that are not closely bound to fluorine. The relative increase in intensity of CF_2 peaks at 292 eV in Figure 4.3(c) and Figure 4.3(d) with the longer treatment times is an indication of the presence of higher amounts of perfluorocarbon polymer plasma deposited on the TiO_2 particles.

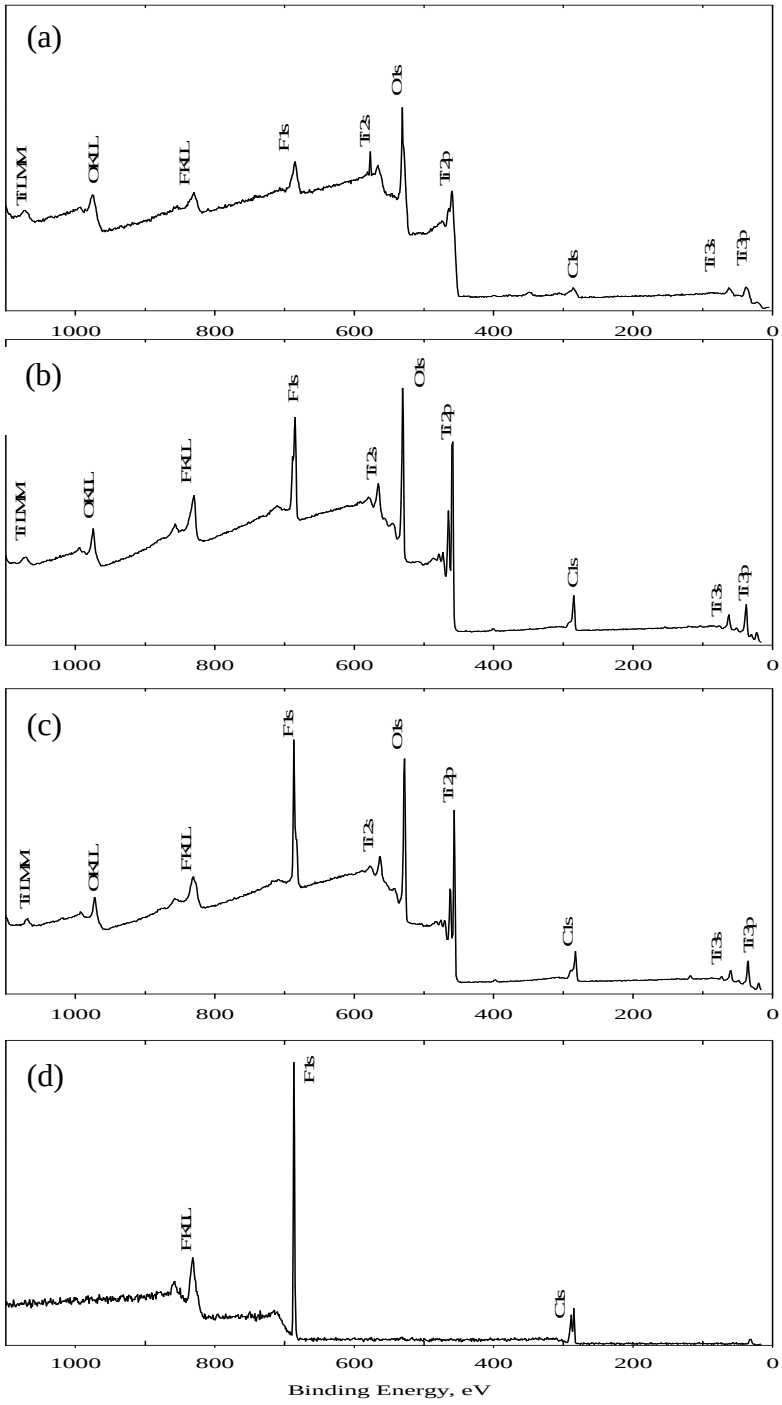

Figure 4.2 XPS survey scan of HFPO plasma coated TiO_2 nanoparticles as a function of deposition times. Plasma deposition was conducted with 10 ms-on/ 10 ms-off duty cycle at 150W peak power (a): 5 minutes, (b): 20 minutes, (c): 30 minutes and (d): 60 minutes

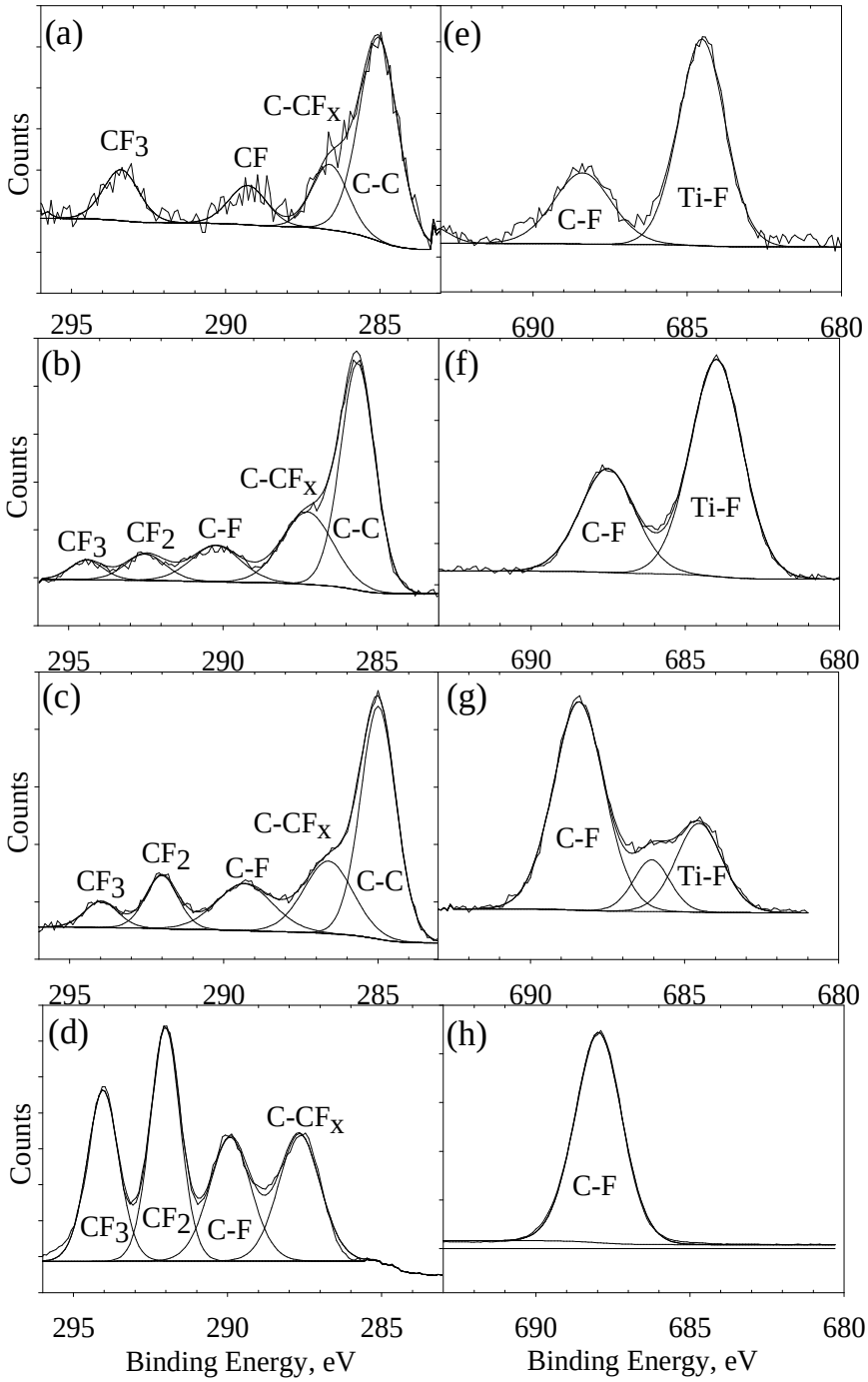

Figure 4.3 High resolution XPS spectra of C(1s): (a) – (d): and F(1s): (e) – (h): of plasma treated TiO_2 at duty cycle of 10 ms_on/10 ms_offfor 5, 20, 30 and 60 minutes, respectively.

The F(1s) XPS spectra, on the right panel of Figure 4.3 (e, f, g and h), clearly indicate a progressive change in the nature of the surface fluorine on the TiO_2 particles with increasing plasma treatment times. Specifically, Ti-F (684.5 eV) was the major fluorine species in the samples treated for 5 and 20 minutes, Figure 4.3(e) and (f). Integration of the two peaks in these figures reveal that the fluorine atom content was present as Ti-F at 70.1 and 66.4% for the samples treated for 5 and 20 minutes, respectively, with the remaining fluorine being present as C-F bonds (binding energy 688.2 eV). However, the fluorine atom XPS spectra are very different for the samples treated for longer times. As shown in Figure 4.3(g) and (h), the catalyst exposed to the plasma for 30 minutes was dominated by fluorine bonds present as perfluorocarbon (67.5%), while the sample treated for 60 minutes reveals only the presence of C-F bonds, as a single F(1s) peak, at 688.2 eV. As indicated by these data, it appears that during the initial plasma treatment period, Ti-F formation dominates, but at the same time some perfluorocarbon is being deposited. As the treatment time increases, the particles are increasingly covered with the perfluorocarbon film, thus obscuring the initially formed Ti-F bonds. Also, one notes that the change of surface chemistry is dependent on plasma treatment times in that only a smaller change in the C(1s) spectrum is observed between Figure 4.3(b) and (c), which corresponds to the shortest plasma treatment time difference among the four samples. However, even during this relatively short time difference, it is noted that the C(1s) changes observed reveal an increase in total CF_x surface functionalities, which is in accord with the overall trend in surface chemistry change from direct TiO_2 fluorination to fluorocarbon coating.

A significantly more dramatic change was observed in contrasting the relative areas of F(1s) photoelectrons between the 20 minutes and 30 minutes runs, as shown in Figure 4.3(f) and (g). This large difference can be attributed to the fact that the increasing fluorocarbon film thickness results in a rapid decrease in the ability to generate photoelectrons from fluorine atoms from the underlying Ti-F functionalities. In connection with this observation, we note that based on film deposition rates during runs carried out under 10/10 ms on/off times, the film thicknesses are 4 and 6 nm for deposition times of 20 and 30 minutes, respectively. The film thickness varies linearly with deposition time under pulsed plasma conditions. Under the XPS conditions employed, using a 75 degree take-off angle, we have previously observed that the X-Ray penetration depth is approximately 5.5 to 6.0 nm. Thus, a particularly sharp decrease in photoelectron emission from Ti-F functionalities would be expected in comparing the relative F atom peak areas, as observed in this study [Figure 4.3(f) and (g)]. Also, the complete disappearance of photoelectrons from the Ti-F functionality is in accord with expectations in that the film thickness after 60 minute deposition time is 12 nm.

The XPS analysis indicates that surface percent of fluorine species increases with increasing treatment time. For example, with a plasma duty cycle of 10 ms_on/10 ms_off, the atom percent of fluorine increased gradually from 10.3% to 25.3% and 43.0% as the plasma treatment times were increased from 5 to 20 and 30 minutes, respectively. The maximum fluorine of 76.7 atom % was observed in the sample treated under the plasma duty cycle of 10 ms_on/10 ms_off for one hour. Also, the percent carbon atoms show a steady increase with increasing deposition times under the duty cycle of 10 ms_on/10

ms_off. In contrast, both the titanium and oxygen atom percents decrease with plasma treatment time, becoming undetectable and 0.7 atom %, respectively, after the 60 minute treatment time. Overall, these data are consistent with a progressively thicker perfluorocarbon film being deposited on the particles, with the film thickness ultimately exceeding the depth of penetration of the X-ray photons from the XPS source. TiO_2 samples which were treated by duty cycle of 10 ms_on/100 ms_off and CW for only 5 minutes had fluorine content of 54.2% and 44.9%, respectively.

The nature of the surface modifications of TiO_2 produced using pulsed 10 ms_on/100 ms_off discharges, as well as CW operational mode, were also investigated. Dramatic differences in surface chemistry were observed in contrasting the XPS spectra obtained for these two different treatments, as shown in Figure 4.4. These differences are noted both for the C(1s) and F(1s) photoelectron spectra. As shown in Figure 4.4(a), the 10/100 sample reveals the over whelming presence of C-F bonds, whereas the CW sample reveals the dominant presence of C atoms not directly bonded to fluorine (Figure 4.4(b)). In accord with the C(1s) spectra, the F(1s) XPS spectrum of the 10/100 sample, Figure 4.4(c), reveals only a single peak of C-F bonds at 688.2 eV, and no presence of Ti-F. In sharp contrast at the highest plasma power input, namely under CW conditions, the contributions of C-F groups is minimal and the only significant fluorine present is in the form of Ti-F, as shown in Figure 4.4(d). Thus, in accord with prior work on HFPO plasma polymerization (Savage et al., 1991), no polymer films are deposited under high power input conditions. Also noted is the fact that the perfluorocarbon films obtained in the presence study, particularly the CF_2 functionality, differ slightly from those

previously published. This difference reflects the fact that the peak power input in the present study of 150 W is significantly lower than the value of 250 W employed in the prior work (Savage et al., 1991).

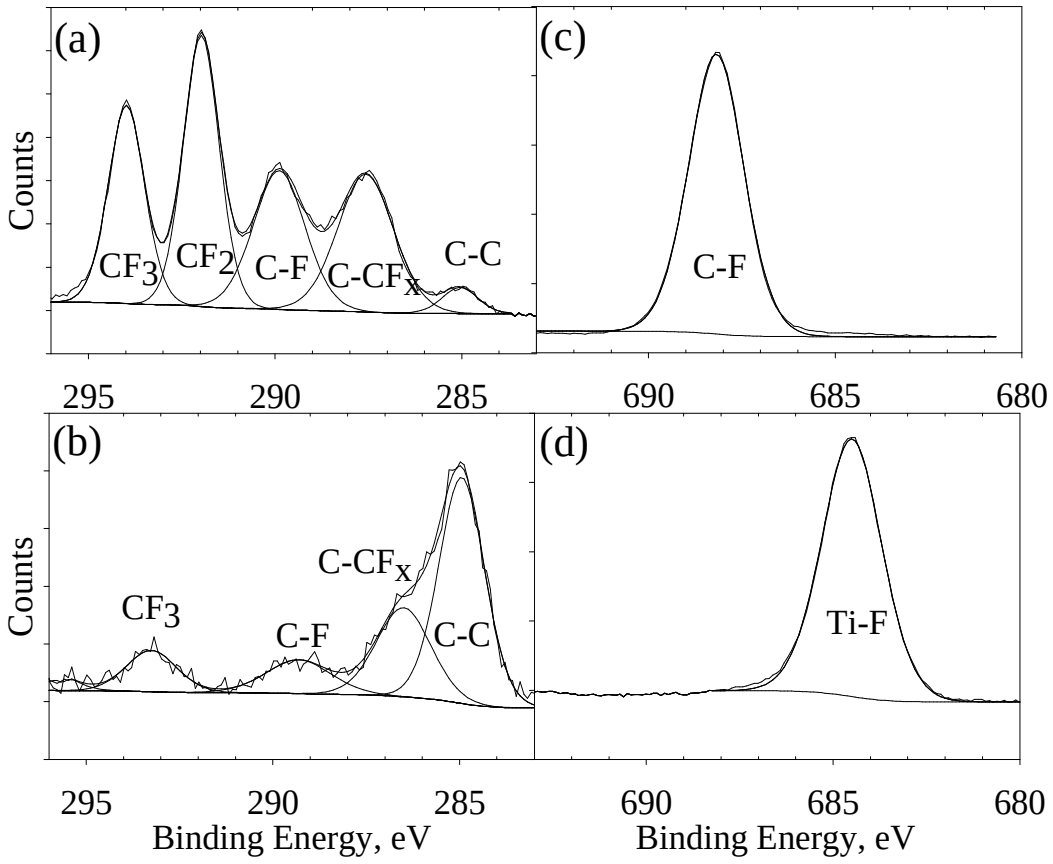

Figure 4.4 High resolution XPS spectra of C(1s): (a) and (b): and F(1s): (c) and (d): of plasma treated TiO2 for 5 minutes in different duty cycles:10 ms_on/100 ms_off and CW, respectively.

The detailed information on the surface composition of the HFPO plasma treated particles obtained from the XPS studies is provided in Table 4.2.

Table 4.2 Chemical Composition of HFPO Plasma Treated TiO_2. The deposition was carried out with 10 ms_on/10 ms_off for 5, 20, 30 and 60 minutes, 10 ms_on/100 ms_off for 5 minutes and CW for 5 minutes

Plasma on/off, ms	Treatment Time, min	Composition			
		C, %	F, %	O, %	Ti, %
10/10	5	10.6	10.3	45.4	33.7
10/10	20	12.1	25.3	39.1	23.5
10/10	30	13.6	43.0	35.3	8.1
10/10	60	22.6	76.7	0.7	ND*
10/100	5	20.1	54.2	9.2	16.5
CW	5	14.5	44.9	22.3	18.3

*ND = Non-detectable

The relative content of C-F and Ti-F fluorine produced under the various plasma conditions employed is summarized in Table 4.3. Under 10 ms_on/10 ms_off condition, the ratio of C-F to Ti-F functionalities varies strongly with the deposition time employed, as shown in this table with the percent C-F groups ranging from ~30% to 100% as the deposition time is increased from 5 to 60 minutes. No time dependence studies were carried out at the other two plasma conditions employed since only one type of F atom containing functionality was observed, namely only C-F at 10/100 ms on/off and only Ti-F under CW conditions.

In summation, these XPS data document the deposition of two distinctly different types of fluorine surface atoms, dependent on the plasma duty cycles employed.

Specifically, higher power depositions result in F atoms covalently bonded to Ti atoms, denoted here as Ti-F. In contrast, lower energy conditions favor deposition of polymeric perfluorocarbon films in which the F atoms are covalently bonded to carbon atoms, denoted as C-F.. Under intermediate power input (10/10 ms) both types of F atom depositions occur, however the Ti-F bonds initially formed are ultimately covered by the perfluorocarbon film.

Table 4.3 Percent of Perfluorocarbon (C-F) and Fluorination (Ti-F) on the TiO_2 Treated with Plasma 10 ms_on/10 ms_off (5, 10, 20, and 60 minutes), 10 ms_on/100 ms_off (5 minutes) and CW (5 minutes)

On time/Off time, ms	Treatment Time, min	Fluorine as	
		Fluorination (Ti-F), %	Perfluorocarbon (C-F), %
10/10	5	70.1	29.9
10/10	10	66.4	33.6
10/10	30	32.5	67.5
10/10	60	0	100
10/100	5	0	100
CW	5	100	0

4.1.3 UV-Vis Spectroscopy of HFPO Plasma Treated TiO_2

The effect of the plasma treatments on the UV-visible absorption spectrum of TiO_2 was investigated using surface reflectance spectroscopy. Figure 4.5 shows the absorbance spectra at wavelength of 250 – 800 nm of untreated and plasma modified catalysts. The absorption of 10 ms_on/100 ms_off (fluorocarbon coating) and CW (fluorinated) samples do not show shifting of the fundamental absorption edge of TiO_2. This result is consistent with several other studies, employing various doping techniques, which report that F-doping did not change the optical absorption properties, particularly not narrowing the band gap of TiO_2 (Czoska et al., 2008, Li et al., 2005, Yu et al., 2009). For example, Czoska et al.(2008) used a sol-gel process as the doping method for TiO_2 powder and observed no shifting in the absorption edge or response to visible of the F-TiO_2 compared with untreated TiO_2. The hydrothermal technique was employed to fluorinate TiO_2 at 150°C by Ye et.al. (2009), the UV-Vis absorption edge of the catalyst was not shifted. Li et al. (2005), employing a spray pyrolysis technique to fluorine dope TiO_2, reported that the optical property of doped material was also unchanged. However, in contrast with the results of this study and those of other research cited above, it should be mentioned that some studies have reported a red shift is observed upon F doping of TiO_2 (Lim et al., 2008, Yu et al., 2002). Lim et al.(2008) reported that co-doping of fluorine and carbon/fluorine shifted the absorption edge and decreased band gap energy to 3.05 and 3.07 eV, respectively. Increased light absorption at wavelength shorter than 400 nm was significant in fluorine doped TiO_2 (Yu et al., 2002). Finally, it is noted that Yamaki et al. (2003), in a computational study, investigated the electronic structure of F-

doped TiO_2 and concluded that localized, high density levels appeared below the valence band. He attributed these levels to F(2p) orbitals without any mixing with the valence or conduction band. As a result, these authors conclude that F doping does not contribute to the changes in the optical absorption spectra of TiO_2. Thus, as detailed above, conflicting results remain concerning the effect of F-doping on the absorption spectra of TiO_2. However, as clearly shown in Figure 4.5, the results of the present study do not reveal any significant change in TiO_2 absorption with particles that XPS data (Figure 4.4) clearly document are fluorine doped.

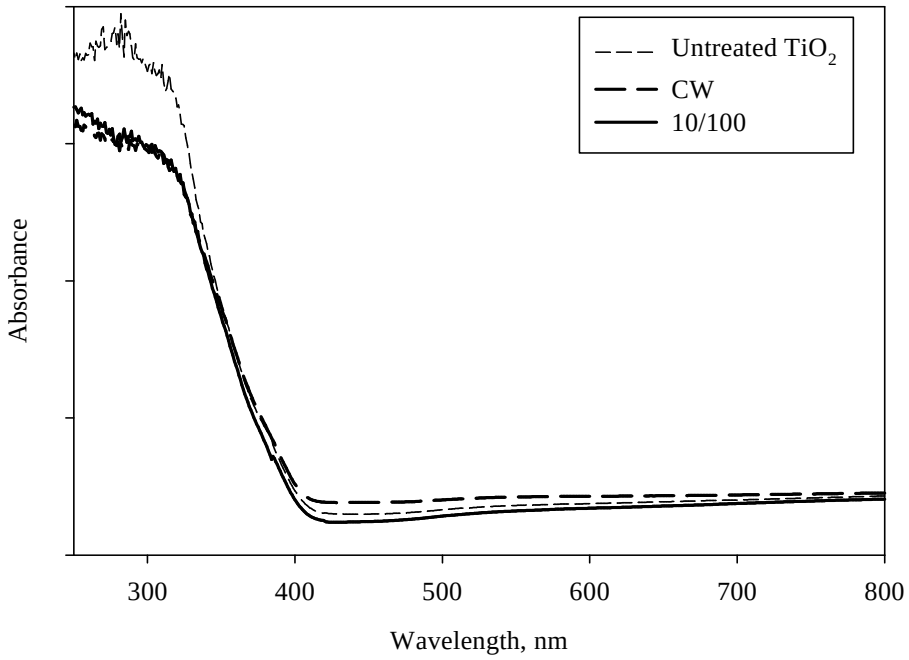

Figure 4.5 UV-Vis absorbance spectra of catalysts. HFPO plasma depositions had been conducted for 5 minutes on CW and 10 ms_on/100 ms_off conditions.

4.1.4 Static Water Contact Angle

Static water contact angles were measured for a number of plasma treated and unmodified TiO_2 samples. The contrast of water contact angle between untreated and plasma modified TiO_2 is illustrated in Figure 4.6 and Table 4.4.

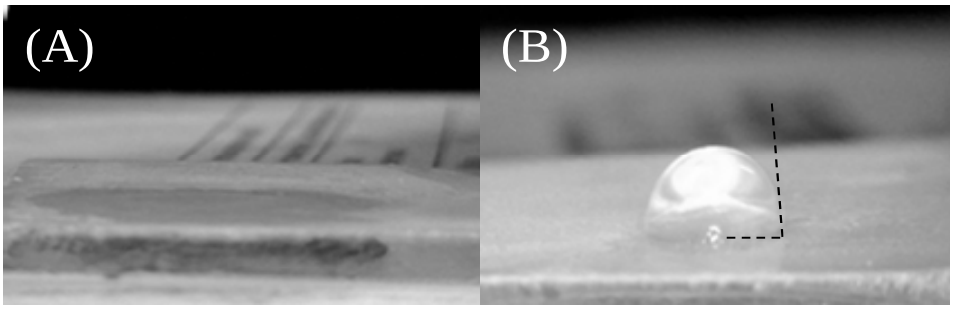

Figure 4.6 Static water contact angle on the TiO_2 coated on glass plate: (A) untreated TiO_2 (B) fluorinated TiO_2 treated by CW plasma at peak power of 150 W for 5 minutes

Table 4.4 Water Contact Angle on TiO_2 Treated with Different Conditions. Plasma depositions were carried out at peak power of 150 W for 5 minutes

Sample	Water Contact Angle, degree
Untreated TiO_2	0 (non measurable)
10 ms_on/100 ms_off	125
10 ms_on/10 ms_off	90
CW	80

As documented by these measurements, the plasma treatments had a profound effect of the wettability of the TiO_2 surfaces in that the TiO_2 particles are converted from hydrophilic to hydrophobic. The untreated TiO_2, containing a high density of surface –OH groups bound to Ti atoms, was completely wettable in that the contact angle of the water droplet was non-measureable. In contrast, the plasma treated samples exhibited very large contact angles and are thus categorized as being hydrophobic. The hydrophobicity is in accord with expectations based on the fluorine content of the treated samples. The higher contact angle, 125°, for the sample treated at the plasma duty cycle of 10 ms_on/100 ms_off is reasonable given the fact that this sample is actually coated with a perfluorocarbon thin film. These results are in accord with those reported by Lim et al. (2008) that TiO_2 co-doped by carbon/fluorine had greater water contact angle than fluorine doped TiO_2. These plasma induced surface energy changes are significant in that the more hydrophobic TiO_2 surfaces will more readily adsorb non-polar compounds, such as m-xylene, while simultaneously minimizing the competitive adsorption of water molecules. This expectation was in fact observed experimentally as described next in this document.

4.2 Adsorption of m-Xylene on Plasma Modified TiO_2 Particles

Experiments were carried out to quantify the effect of plasma surface modification on the direct adsorption of m-xylene compared to that on untreated TiO_2. Figure 4.7 shows the amount of m-xylene adsorbed on the catalysts in 0% of relative humidity environment. The untreated TiO_2 has lower adsorption ability than HFPO plasma treated TiO_2. The adsorption amount of m-xylene on standard TiO_2 is 0.453 mg/g

of catalyst. Larger amounts of xylene, namely 0.529 and 0.552 g/mg, were adsorbed onto perfluorocarbon coated and directly fluorinated TiO_2, respectively. Overall, it was observed that an average of 12±2% increased adsorption of the m-xylene was observed on the plasma treated TiO_2 compared to the untreated materials.

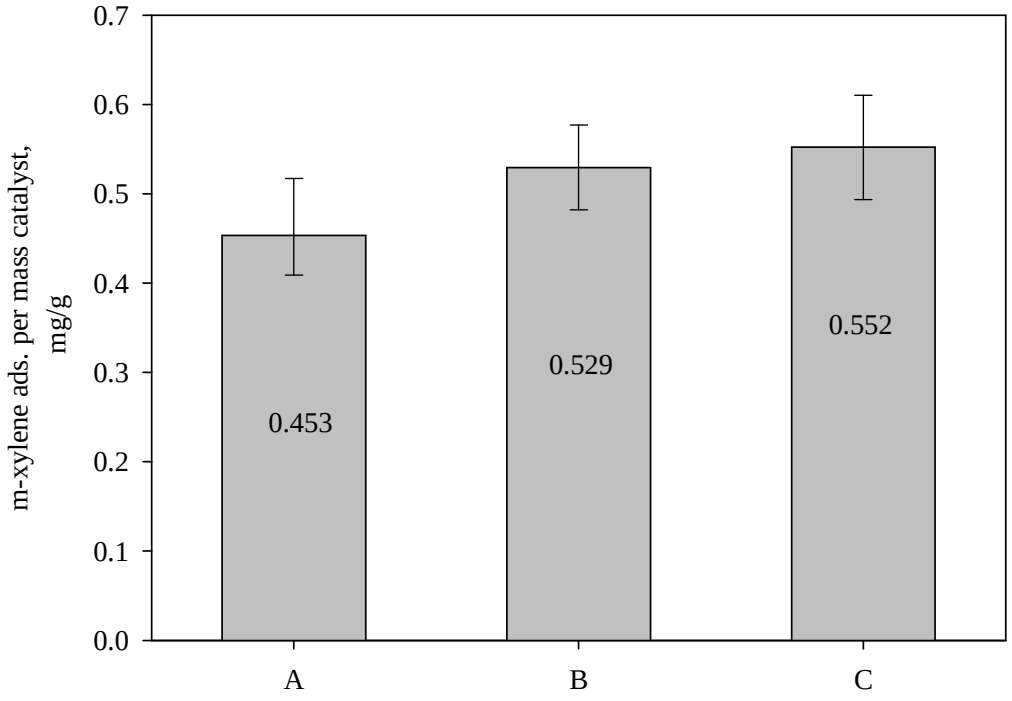

Figure 4.7 Adsorption of m-xylene on (A) untreated TiO_2 (B) 10 ms_on/100 ms_off treated (C) CW plasma treated

4.3 Evaluation of the Photocatalytic Activities of HFPO Plasma Treated and Standard TiO_2

4.3.1 Photodegradation of m-Xylene and its Photocatalytic Oxidation by Standard TiO_2

Initial control experiments were conducted to examine how m-xylene responds to exposure to UV light, with and without TiO_2 present in the reactor. For this purpose, the

concentration of m-xylene was monitored as a function of the irradiation time, all other variables held constant. The ratio of the concentration of xylene remaining to that present before UV light initiation (C/C_0) versus irradiation time is plotted in Figure 4.8. The initial concentration of xylene was 1000 ppm in air, which represents its value after stabilization in the dark for 60 minutes. In the absence of TiO_2, the plot of C/C_0 remains essentially constant, even after 120 minutes of continuous UV radiation, as shown by the top curve in Figure 4.8. This result reveals that no decomposition of the xylene occurs by direct photolysis of the xylene or by any surface promoted route.

However, as shown by the lower curve, the photocatalytic oxidation of m-xylene was observed when TiO_2 was inserted to the reactor. In fact, only 32% of the original xylene remained after 140 minutes of irradiation. The TiO_2 employed in this run was subjected to 10 minutes of O_2 plasma discharge to remove any adventitious carbon adsorbed on the surface.

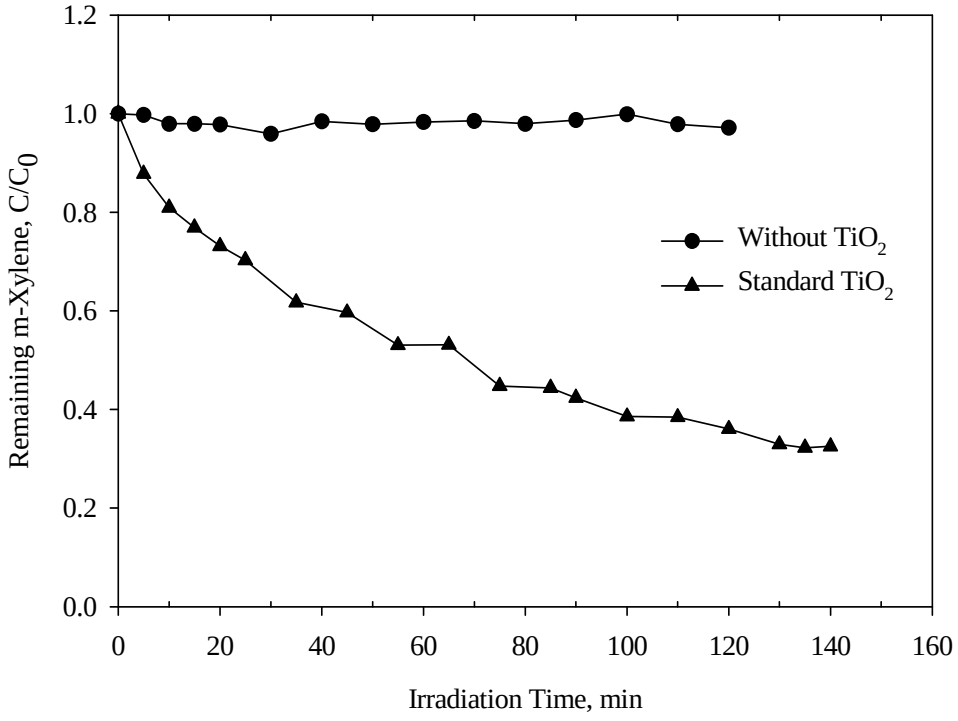

Figure 4.8 The effect of UV irradiation on the concentration of m-xylene and the degradation of m-xylene using TiO_2 that was pre-treated by oxygen plasma as photocatalyst

4.3.2 Photocatalytic Oxidation of m-Xylene by HFPO Treated TiO_2

The photocatalytic oxidation rates of gaseous m-xylene were experimentally determined using both the directly fluorinated and fluorocarbon coated TiO_2 nanoparticles. Non-plasma treated TiO_2 samples, of identical amount as that used for the plasma treated samples, were employed as controls to assess the efficacy of the plasma surface modifications. The measurements were made by monitoring the concentrations of unreacted m-xylene as a function of reaction times.Figure 4.9, the photocatalysed degradation data of m-xylene are presented as a function of the plasma treatment times, under pulsed 10 ms_on/10 ms_off conditions, employed to modify the TiO_2. The curves

shown here represent the remaining m-xylene obtained by joining the successive data points.

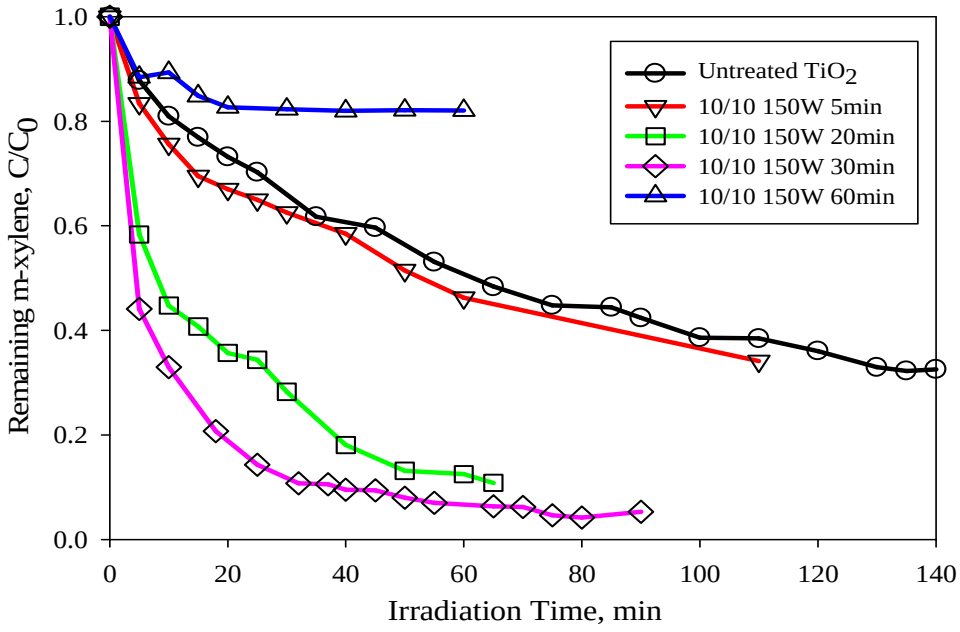

Figure 4.9 Effect of 10 ms_on/10 ms_off pulsed plasma treatment times on photocatalytic oxidation of m-xylene as compared to untreated TiO_2.

As shown in Figure 4.9, the overall catalytic activity of the plasma fluorinated TiO_2 can be much higher than that of the untreated TiO_2. A steady increase in activity of the TiO_2 was observed as the plasma treatment times were progressively increased from 5, to 20, to 30 minutes. However, a much longer plasma treatment time of 60 minutes resulted in a sharp decrease in the TiO_2 oxidation of the xylene. In fact, the oxidation rate observed for the 60 minute sample is extremely low, as shown, being significantly less than that observed for the untreated sample.

Figure 4.10 shows a comparison of the catalytic oxidation rates of m-xylene by the catalysts as a function of the three different plasma treatment processes (10 ms_on/10 ms_off, 10 ms_on/100 ms_off, and CW) employed in modifying the TiO_2. As noted above, the CW plasma results in direct fluorination of TiO_2, whereas use of the relatively low duty cycle pulsed plasma of 10 ms_on/100 ms_off results only in deposition of a perfluorocarbon film on the particles. In contrast, the 10/10 ms on/off runs involve simultaneous direct fluorination and perfluorocarbon film deposition processes. Plasma treatment times for three samples were 5 minutes since it was observed that the optimum PCO activity observed for the CW and 10/100 ms on/off runs occurs after only 5 minutes of plasma treatment. The result of 10 ms_on/100 ms_off treated for 30 minutes is also shown in this figure to compare the best m-xylene oxidations obtained from all three plasma conditions.

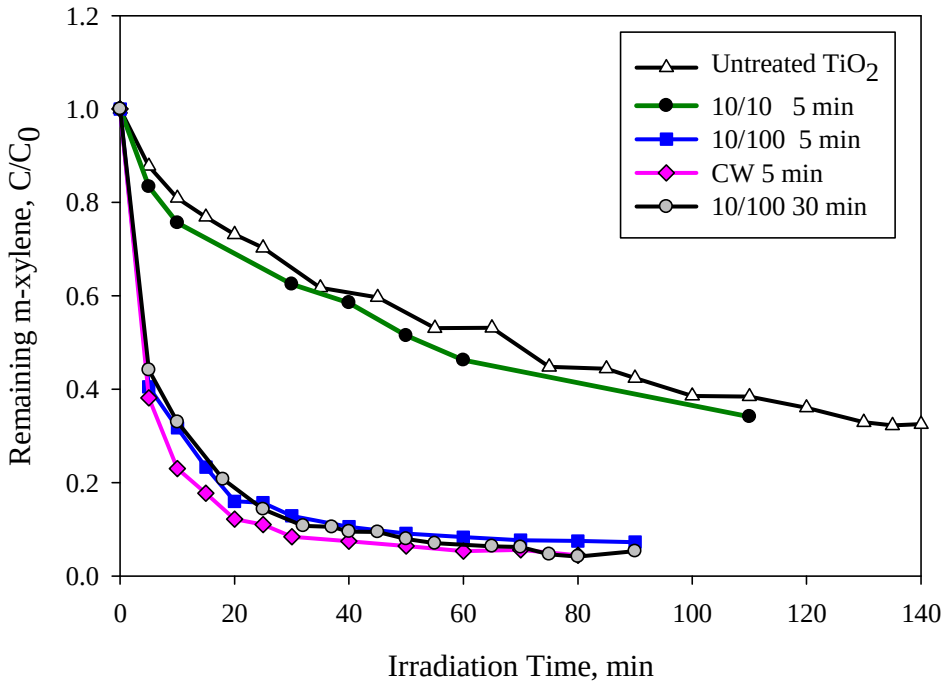

Figure 4.10 Comparison of the photocatalytic oxidation of m-xylene by untreated TiO_2, plasma treated at on/off time of 10/10, 10 /100, and CW for 5 minutes and 10/10 for 30 minutes.

The above result reflects the fact that under CW conditions only the direct fluorination occurs and this apparently occurs to completion in a relatively short time. The time dependence difference between the 10/10 and 10/100 ms on:off treatments is a reflection of the difference in film deposition rates, which was 0.2 nm/min for the 10/10 and 0.7 nm/min for the 10/100 treated samples, respectively. Thus, the perfluorocarbon film thickness reaches its optimum value much faster under the 10/100 condition. In general, both the directly fluorinated and the fluorocarbon coated samples produced dramatically increased photocatalytic oxidation of the m-xylene relative to that observed with untreated TiO_2 over this short time period. However, the 10 ms_on/10 ms_off treated sample, treated for this short 5 minute period, exhibited only a relatively small

improvement of photocatalytic oxidation over that of untreated TiO_2. This latter result suggests that under the 10/10 condition incomplete fluorination and incomplete perfluorocarbon film formation occurs during the short 5 minute deposition time. However, much longer treatment time, 30 minutes, for 10 ms_on/10 ms_off condition is needed to produce comparable m-xylene oxidation to the other two conditions employed for only 5 minutes.

The optimum treatment time of CW condition was observed at 5 minutes. The shorter treatment time of 3 minutes produced less active photocatalyst than that of 5 minutes as shown in Figure 4.11. After plasma treatment times of 10 minutes, the catalytic activity for the CW sample begins to decrease reflecting possible damage to the TiO_2 particles at this high power input condition.

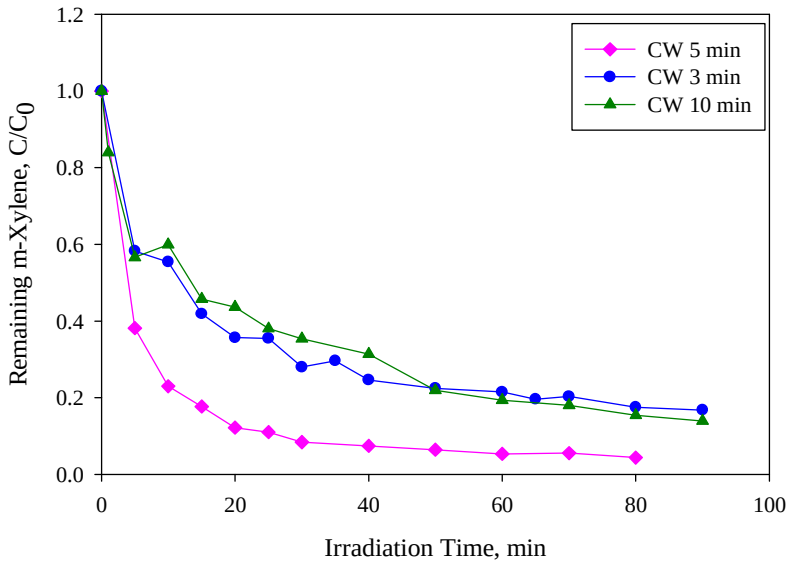

Figure 4.11 Comparison of the photocatalytic oxidation of m-xylene by CW plasma treated TiO_2 for 3, 5 and 10 minutes.

The photocatalytic oxidation rates of the m-xylene were analyzed in terms of reaction order. The best fit of the conversion rates was determined to be first-order in m-xylene for all the samples of TiO_2 employed. The first order decay plots, which reveal R^2 correlation factors ranging from 0.999 to 0.948, are shown in the Figure 4.12 and Table 4.5. The rate constants increase markedly with increasing plasma treatment periods of 5, 20 and 30 minutes for samples subjected to the identical duty cycle of 10 ms_on/10 ms_off. The highest rate constant among samples treated under the pulse plasma 10/10 on to off ratio was 0.0566 min^{-1}, which is a factor of 4.7 times larger than that observed for the untreated TiO_2. However, as shown in Figure 4.12(a), it is also interesting to note that the rate constant of the sample treated for 60 minutes is significantly lower than that of untreated TiO_2.

In terms of rate constant as a function of plasma duty cycle using the same treatment duration in Figure 4.12(b), the highest rate constant, 0.0736 min^{-1}, was obtained for the fluorinated sample treated for 5 minutes under CW conditions. This value is slightly higher than that of the 10/100 (5 minutes treated) and 10/10 (30 minutes treated) samples, 0.0609 and 0.599 min^{-1}, respectively. These values are much larger than that obtained for the untreated TiO_2, which was 0.012 min^{-1}. The rate constant observed for the sample treated for 5 minutes using duty cycle of 10 ms_on/10 ms_off is 0.020 min^{-1}, which is only slightly higher than that for the untreated sample.

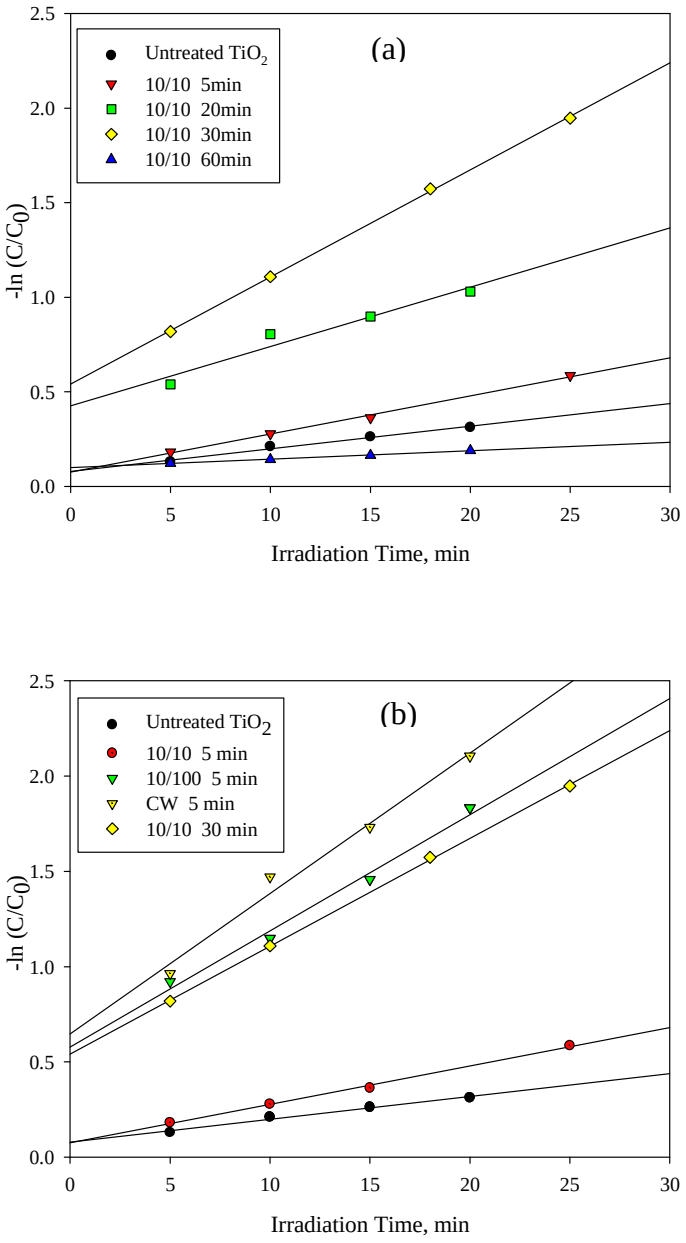

Figure 4.12 First-order plots of initial m-xylene degradation. (a) duty cycle of 10/10 treated for various durations (b) duty cycle of 10/10, 10/100, CW treated for 5 minutes and 10/10 treated for 30 minutes.

Table 4.5 First-Order Rate Constant of m-Xylene Degradation.

Plasma on/off Time, ms/ms	Treatment Time, min	Rate Constant, min^{-1}	R^2
Untreated	0	0.0120	0.984
10/10	5	0.0202	0.995
10/10	20	0.0314	0.948
10/10	30	0.0566	0.999
10/10	60	0.0044	0.997
10/100	5	0.0609	0.988
CW	5	0.0736	0.984

4.3.3 Reproducibility of Photocatalytic Oxidation of m-Xylene by Fluorinated TiO_2

In order to verify that the obtained data from the experiments are reproducible, the repeat tests were conducted to see the variation of the results between runs. The results of photocatalytic oxidation of m-xylene by fluorinated TiO_2 were shown in Figure 4.13. Fluorinated TiO_2 samples were prepared under CW plasma for the duration of 5 minutes. The plots show that two separate experiments gave the same results with marginal variation which is the evidence that the results of these photocatalytic oxidation of m-xylene by TiO_2 are reproducible.

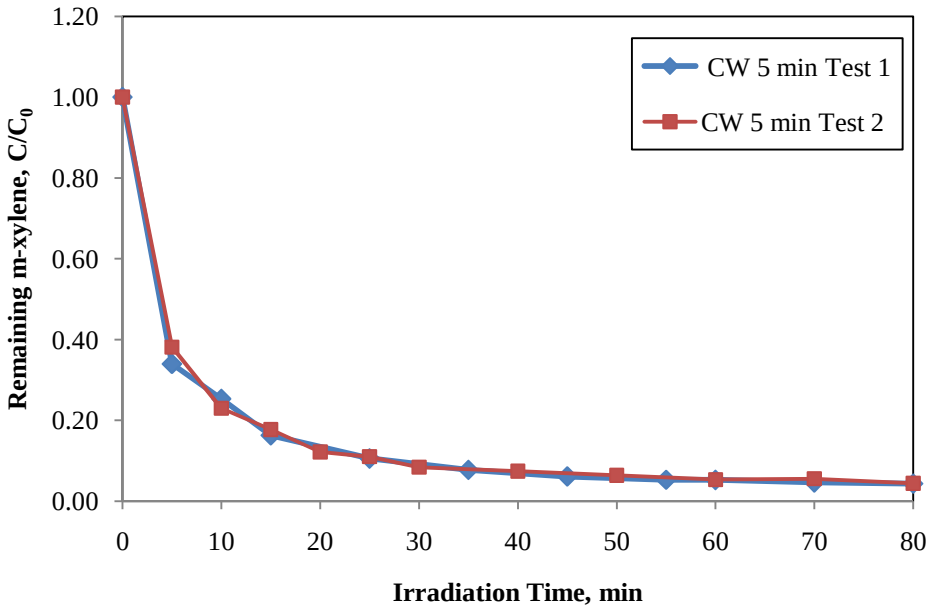

Figure 4.13 Reproducibility of m-xylene photodegradation by fluorinated TiO_2

4.3.4 Photocatalytic Oxidation of Acetaldehyde by HFPO Treated TiO_2

As noted earlier, HFPO plasma treatment transforms TiO_2 surfaces from hydrophilic to hydrophobic, and this transformation was effective in accelerating the photocatalytic oxidation of non-polar m-xylene molecules. Thus, it was felt to be of interest to investigate how effective HFPO plasma modified TiO_2 particles would be in providing photocatalytic oxidation of a non-polar compound. Acetaldehyde (CH_3CHO), a known component in air pollution with respect to contributing to smog formation, was chosen for this purpose. Since acetaldehyde is significantly more easily oxidized than xylene, the emphasis in this study focused on a comparison of oxidation rate of CH_3CHO by treated and untreated TiO_2 particles. For this purpose, the fluorine modified TiO_2

employed was produced using the CW plasma treatment for 5 minutes which produces direct fluorination.

The photo-oxidation results obtained with untreated and fluorinated TiO_2, using the analogous approach as that employed with xylene, are shown in Figure 4.14.

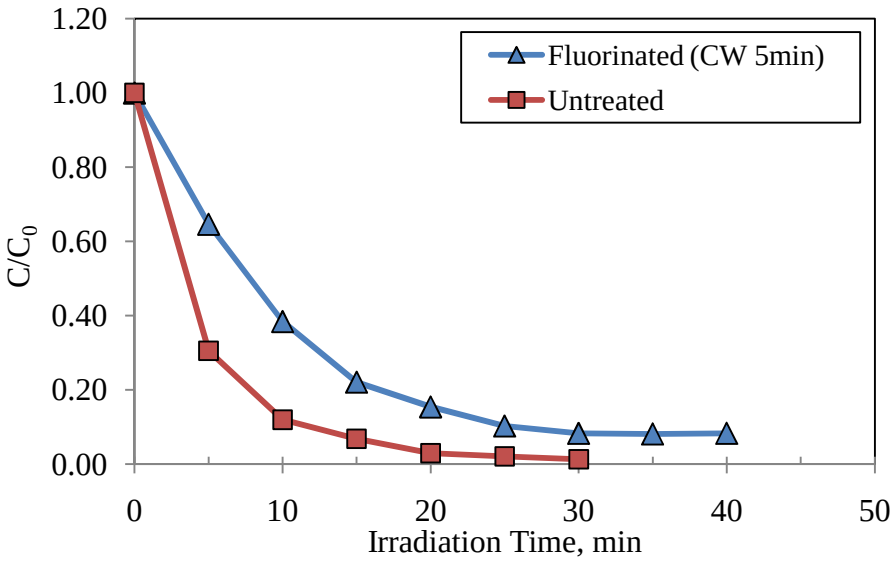

Figure 4.14 Photocatalytic activity of untreated and fluorinated TiO_2 to oxidize acetaldehyde

Interestingly, as shown in this figure, and in sharp contrast with the xylene results, the untreated TiO_2 catalyst exhibited better photocatalytic oxidation activity than the fluorinated samples. For example, 97% of the initial CH_3CHO was consumed within 20 minutes, compared with 85% consumption for the plasma modified catalyst.

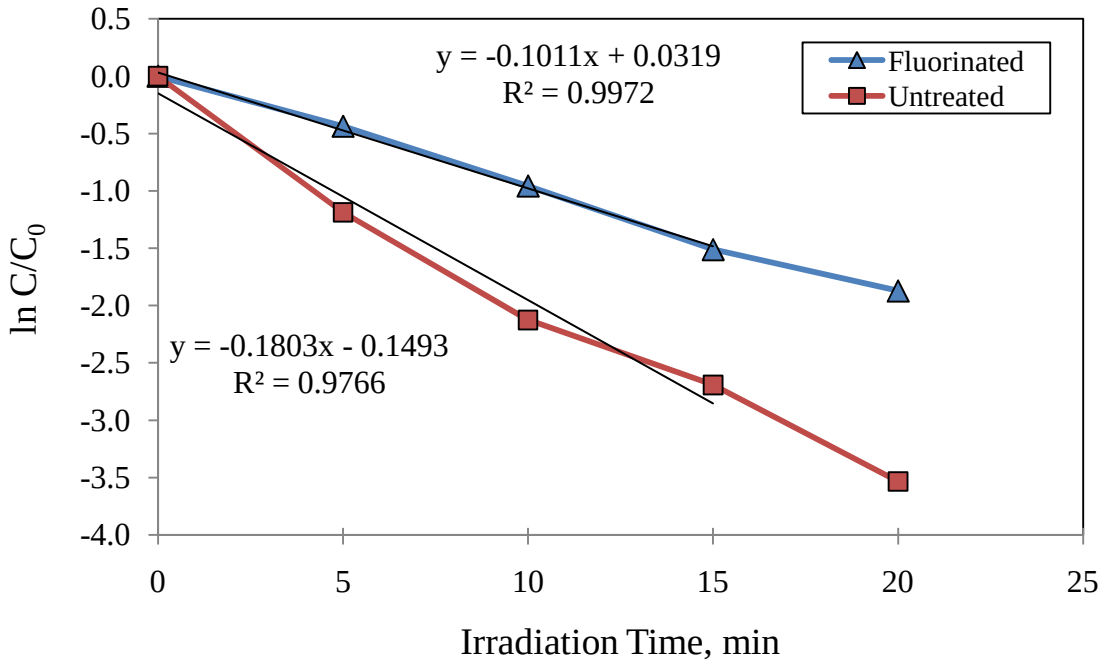

Figure 4.15 Linear fits for acetaldehyde degradation by untreated and fluorinated TiO_2. CW plasma was employed for 5 minutes.

Kinetic treatment of the rate data is shown in Figure 4.15 in terms of first order decay plots. From the slopes of these first order plots, rate constants of 0.180 min^{-1}, for the untreated TiO_2, and 0.101 min^{-1}, for the plasma treated sample, are obtained. This result is what would be anticipated, given that acetaldehyde is a polar compound, and the fact that a hydrophobic surface would be expected to decrease adsorption of polar compounds. These results are similar to those of a study by Ooka et al (2004) who reported that the photooxidation rate of ethanol, a polar compound, over standard P-25 TiO_2 was double the rate of that obtained over hydrophobic pillared clay TiO_2. It was explained that higher hydrophobicity on pillared clay decreased ethanol adsorption and reduced its photocatalytic degradation. It is also of interest to compare the relative

catalytic activities of xylene and acetaldehyde observed in this study. For example, with respect to untreated TiO_2, the oxidation of acetaldehyde is significantly faster, 0.180 min^{-1}, than the value of 0.012 min^{-1} observed for xylene. The higher reactivity of the acetaldehyde is in accord with expectations based on its greater reactivity, as introduced by the relatively labile C-H bond of the CHO group.

4.3.5 Photocatalytic Oxidation of Elemental Mercury by HFPO Treated TiO_2

It is well established that elementary mercury (Hg^0) is an atmospheric pollutant, whose main source is from coal powered power plants. For that reason, studies of the potential use of HFPO treated TiO_2 to provide PCO of Hg^0 were conducted. Directly fluorinated TiO_2, prepared by CW plasma for 5 minutes, was employed as the photocatalyst to remove Hg^0 in the air stream in which initial concentration was 500 $\mu g/m^3$. The plots of photocatalytic oxidation of Hg^0 by fluorinated TiO_2 and untreated TiO_2 are shown in Figure 4.16.

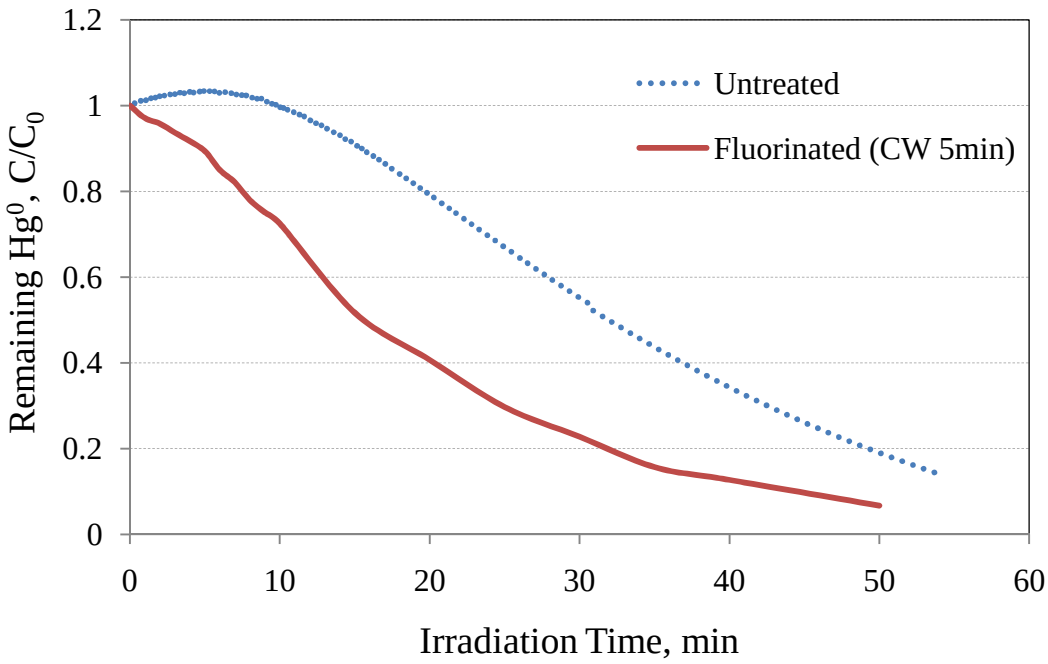

Figure 4.16 Photocatalytic activity of untreated and fluorinated TiO_2 to remove elemental mercury

As shown in Figure 4.16, the fluorinated TiO_2 showed higher photocatalytic activity than untreated TiO_2 to degrade Hg^0. The untreated catalyst exhibited steady rate of removal throughout the experiment whereas higher removal rate were observed at the initial state and slightly declined after 35 minutes in fluorinated sample. The kinetic plots of Hg^0 oxidation are expressed in Figure 4.17.

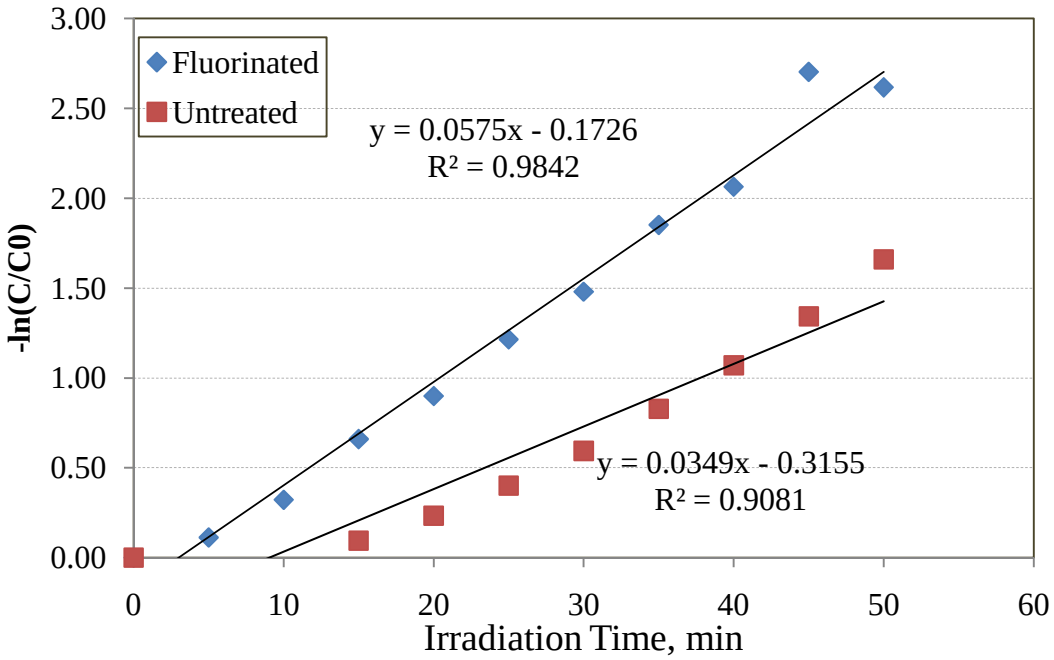

Figure 4.17 Linear fits for elemental mercury degradation by untreated and fluorinated TiO_2

First order reactions of Hg^0 photooxidation are observed in Figure 4.17. The plasma fluorinated TiO_2 exhibited slightly higher photoreactivity in terms of the initial oxidation rate, and percent Hg^0 removal, than the untreated sample. The removal efficiency higher than 80% was achieved from both samples at 50 minutes of the reactions. The removal rate of Hg^0 obtained from plasma treated TiO_2 was 1.6 times greater than that of the non-treated TiO_2.

4.4 Effect of Relative Humidity on the Photocatalytic Oxidation of m-Xylene

In light of the fact that the relative humidity (RH) of real atmospheres can vary significantly, a catalyst that can maintain high activity over a wide range of humidity would be highly beneficial. For this reason, we examined the utility of our plasma surface

modification technology in terms of improving the TiO_2 catalyst efficacy over a broad range of humidity. Herein, we report on the effect of water vapor on the photooxidation of m-xylene using plasma modified and untreated TiO_2 catalysts.

Figure 4.18 demonstrates the effect of relative humidity in the air stream on the degradation rate of m-xylene by standard TiO_2. A small difference in m-xylene destruction rates are observed in the lower levels of relative humidities ranging from 0 to 40%. A slight optimum pollutant removal rate was observed at a RH of 10%; however, the overall effect of RH changes from 0 to 40% was rather minor in scope. In contrast, higher RH values of 60% and 80% had a strong inhibition effect on the rate of m-xylene removal, with the rate decrease being more pronounced for the 80% value. These results are similar to Kim and Lee's study, which found that varying RH from 0-50% did not impact trichloroethylene (TCE) destruction; however, humidities exceeding 50% inhibited TCE removal (Kim and Lee, 2001).

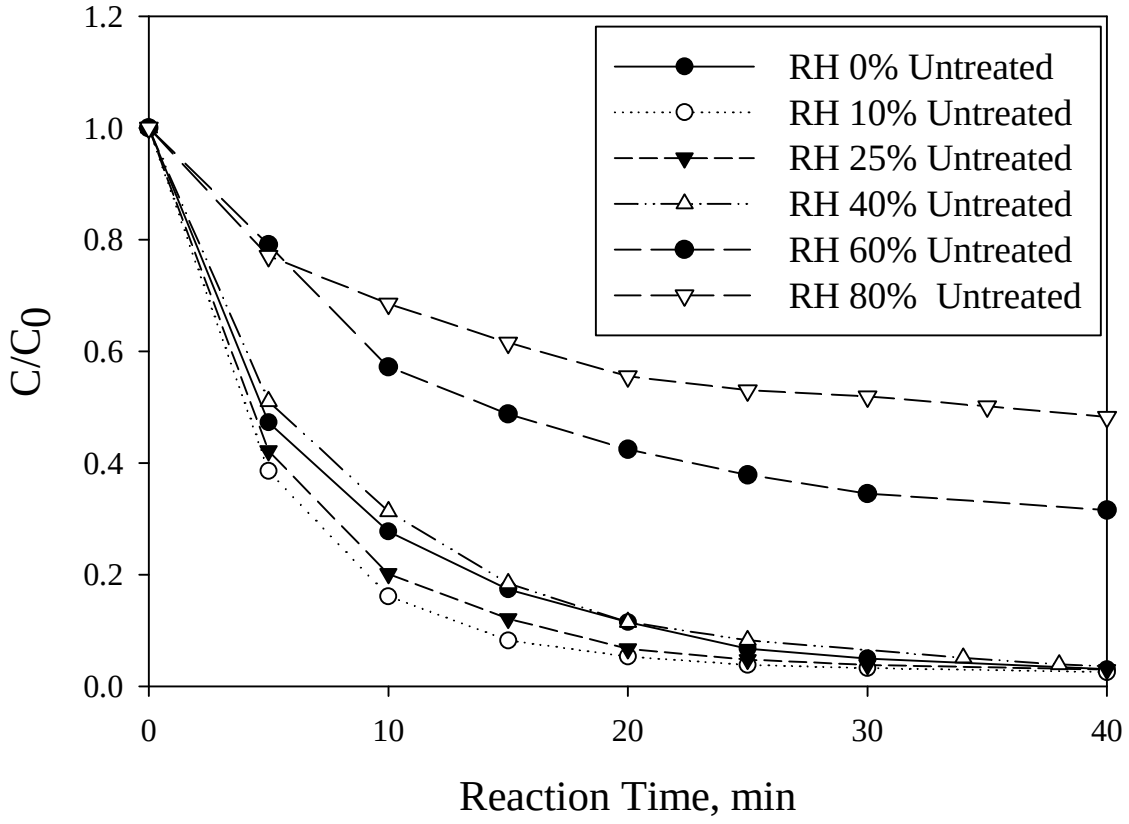

Figure 4.18 Photocatalytic activities of untreated TiO2 to remove m-xylene at different relative humidity values

The pattern of the effect of RH when fluorinated TiO_2, produced by CW plasma, was employed is similar to the untreated catalyst, with the exception that m-xylene was oxidized at a much higher rate. As illustrated in Figure 4.19, the difference between m-xylene removal rates was marginal over the RH rang of 0 to 40% when HFPO plasma modified TiO_2 was used, as the as the rate plots are essentially overlapping over this range of R.H values. A noticeable decrease in xylene removal rates was observed when the RH levels were raised to 60 and 80%, with the higher value again producing the

lower activity. However, the degradations of m-xylene by fluorinated TiO_2 are significantly higher than that of untreated TiO_2. Overall, the kinetic data obtained reveal that the modified catalyst is less sensitive to relative humidity levels in the air stream than the untreated TiO_2 at high level of RH in the gas stream.

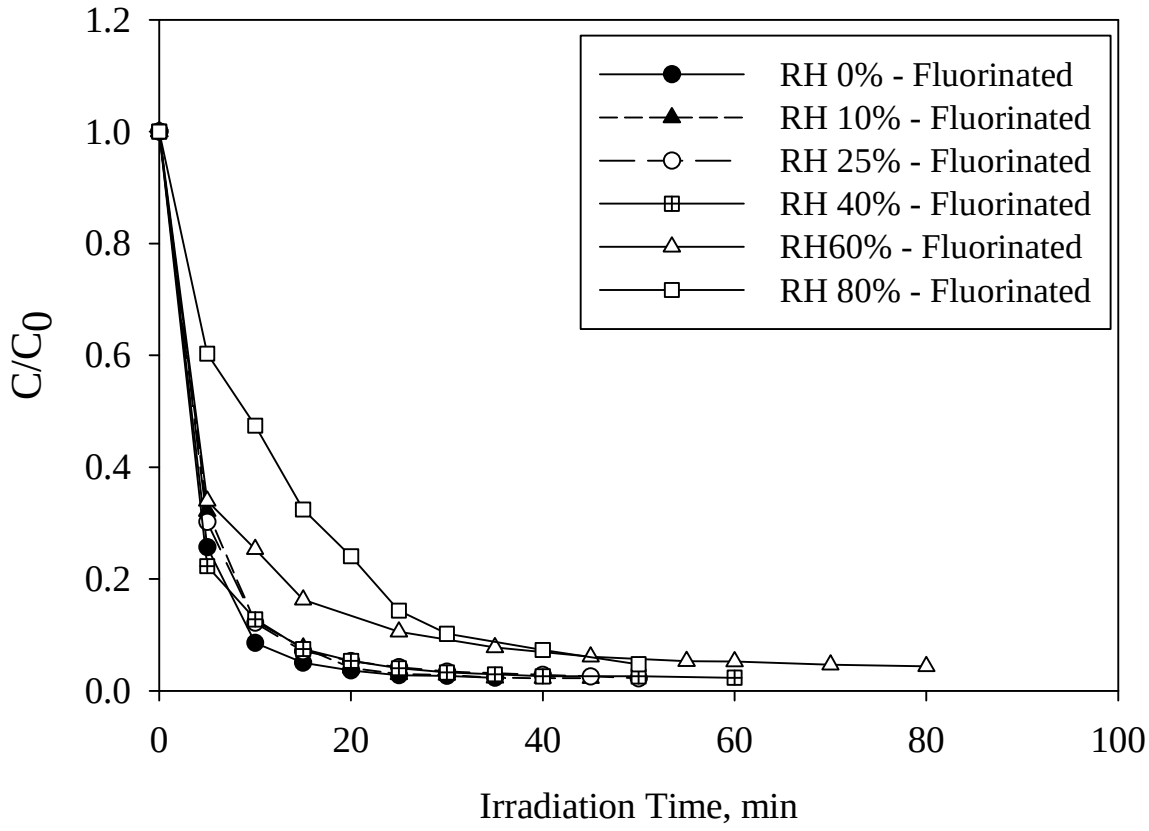

Figure 4.19 Photocatalytic activities of plasma fluorinated TiO_2 to remove m-xylene at different relative humidity levels. TiO_2 was treated by CW plasma for 5 minutes.

In order to quantify the photocatalytic activities of the untreated and fluorinated TiO_2 under various RH conditions, the initial oxidation rates of m-xylene were plotted to compare the efficiency of each catalyst. The first few data points were used in

determining the rate constant since they fitted well with first order reaction kinetics. The plots of $\ln(C/C_0)$ versus irradiation time of untreated and plasma fluorinated TiO_2 are shown in Figure 4.20 and Figure 4.21, respectively. The initial removal rate constants of m-xylene were determined by the slopes of the best fit lines. Initial rate of oxidations and their R^2 value are presented in Table 4.6. The optimum removal rate by untreated TiO_2, observed under 10% RH is 0.1675 min^{-1}, followed by RH values of 25, 0, 40, 60 and 80%, respectively. A value of 0.0281 min^{-1} was observed under 80% RH.

A greater photocatalytic activity was obtained from the fluorinated TiO_2, with the initial rates of degradation being higher than that of untreated TiO_2 under all RH conditions employed. When the RH levels in the system were in the range of 0 – 40%, the rates of reaction were relatively high and the differences were marginal as the trend lines are overlapping. The reaction rate was approximately 0.23 min^{-1} over this 0 to 40% RH range when the fluorinated TiO_2 was used. However, the m-xylene removal rates dropped after higher amounts of water vapor were introduced to the PCO reactor. The initial oxidation rates decreased to 0.1147 min^{-1} and 0.0694 min^{-1} when the RH reached 60 and 80%, respectively.

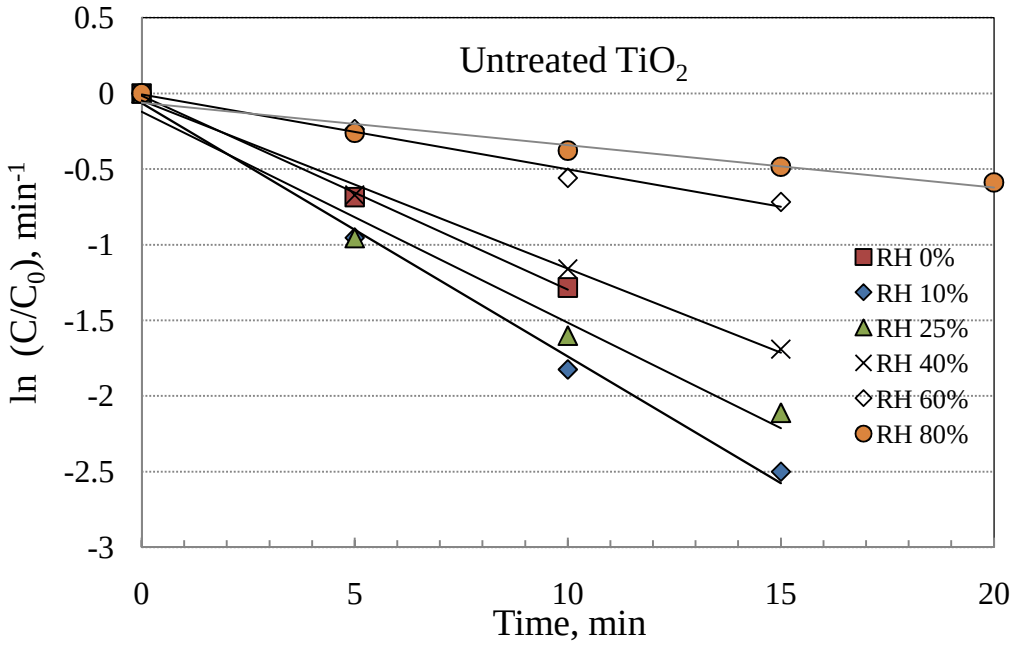

Figure 4.20 Initial oxidation rate of m-xylene by untreated TiO_2 at different relative humidity values

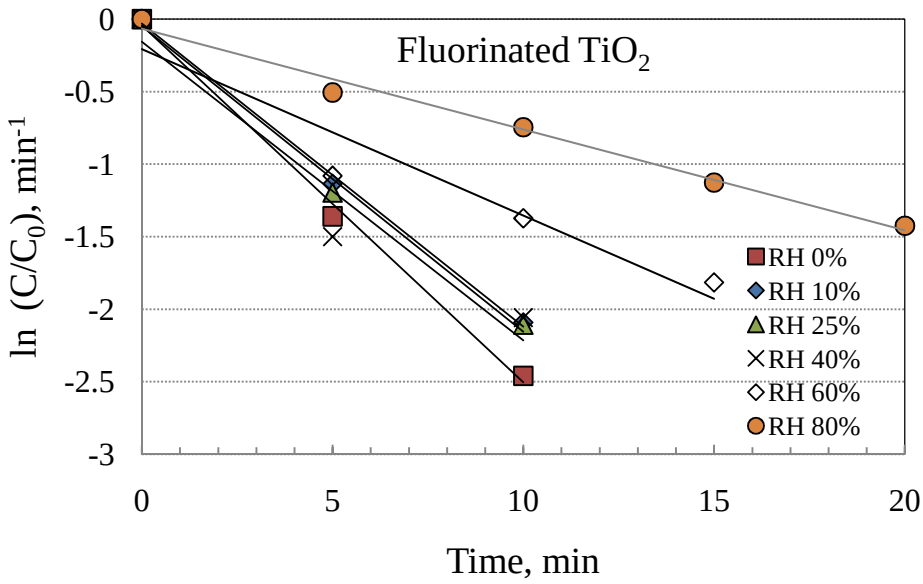

Figure 4.21 Initial oxidation rate of m-xylene by fluorinated TiO_2 at different relative humidity values.

Table 4.6 Initial Rate of Oxidation by Untreated and Fluorinated TiO_2.

RH, %	Untreated TiO_2			Fluorinated TiO_2			Difference of k-value, %
	k, min^{-1}	R^2	N	k,min^{-1}	R^2	N	
0	0.1283	0.9985	3	0.2459	0.9963	3	47.82
10	0.1675	0.9944	4	0.2090	0.9975	3	19.86
25	0.1396	0.9793	4	0.2107	0.9939	3	33.74
40	0.1112	0.9951	4	0.2058	0.9347	3	45.97
60	0.0495	0.9852	4	0.1147	0.9188	4	56.84
80	0.0281	0.9528	5	0.0694	0.9881	5	59.51

The plots of k-values of untreated and fluorinated TiO_2 are shown in Figure 4.22. It is clearly seen that fluorinated TiO_2 had higher k values than the untreated TiO_2 for all RH levels. However, they expressed similar trends which k values decreased at higher RH. The lowest values for the rate constant of both catalysts are observed at a RH of 80%.

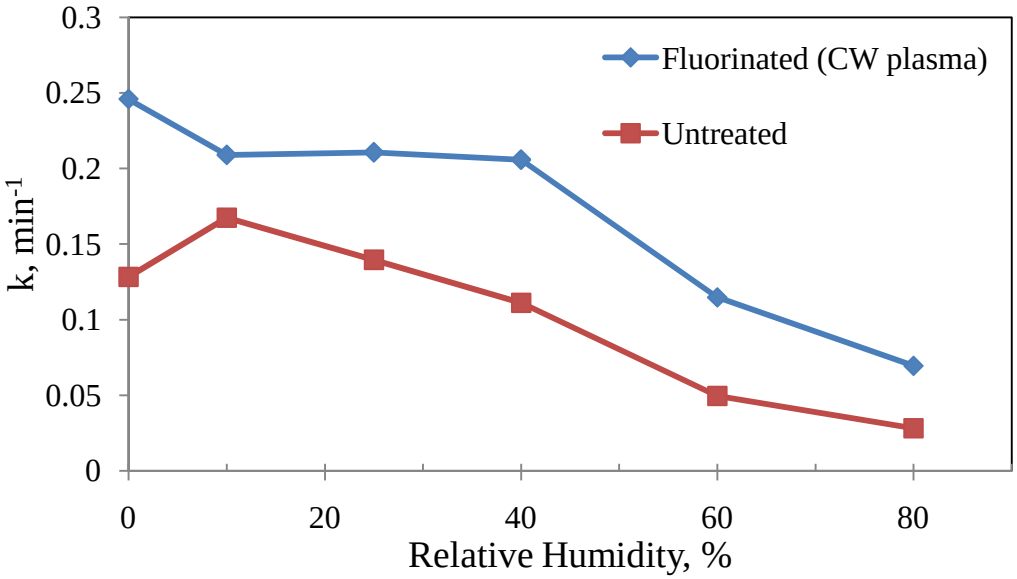

Figure 4.22 Relationship between k-values and relative humidity obtained from untreated and fluorinated TiO_2

4.5 Deactivation and Regeneration of TiO_2 Photocatalyst by Oxygen Plasma Treatment

4.5.1 Catalyst Deactivation

Deactivation of catalysts is an inherent problem in any catalytic system (Kaewgun and Lee, 2010, Park and Na, 2008). After a certain period of usage, it is not uncommon to observe a rapid decrease in photocatalytic activity with continued irradiation periods. In order to investigate the degradation of plasma modified photocatalyst, a sample of fluorinated TiO_2 was used in photocatalytic oxidation of m-xylene for 4 consecutive runs, all reaction conditions remaining constant in each run. The rates of xylene removal observed during this 4 run sequence are shown in Figure 4.23 and Table 4.7.

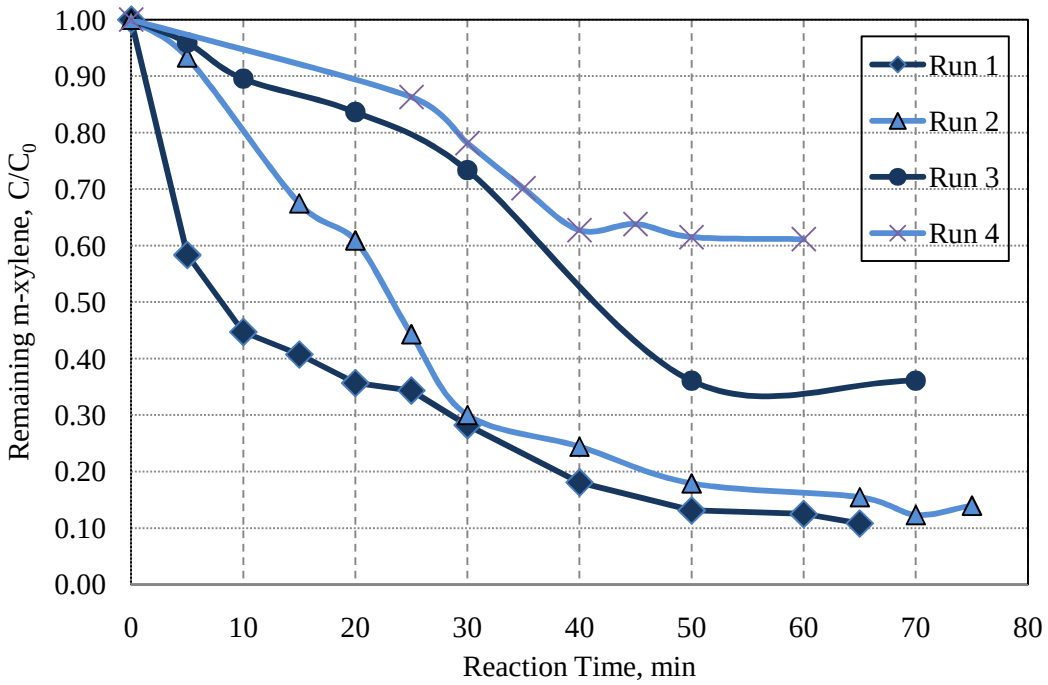

Figure 4.23 Deactivation of fluorinated TiO_2 during m-xylene degradation.

Table 4.7 Conversion of m-Xylene at 20 minutes and Maximum Conversions.

Run Number	% Conversion after 20 min.	Maximum % Conversion
1	64%	90% (65 min.)
2	40%	88% (70 min.)
3	16%	64% (55 min.)
4	10%	39% (60 min.)

In the first run, fluorinated TiO_2 efficiently decomposed m-xylene, more than 60% of the pollutant was photooxidized within 20 minutes. The total percent conversion was 90% after 65 minutes of UV irradiation. An apparent slight catalyst deactivation was observed in the second run in that the 60% m-xylene removal was observed only after 25 minutes of irradiation, with a slightly higher amount of xylene remaining at long reaction times compared to the initial run. As shown in Figure 4.23, the rate of catalyst deactivation became significantly more apparent in the subsequent two runs. For example, only 15% of the xylene was consumed over the 20 minute reaction time in run 3 and this had further decreased to only 10% in the first 20 minutes in the 4^{th} run. Obviously, the performance of the modified TiO_2 deteriorated rapidly with the increasing photooxidation time.

It should be noted that the color of the fresh TiO_2 has a white-grey color which is the typical color of titanium dioxide. The color of TiO_2 was changed from white into yellow after it had been employed to decompose m-xylene. The changing of TiO_2 color indicates accumulation of intermediates or partially oxidized species adsorbed on the active sites of TiO_2.

In order to investigate the nature of the catalyst deactivation observed, XPS spectra were carried out for the unreacted and the reacted catalyst, after run number 2. The XPS survey spectra of fresh fluorinated TiO_2 and after the two photocatalytic oxidation runs are shown in Figure 4.24. The major differences in these two spectra are the sharp decrease in the intensity of the F atom peak, accompanied by an increase in surface C atom content, in contrasting new and used catalyst. The composition of carbon

species is higher after photooxidation of m-xylene. Carbon compounds increase from 14.5% to 22.81% which is evidence that there are carbonaceous molecules produced and deposited on the surface during the m-xylene photooxidation.

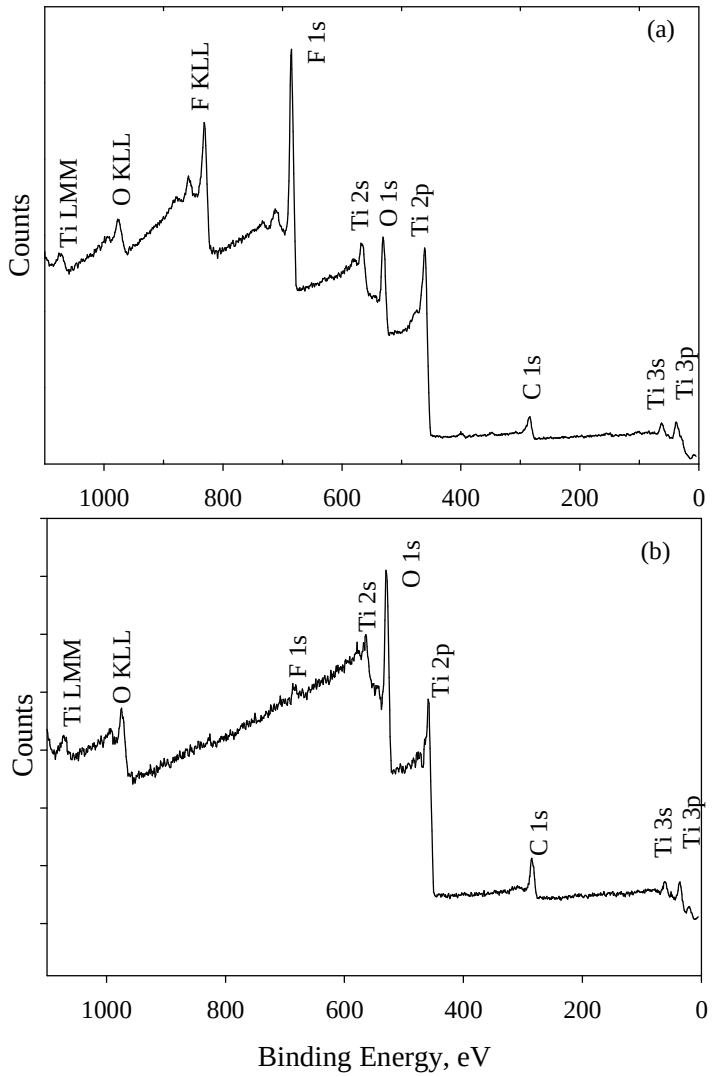

Figure 4.24 Survey XPS spectra of fluorinated TiO_2 (a) before reaction (b) fluorinated TiO_2 after reaction with m-xylene.

4.5.2 Catalyst Reactivation

Oxygen plasma treatment is a convenient single step that could remove carbonaceous molecules from the substrate. Moreover, the processing time of oxygen treatment is relatively short compare to other techniques. In this study, regeneration of used catalyst by oxygen plasma was conducted on fluorinated TiO_2. Two oxygen treatment durations were employed, namely 3 minutes and 10 minutes. During the regeneration process, the plasma conditions employed were 10 ms_on/10 ms_off, peak input power of 150 W and pressure of 160 mTorr. The recoveries of photoactivity are shown in Figure 4.25, along with the activities of the used catalysts in the successive four runs before regeneration.

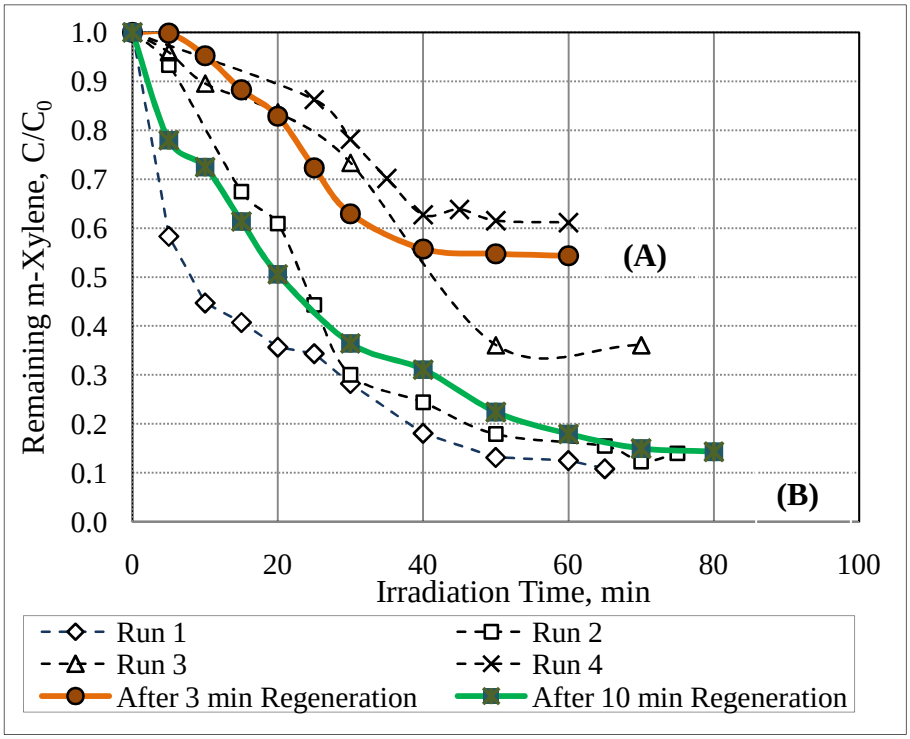

Figure 4.25 Photocatalytic activity of regenerated TiO_2 using O_2 plasma for: (A) 3 minutes and (B) 10 minutes

After being regenerated by O_2 plasma for 3 minutes, the color of TiO_2 sample was changed from brown to brighter yellow. A partial improvement of photodegradation of m-xylene was noticed when TiO_2 was exposed to O_2 plasma for a short period of 3 minutes. The m-xylene conversion was improved by approximately 11% over the used catalyst from run 4. In contrast, the activity of TiO_2 was nearly 100% recovered after being regenerated for 10 minutes. The photoreactivity was just slightly lower than that of the fresh photocatalyst. By using 10 minutes oxygen regeneration, m-xylene conversion was as high as 85.7% compared to 90% and 88% which were observed from the fresh catalyst and after run 1 sample, respectively.

A longer time, namely 15 minutes, of O_2 plasma regeneration was applied to the catalyst in order to achieve higher percent recovery. However, the TiO_2 nanoparticles which were coated on the glass plate were almost completely removed from the glass surface by the etching of O_2 plasma. Therefore, 15 minutes duration of O_2 cleaning is excessive to regenerate TiO_2 coated on glass plate.

4.6 Discussion on HFPO Plasma Treated TiO_2

The basic objective of the present study was to examine the feasibility of employing a plasma treatment process to improve the photocatalytic activity of TiO_2 for destruction of atmospheric VOCs. As documented in the results, both the direct plasma fluorination of TiO_2, as well as deposition of thin perfluorocarbon coatings on the TiO_2, were remarkably effective in enhancing the photocatalytic oxidation of m-xylene. The activity with respect to xylene is significant in that this particular pollutant is certainly not one of the more easily oxidized VOC pollutants. Thus it would appear to be reasonable to

assume that the enhanced activity of the plasma treated TiO_2 observed in this study should be applicable to a broader range of atmospheric VOCs.

It is interesting to note that the effectiveness of the plasma surface modification process is strongly dependent on the duty cycle and time of the plasma discharge employed. Under the same treatment period of 5 minutes, duty cycle of 10 ms_on/10 ms_off formed less fluorine species on the surface than the 10 ms_on/100 ms_off and CW. As a result, the photocatalytic activities of TiO_2 treated by duty cycle of 10 ms_on/10 ms_off were highly dependent on plasma treatment times. In general, the degradation rate of the m-xylene increased with increasing plasma treatment times, or in other words, with the amount of fluorine on the surface. The photocatalytic activities, which were observed in CW and 10 ms_on/100 ms_off treated for 5 minutes and 10 ms_on/10 ms_off treated for 30 minutes, are comparable. Interestingly, as shown by the XPS data, the surface fluorine atom percent is relatively similar for all three samples, varying from 45 to 55 atom % F. This result is in agreement with the study of Park and Choi (2005), who report more rapid photocatalytic degradation of stearic acid with TiO_2 particles having higher surface fluoride concentration. However, there is clearly an optimum plasma treatment time in maximizing the photocatalytic oxidation rates achievable, as shown by the data presented in Figure 4.9 for samples prepared at 10/10 over a wide range of plasma treatment times. As these data reveal, increasing the treatment time from 30 to 60 minutes resulted in a sharp decrease in photocatalytic activity of the TiO_2. This decrease is attributed to the deposition of an excessively thick perfluorocarbon film on the particles during the 60 minute deposition. The XPS data

confirm this fact in that no photoelectrons are detected from Ti atoms (and virtually no photoelectrons from O atoms) after the 60 minute process. It is reasonable to assume that the thicker perfluorocarbon films both minimize the penetration of the 366 nm UV incident photons to the TiO_2 surfaces, as well as increase the surface electron-hole recombination rates relative to the access of these species by the adsorbed xylene molecules.

It is interesting to note that both the direct surface fluorination and deposition of thin perfluorocarbon film are highly effective in promoting increased TiO_2 photocatalytic activity. It appears reasonable to infer that the enhanced activity observed in the present study involves a combination of the presence of fluorine atoms, which reduce recombination rates of electrons and holes, coupled with the conversion of the TiO_2 surface from hydrophilic to hydrophobic character. Photo-generated electrons are strongly attracted to fluorine since it is the most electronegative element (Yu et al., 2009). Consequently, the life time of electrons and holes would be lengthened since electron capture by the F atoms localizes conduction band electrons, thus delaying electron-hole recombination rates. The increased hydrophobicity after plasma treatments should play an important role in helping to promote more facile adsorption of the non-polar m-xylene molecules onto the catalyst surfaces, thus increasing the potential rate of their photooxidation. In fact, as shown in Figure 4.7, an enhanced direct adsorption of xylene on the fluorinated TiO_2 was observed. The increased hydrophobicity is quite dramatic, as shown by the water contact angle measurements. Finally, we note that there is no evidence that the plasma treatment process has altered the absorption band width of the

TiO_2: the reflectance absorption spectra of the treated and untreated TiO_2 are essentially identical, as shown in Figure 4.5. In this context, it is interesting to note that the recent report by Liu et al (2006) of treatment of TiO_2 with N_2 plasma to produce N-doped TiO_2 also resulted in increased photocatalytic activity of the TiO_2, as shown in the reduction of Cr(VI) in solution studies. In this work, the increased catalytic activity is attributed to a shift in TiO_2 adsorption to longer wavelength with N atom doping. As in the present work, evidence was also presented for an optimum plasma treatment time with respect to maximizing the photocatalytic activity.

Based on the rate constants observed, it is clear that the plasma treatment of TiO_2 can provide significantly enhanced photocatalytic oxidation rates for these materials. The rate constant for the 5 minute CW and 10/100 treated sample, namely 0.0736 min^{-1} and 0.0609 min^{-1}, are factors of 6.1 and 5.1 times larger, respectively, than that observed for the untreated TiO_2 material. These enhanced activity factors are higher than the results observed in other works where the factors were ranging from 1.21 to 3 times of the untreated materials (Lv et al., 2010, Vijayabalan et al., 2009, Yang et al., 2007, Yu et al., 2009).

In contrast, the photocatalytic oxidation of acetaldehyde by fluorinated TiO_2 is slower than that of standard TiO_2. A good measure of the difference in polarity between acetaldehyde and xylene is the octanol/water partition coefficient (log P_{ow}) which is used to define the relative water solubility of a compound. The value of log P_{ow} of acetaldehyde is 0.63 (Acros Organics, 2009) which is much less than that of m-xylene, 3.20 (International Labour Organization., 2008). This means that acetaldehyde has much

higher affinity for water vs. octanol, compared to m-xylene. As a result, it is presumably easier for acetaldehyde to access the active sites of standard TiO_2 than that of the hydrophobic fluorinated TiO_2. As a result, a higher photooxidation rate of acetaldehyde is observed on the untreatedTiO_2. The higher degradation rate of a polar substance, such as acetaldehyde on the untreated TiO_2 catalyst, agrees with a study of Ooka et al (2004) that the photooxidation rate of ethanol over standard P-25 TiO_2 was 2 times higher than that of hydrophobic pillared clay TiO_2. The hydrophobicity of pillared clay inhibited ethanol, which is a polar compound, from being adsorbed on the catalyst. However, the decreasing of electrons-holes recombination in plasma modified TiO_2 would compensate the loss of efficiency from hydrophobic surface that preventing accessing of acetaldehyde. Further investigations of catalytic photodegradation of other compounds by modified TiO_2 would be useful in helping to assess the overall effect of the hydrophobicity created by the HFPO plasma treatment on the degradation activity

The promotional effect of direct fluorination of TiO_2 on Hg^0 removal is similar to the effect that was observed with m-xylene. Fluorine on the TiO_2 surface effectively improves photooxidation of Hg^0. As noted earlier, this result can be rationalized in terms of fluorine decreasing electron-hole recombination rates and/or creation of a hydrophobic catalytic surface favoring adsorption of the mercury. Li and Wu (2006) reported that increasing relative humidity in the air stream suppressed Hg^0 photooxidation because of competitive adsorption of water and Hg^0. Thus, hydrophobicity of fluorinated TiO_2 would be beneficial to adsorption and photocatalytic oxidation of Hg^0.

The effects of water vapor on photocatalytic oxidation of m-xylene are relatively similar for both untreated and plasma fluorinated TiO_2. The rates of m-xylene degradation are marginally changed over RH variations from 0 to 40%. An inhibition effect of water vapor of photodegradation rates becomes noticeable when the RH is raised to 60% and 80% for both treated and untreated catalysts. It is also apparent that the fluorinated TiO_2 exhibits higher rate of m-xylene degradation than the untreated TiO_2 at all RH levels employed. In general, a low RH level would be expected to be beneficial for m-xylene removal because water molecules are a source of $OH^{\bullet}$ which could effectively oxidize m-xylene. However, at higher RH values of 60% and 80%, competitive adsorption between water molecules and m-xylene for adsorption on catalytic sites occur. It is presumed that more than one monolayer of water molecule are formed and, as such, limits m-xylene access to the surface of TiO_2. Interestingly, in case of the fluorinated TiO_2, the maximum m-xylene degradation rate is actually observed when the RH is 0%. This result indicates that under this condition which favors xylene adsorption, sufficient $OH^{\bullet}$ may be effectively produced from surface hydroxyl groups, perhaps formed by the hydrolysis of water during the slurry coating of TiO_2 on the glass plate. This possibility, coupled with the expected F-induced decrease in electron-hole recombination rates, would account the increased photooxidation rates observed with the F-doped TiO_2 catalysts.

Finally, we note that, with respect to catalyst stability, it was observed that the PCO activity decreased slowly when the same catalyst was employed in a sequence of successive runs. As shown in Figure 4.23 after 4 consecutive runs, the photocatalytic

activity of the catalyst has significantly diminished XPS analysis of the used catalyst revealed an increase in the C(1s) photo electron peaks between 285eV and 288eV, which corresponds to the presence of non-fluorinated carbon atoms. The experimental results revealed that oxygen plasma cleaning of 3 minutes was not long enough to regenerate the exhausted TiO_2 since the photoreactivity was still substantially lower than that of the newly treated TiO_2. However, it was also observed that subjection of the used catalysts to a 10 minute pure oxygen plasma restored its PCO activity to close to its original value. Thus it is possible to essentially remove the carbonaceous material formed during the PCO runs, without significantly disturbing the fluorine functionalities.

In conclusion, the use of a relatively simple plasma treatment process has been shown to accelerate significantly the photocatalytic oxidation rate of TiO_2. It will be of interest, in future studies, to determine if other plasma surface treatment processes might duplicate, or even exceed, the acceleration rates obtained in the present study. In addition, the results obtained in this study suggest that it would be interest to also examine the generality of this process in improving the photocatalytic activity of other photooxidative catalytic materials.

CHAPTER 5

CONCLUSIONS AND RECOMMENDATIONS

5.1 Conclusions

It has been demonstrated that plasma processing provides a viable route to enhancing the photocatalytic activity of TiO_2 particles. Using a perfluorocarbon monomer, it was shown that under highly energetic continuous wave (CW) plasma conditions, direct fluorination of the TiO_2 was obtained. In contrast, under less energetic conditions such as low duty cycle pulsed plasmas, thin layers of perfluorocarbon polymeric films were deposited on the TiO_2. Both direct fluorination and perfluorocarbon film deposition are observed on the TiO_2 surface when intermediate power input was employed. In all cases, the deposition of fluorine species dramatically changed surface character of TiO_2 from hydrophilic to highly hydrophobic. However, the UV-visible absoption spectrum of TiO_2 was unaffected by plasma depositions.

Modified TiO_2 exhibited significantly higher photocatalytic activity in degrading m-xylene. It was discovered that relatively short plasma treatment times are required to achieve enhanced catalytic activity of the TiO_2. Plasma treatment, either direct fluorination or coating of perfluorocarbon film, for only 5 minutes dramatically enhanced photocatalytic oxidation rates for these materials. However, excessive coating of perfluorocarbon film, which limits contact between the xylene and the TiO_2, resulted in severely retarded photocatalyst activity. Initial degradation rates of m-xylene, treated

as first order processes, provided rate constants obtained for fluorinated and perfluorocarbon coated TiO_2 which were 6.1 and 5.1 times larger, respectively, than that of the untreated TiO_2.

In contrast, fluorinated TiO_2 exhibited less reactivity in photocatalytic oxidation of acetaldehyde than the untreated catalyst. This result suggests that the hydrophobicity of the fluorinated materials reduce the adsorption of a polar molecule such as acetaldehyde relative to its adsorption on the untreated hydrophilic TiO_2 particles. Thus, the experimentally observed improvement of initial rate constants observed in fluorine plasma treated TiO_2 with xylene might be applicable to other non-polar substances which are similar to m-xylene but may not applicable to polar compounds such as acetaldehyde. In accord with this concept, it is noted that the photocatalytic oxidation of elemental mercury was promoted on fluorinated TiO_2, which would be accord with the non-polar character of elemental mercury.

The effect of relative humidity (RH) on the rate of photooxidation of m-xylene was examined using both untreated and fluorinated TiO_2 as catalysts. Overall, the untreated TiO_2 appeared to exhibit more sensitivity to RH valued than the fluorinated material. In the case of the untreated TiO_2, a RH of 10% was observed to provide optimum catalytic activity for m-xylene removal. At RH values higher than 10%, degradation rates were inversely proportional to the RH. The photocatalytic activity of the fluorinated material was less affected by RH, as essentially the same photooxidation rates were obtained for RH values ranging of 0 – 40%. However, photooxidation of m-xylene was inhibited under higher RH of 60% and 80% for the F-doped material.

Finally, deactivation of fluorinated TiO_2 was found when it was employed in a succession of runs. However, it was shown that use of an oxygen plasma treatment provides effective regeneration of the catalyst. The effectiveness of the oxygen plasma treatment is ascribed to its efficient removal of carbonaceous deposits from the surface of catalyst. Oxygen plasma treatment of only 10 minutes was shown to essentially restore catalytic activity of the TiO_2 to its original value.

5.2 Recommendations

Based on the encouraging results obtained, further studies could include exploring the utility of employing F-doped TiO_2 for oxidation of other gaseous pollutant substances. In particular, it would be of value to investigate further the effect of the molecular structure of the pollutant, in terms of its polar or non-polar character, with respect to their photodegradation as functions of relative humidities. The present work can also serve as a spring board to examine the efficacy of using plasma processing to investigate the preparation of controlled catalyst doping by atoms other than fluorine, for example nitrogen and carbon, with TiO_2 as well as other catalytic materials. Since VOCs cover a broad spectrum of functional groups and molecular structures, it is reasonable to assume that different plasma treatments may provide surfaces that are particularly effective in achieving photocatalytic destruction of specified VOCs. Thus it would be of significant interest to examine the efficacy of employing various plasma doped TiO_2 particles. Conceivably, this could lead to use of a catalytic bed containing a mixture of TiO_2 doped particles which could provide simultaneous effective degradation of a wide range of VOC molecules.

Many additional concerns must be considered and addressed prior to experimental application of the TiO2 doped treatment process. For example, pilot scale testing of plasma treated TiO_2 under field conditions should be employed to help elucidate the effects of other key variables such as gas flow rate, gas temperature, size of the PCO reactor, and the interaction of other substances in the gas stream ,in particular particulates, on the efficiency of the PCO process to remove VOCs. The pilot scale studies should include integration of the plasma treatment and PCO reactor as this would reduce construction costs, space requirement and PCO reactor down time during the regeneration of deactivated TiO_2. Finally, capital and operating costs for field-scale systems would need to be estimated.

REFERENCES

1. A&WMA (2000). *Air Pollution Engineering Manual*, Wiley-Interscience.
2. Abou Asi, M., He, C., Su, M., Xia, D., Lin, L., Deng, H., Xiong, Y., Qiu, R., and Li, X.-z. (2011). "Photocatalytic reduction of CO_2 to hydrocarbons using AgBr/TiO_2 nanocomposites under visible light." *Catalysis Today*, doi:10.1016/j.cattod.2011.02.055.
3. Acros Organics (2009). "Material Safety Data Sheet - Acetaldehyde." http://www.wku.edu/msds/docs/307.pdf. (July 1, 2011, 2011).
4. Alberici, R. M., and Jardim, W. F. (1997). "Photocatalytic destruction of VOCs in the gas-phase using titanium dioxide." *Applied Catalysis B: Environmental*, 14(1-2), 55-68.
5. Alptekin, G., Monroe, J., Amalfitano, R., and Copeland, R. "Sorbents for mercury removal from coal-derived synthesis gas " *Proc., Proceedings - Annual International Pittsburgh Coal Conference*, Pittsburgh Coal Conference, University of Pittsburgh.
6. Ananpattarachai, J., Kajitvichyanukul, P., and Seraphin, S. (2009). "Visible light absorption ability and photocatalytic oxidation activity of various interstitial N-doped TiO2 prepared from different nitrogen dopants." *Journal of Hazardous Materials*, 168(1), 253-261.

7. Augugliaro, V., Loddo, V., Palmisano, G., and Palmisano, L. (2010). *Clean by Light Irradiation: Practical Applications of Supported TiO_2,* RSC Publishing, Cambridge, UK.

8. Beamson, G., and Briggs, D. (1992). *High resolution XPS of organic polymers: the Scienta ESCA300,* John Wiley & Sons Ltd, West Sussex, England.

9. Boonstra, A. H., and Mutsaers, C. A. H. A. (1975). "Relation between the photoadsorption of oxygen and the number of hydroxyl groups on a titanium dioxide surface." *The Journal of Physical Chemistry*, 79(16), 1694-1698.

10. Boulamanti, A. K., Korologos, C. A., and Philippopoulos, C. J. (2008). "The rate of photocatalytic oxidation of aromatic volatile organic compounds in the gas-phase." *Atmospheric Environment*, 42(34), 7844-7850.

11. Cao, L., Gao, Z., Suib, S. L., Obee, T. N., Hay, S. O., and Freihaut, J. D. (2000). "Photocatalytic Oxidation of Toluene on Nanoscale TiO_2 Catalysts: Studies of Deactivation and Regeneration." *Journal of Catalysis*, 196(2), 253-261.

12. Chen, M. L., Zhang, F. J., Zhang, K., Meng, Z. D., and Oh, W. C. (2010). "Fabrication of M-CNT/TiO2 (M=Cr, Mn and Fe) composites and the effect of transition metals on their photocatalytic activities." *Journal of Chemical Research*, 34, 283-287.

13. Chen, Y., Chen, F., and Zhang, J. (2009). "Effect of surface fluorination on the photocatalytic and photo-induced hydrophilic properties of porous TiO_2 films." *Applied Surface Science*, 255(12), 6290-6296.

14. Cheng, Y., Sun, H., Jin, W., and Xu, N. (2007). "Effect of preparation conditions on visible photocatalytic activity of titania synthesized by solution combustion method." *Chinese Journal of Chemical Engineering*, 15(2), 178-183.

15. Cho, J., Denes, F. S., and Timmons, R. B. (2006). "Plasma processing approach to molecular surface tailoring of nanoparticles: Improved phtocatalytic ativity of TiO_2." *Chemistry of Materials*, 18(13), 2989-2996.

16. Cho, J. H. (2005). "RF pulsed plasma surface modification of titanium dioxide nanoparticles for environmental applications ." Ph. D. Dissertation, The University of Texas at Arlington. .

17. Cho, Y., Choi, W., Lee, C.-H., Hyeon, T., and Lee, H.-I. (2001). "Visible Light-Induced Degradation of Carbon Tetrachloride on Dye-Sensitized TiO_2." *Environmental Science & Technology*, 35(5), 966-970.

18. Coronado, J. M., Zorn, M. E., Tejedor-Tejedor, I., and Anderson, M. A. (2003). "Photocatalytic oxidation of ketones in the gas phase over TiO_2 thin films: a kinetic study on the influence of water vapor." *Applied Catalysis B: Environmental*, 43(4), 329-344.

19. Czoska, A. M., Livraghi, S., Chiesa, M., Giamello, E., Agnoli, S., Granozzi, G., Finazzi, E., Valentin, C. D., and Pacchioni, G. (2008). "The nature of defects in fluorine-doped TiO_2." *The Journal of Physical Chemistry C*, 112(24), 8951-8956.

20. D'Hennezel, O., and Ollis, D. F. (1997). "Trichloroethylene-Promoted Photocatalytic Oxidation of Air Contaminants." *Journal of Catalysis*, 167(1), 118-126.

21. D'Hennezel, O., Pichat, P., and Ollis, D. F. (1998). "Benzene and toluene gas-phase photocatalytic degradation over H_2O and HCl pretreated TiO_2: by-products and mechanisms." *Journal of Photochemistry and Photobiology A: Chemistry*, 118(3), 197-204.

22. Di Paola, A., MarcÃ, G., Palmisano, L., Schiavello, M., Uosaki, K., Ikeda, S., and Ohtani, B. (2001). "Preparation of Polycrystalline TiO2 Photocatalysts Impregnated with Various Transition Metal Ions: Characterization and Photocatalytic Activity for the Degradation of 4-Nitrophenol." *The Journal of Physical Chemistry B*, 106(3), 637-645.

23. Einaga, H., Futamura, S., and Ibusuki, T. (2002). "Heterogeneous photocatalytic oxidation of benzene, toluene, cyclohexene and cyclohexane in humidified air: Comparison of decomposition behavior on photoirradiated TiO_2 catalyst." *Applied Catalysis B: Environmental*, 38(3), 215-225.

24. EPA, U. S. (2009). "Integrated Risk Information System (IRIS)." http://www.epa.gov/iris/index.html. (June 7, 2011, 2011).

25. Evonik Industries (2011). "Photocatalytic effect with AEROSIL fumed silica." http://www.aerosil.com/product/aerosil/en/effects/photocatalyst/pages/default.aspx. (July 14, 2011, 2011).

26. Fujishima, A., and Honda, K. (1972). "Electrochemical Photolysis of Water at a Semiconductor Electrode." *Nature*, 238(5358), 37-38.

27. Geng, Q., and Chen, N. (2011). "Photocatalytic Degradation of a Gaseous Benzene-Toluene Mixture in a Circulated Photocatalytic Reactor." *Chemical Engineering & Technology*, 34(3), 400-408.

28. Geng, Q., Guo, Q., and Yue, X. (2010). "Adsorption and Photocatalytic Degradation Kinetics of Gaseous Cyclohexane in an Annular Fluidized Bed Photocatalytic Reactor." *Industrial & Engineering Chemistry Research*, 49(10), 4644-4652.

29. Granite, E. J., King, W. P., Stanko, D. C., and Pennline, H. W. (2008). "Implications of mercury interactions with band-gap semiconductor oxides." *Main Group Chemistry*, 7(3), 227-237.

30. Gregg, S. J., and Sing, K. S. W. (1982). *Adsorption, surface area and porosity -2nd ed.*, Academic Press INC., New York, United States.

31. International Labour Organization. (2008). "m-Xylene." http://www.ilo.org/legacy/english/protection/safework/cis/products/icsc/dtasht/_icsc00/icsc0085.htm. (July 1, 2011, 2011).

32. Jeon, S. H., Eom, Y., and Lee, T. G. (2008). "Photocatalytic oxidation of gas-phase elemental mercury by nanotitanosilicate fibers." *Chemosphere*, 71(5), 969-974.

33. Jo, W.-K., and Yang, C.-H. (2009). "Granular-activated carbon adsorption followed by annular-type photocatalytic system for control of indoor aromatic compounds." *Separation and Purification Technology*, 66(3), 438-442.

34. Kaewgun, S., and Lee, B. I. (2010). "Deactivation and regeneration of visible light active brookite titania in photocatalytic degradation of organic dye." *Journal of Photochemistry and Photobiology A: Chemistry*, 210(2-3), 162-167.

35. Kampa, M., and Castanas, E. (2008). "Human health effects of air pollution." *Environmental Pollution*, 151(2), 362-367.

36. Kaneko, M., and Okura, I. (2002). *Photocatalysis :science and technology* Kodansha ;Springer, Tokyo.

37. Kim, J., and Lee, T. (2001). "Effect of humidity on the photocatalytic degradation of trichloroethylene in gas phase over TiO_2 thin films treated by different conditions." *Korean Journal of Chemical Engineering*, 18(6), 935-940.

38. Koppenol, W. H., and Liebman, J. F. (1984). "The oxidizing nature of the hydroxyl radical. A comparison with the ferryl ion (FeO^{2+})." *The Journal of Physical Chemistry*, 88(1), 99-101.

39. Koppman, R. (2007). *Volatile Organic Compounds in the Atmosphere*, Blackwell Publishing Ltd, United Kingdom.

40. Kwok, E. S. C., Aschmann, S. M., Atkinson, R., and Arey, J. (1997). "Products of the gas-phase reactions of o-, m- and p-xylene with the OH radical in the presence and absence of NO_x." *J. Chem. Soc., Faraday Trans.*, 93(16), 2847-2854.

41. Lamborg, C. H., Fitzgerald, W. F., O'Donnell, J., and Torgersen, T. (2002). "A non-steady-state compartmental model of global-scale mercury biogeochemistry with interhemispheric atmospheric gradients." *Geochimica et Cosmochimica Acta*, 66(7), 1105-1118.

42. Lawless, D., Serpone, N., and Meisel, D. (1991). "Role of hydroxyl radicals and trapped holes in photocatalysis. A pulse radiolysis study." *The Journal of Physical Chemistry*, 95(13), 5166-5170.

43. Lenk, T. J., Hallmark, V. M., Hoffmann, C. L., Rabolt, J. F., Castner, D. G., Erdelen, C., and Ringsdorf, H. (1994). "Structural Investigation of Molecular Organization in Self-Assembled Monolayers of a Semifluorinated Amidethiol." *Langmuir*, 10(12), 4610-4617.

44. Lewandowski, M., and Ollis, D. F. (2003a). "Halide acid pretreatments of photocatalysts for oxidation of aromatic air contaminants: rate enhancement, rate inhibition, and a thermodynamic rationale." *Journal of Catalysis*, 217(1), 38-46.

45. Lewandowski, M., and Ollis, D. F. (2003b). *Semiconductor Photochemistry and Photophysics* Marcel Dekker Ltd

46. Li, D., Haneda, H., Labhsetwar, N. K., Hishita, S., and Ohashi, N. (2005). "Visible-light-driven photocatalysis on fluorine-doped TiO_2 powders by the creation of surface oxygen vacancies." *Chemical Physics Letters*, 401(4-6), 579-584.

47. Li, H., Li, Y., Wu, C.-Y., and Zhang, J. (2011). "Oxidation and capture of elemental mercury over SiO_2-TiO_2-V_2O_5 catalysts in simulated low-rank coal combustion flue gas." *Chemical Engineering Journal*, 169(1-3), 186-193.

48. Li, Y., and Wu, C.-Y. (2006). "Role of moisture in adsorption, photocatalytic oxidation, and reemission of elemental mercury on a SiO_2-TiO_2 nanocomposite." *Environmental Science & Technology*, 40(20), 6444-6448.

49. Li, Y., and Wu, C.-Y. (2007). "Kinetic study for photocatalytic oxidation of elemental mercury on a SiO_2-TiO_2 nanocomposite." *Environmental Engineering Science*, 24(1), 3-12.

50. Lim, M., Zhou, Y., Wood, B., Guo, Y., Wang, L., Rudolph, V., and Lu, G. (2008). "Fluorine and carbon codoped macroporous titania microspheres: highly effective photocatalyst for the destruction of airborne styrene under visible light." *The Journal of Physical Chemistry C*, 112(49), 19655-19661.

51. Liu, C., Ma, Z., Li, J., and Wang, W. (2006). "Study on Modification of Nano-Sized Anatase Titanium Dioxide by Nitrogen-Plasma " *Plasma Science and Technology*, 8(3), 311-315.

52. Liu, S., and Chen, Y. (2009). "Enhanced photocatalytic activity of TiO_2 powders doped by Fe unevenly." *Catalysis Communications*, 10(6), 894-899.

53. Lv, K., Yu, J., Deng, K., Sun, J., Zhao, Y., Du, D., and Li, M. (2010). "Synergistic effects of hollow structure and surface fluorination on the photocatalytic activity of titania." *Journal of Hazardous Materials*, In Press, Corrected Proof.

54. Maggos, T., Bartzis, J. G., Leva, P., and Kotzias, D. (2007). "Application of photocatalytic technology for NO_x removal." *Applied Physics A: Materials Science & Processing*, 89(1), 81-84.

55. McLarnon, C. R., Granite, E. J., and Pennline, H. W. (2005). "The PCO process for photochemical removal of mercury from flue gas." *Fuel Processing Technology*, 87(1), 85-89.

56. McLintock, I. S., and Ritchie, M. (1965). "Reactions on titanium dioxide; photo-adsorption and oxidation of ethylene and propylene." *Transactions of the Faraday Society* 61, 1007 - 1016.

57. Mo, J., Zhang, Y., Xu, Q., Lamson, J. J., and Zhao, R. (2009). "Photocatalytic purification of volatile organic compounds in indoor air: A literature review." *Atmospheric Environment*, 43(14), 2229-2246.

58. Moser, J., Grätzel, M., and Gallay, R. (1987). "Inhibition of Electron-Hole Recombination in Substitutionally Doped Colloidal Semiconductor Crystallites." *Helvetica Chimica Acta*, 70(6), 1596-1604.

59. Muggli, D. S., and Ding, L. (2001). "Photocatalytic performance of sulfated TiO_2 and Degussa P-25 TiO_2 during oxidation of organics." *Applied Catalysis B: Environmental*, 32(3), 181-194.

60. Obee, T. N., and Brown, R. T. (1995). "TiO_2 photocatalysis for indoor air applications: Effects of humidity and trace contaminant levels on the oxidation rates of formaldehyde, toluene, and 1,3-butadiene." *Environmental Science & Technology*, 29(5), 1223-1231.

61. Ollis, D. F. (2000). "Photocatalytic purification and remediation of contaminated air and water." *Comptes Rendus de l'Académie des Sciences - Series IIC - Chemistry*, 3(6), 405-411.

62. Ooka, C., Yoshida, H., Suzuki, K., and Hattori, T. (2004). "Effect of surface hydrophobicity of TiO_2-pillared clay on adsorption and photocatalysis of gaseous molecules in air." *Applied Catalysis A: General*, 260(1), 47-53.

63. Oppenlander, T. (2003). *Photochemical Purification of Water and Air*, Wiley-VCH Verlag GmbH & Co. KGaA, Weinheim, Germany.

64. Pan, H., Gu, B., and Zhang, Z. (2009). "Phase-Dependent Photocatalytic Ability of TiO_2: A First-Principles Study." *Journal of Chemical Theory and Computation*.

65. Park, H., and Choi, W. (2004a). "Effects of TiO_2 surface fluorination on photocatalytic reactions and photoelectrochemical behaviors." *The Journal of Physical Chemistry B*, 108(13), 4086-4093.

66. Park, J. S., and Choi, W. (2004b). "Enhanced Remote Photocatalytic Oxidation on Surface-Fluorinated TiO_2." *Langmuir*, 20(26), 11523-11527.

67. Park, J. S., and Choi, W. (2005). "Remote Photocatalytic Oxidation Mediated by Active Oxygen Species Penetrating and Diffusing through Polymer Membrane over Surface Fluorinated TiO_2." *Chemistry Letters*, 34(12), 1630-1631.

68. Park, O. H., and Na, H. Y. (2008). "Photocatalytic degradation of toluene vapour using fixed bed multichannel photoreactors equipped with TiO_2 coated fabrics." *Environmental Technology*, 29(9), 1001 - 1007.

69. Peral, J., and Ollis, D. F. (1992). "Heterogeneous photocatalytic oxidation of gas-phase organics for air purification: Acetone, 1-butanol, butyraldehyde, formaldehyde, and m-xylene oxidation." *Journal of Catalysis*, 136(2), 554-565.

70. Pichat, P. (2010). "Some views about indoor air photocatalytic treatment using TiO_2: Conceptualization of humidity effects, active oxygen species, problem of C1-C3 carbonyl pollutants." *Applied Catalysis B: Environmental*, 99(3-4), 428-434.

71. Portela, R., Suárez, S., Rasmussen, S. B., Arconada, N., Castro, Y., Durán, A., Ávila, P., Coronado, J. M., and Sánchez, B. (2010). "Photocatalytic-based strategies for H_2S elimination." *Catalysis Today*, 151(1-2), 64-70.

72. Quici, N., Vera, M. L., Choi, H., Puma, G. L., Dionysiou, D. D., Litter, M. I., and Destaillats, H. (2010). "Effect of key parameters on the photocatalytic oxidation of toluene at low concentrations in air under 254 + 185 nm UV irradiation." *Applied Catalysis B: Environmental*, 95(3-4), 312-319.

73. Raillard, C., Hequet, V., Cloirec, P. L., and Legrand, J. (2005). "TiO_2 coating types influencing the role of water vapor on the photocatalytic oxidation of methyl ethyl ketone in the gas phase." *Applied Catalysis B: Environmental*, 59(3-4), 213-220.

74. Rajeshwar, K. (1995). "Photoelectrochemistry and the environment." *Journal of Applied Electrochemistry*, 25(12), 1067-1082.

75. Rene, E., Murthy, D., and Swaminathan, T. (2010). "Effect of flow rate, concentration and transient—state operations on the performance of a biofilter treating xylene vapors." *Water Air Soil Pollut*, 211(1), 79-93.

76. Sattler, M. L., and Liljestrand, H. M. (2003). "Method for predicting photocatalytic oxidation rates of organic compounds." *Journal of the Air and Waste Management Association*, 53(1), 3-12.

77. Savage, C. R., Timmons, R. B., and Lin, J. W. (1991). "Molecular control of surface film compositions via pulsed radio-frequency plasma deposition of perfluoropropylene oxide." *Chemistry of Materials*, 3(4), 575-577.

78. Snider, G., and Ariya, P. (2010). "Photo-catalytic oxidation reaction of gaseous mercury over titanium dioxide nanoparticle surfaces." *Chemical Physics Letters*, 491(1-3), 23-28.

79. Sun, H., Wang, S., Ang, H. M., Tadé, M. O., and Li, Q. (2010). "Halogen element modified titanium dioxide for visible light photocatalysis." *Chemical Engineering Journal*, 162(2), 437-447.

80. Timmons, R. B., and Griggs, A. J. (2004). *Pulsed Plasma Polymerization*, Imperial College Press, London, UK.

81. Tomasic, V., Jovic, F., and Gomzi, Z. (2008). "Photocatalytic oxidation of toluene in the gas phase: Modelling an annular photocatalytic reactor." *Catalysis Today*, 137(2-4), 350-356.

82. Tseng, H. H., Wei, M. C., Hsiung, S. F., and Chiou, C. W. (2009). "Degradation of xylene vapor over Ni-doped TiO_2 photocatalysts prepared by polyol-mediated synthesis." *Chemical Engineering Journal*, 150(1), 160-167.

83. U.S. EPA (1997). "Mercury Study Report to Congress." Office of Air Quality Planning & Standards, and Office of Research and Development, eds.

84. U.S. EPA (2009). "Air Pollutants." http://www.epa.gov/ebtpages/airairpollutants.html. (2009/9/27, 2009).

85. U.S. EPA (2011). "Ground-level Ozone." http://www.epa.gov/air/ozonepollution/basic.html. (June 7, 2011, 2011).

86. Vijayabalan, A., Selvam, K., Velmurugan, R., and Swaminathan, M. (2009). "Photocatalytic activity of surface fluorinated TiO2-P25 in the degradation of Reactive Orange 4." *Journal of Hazardous Materials*, 172(2-3), 914-921.

87. Vildozo, D., Ferronato, C., Sleiman, M., and Chovelon, J.-M. (2010). "Photocatalytic treatment of indoor air: Optimization of 2-propanol removal using a response surface methodology (RSM)." *Applied Catalysis B: Environmental*, 94(3-4), 303-310.

88. Wang, Y., and Zhang, J. (2006). "Investigations of Pulse-Plasma-Polymer coating on TiO_2 nanoparticles and their dispersion." *Journal of Macromolecular Science: Physics*, 45(5), 899-909.

89. World Health Organization (1997). "Xylenes." World Health Organization.

90. Xie, C., Xu, Z., Yang, Q., Li, N., Zhao, D., Wang, D., and Du, Y. (2004). "Comparative studies of heterogeneous photocatalytic oxidation of heptane and toluene on pure titania, titania-silica mixed oxides and sulfated titania." *Journal of Molecular Catalysis A: Chemical*, 217(1-2), 193-201.

91. Xu, C., Cao, L., Su, G., Liu, W., Liu, H., Yu, Y., and Qu, X. (2010). "Preparation of ZnO/Cu_2O compound photocatalyst and application in treating organic dyes." *Journal of Hazardous Materials*, 176(1-3), 807-813.

92. Yamaki, T., Umebayashi, T., Sumita, T., Yamamoto, S., Maekawa, M., Kawasuso, A., and Itoh, H. (2003). "Fluorine-doping in titanium dioxide by ion implantation technique." *Nuclear Instruments and Methods in Physics Research Section B: Beam Interactions with Materials and Atoms*, 206, 254-258.

93. Yamashita, H., Maekawa, K., Nakao, H., and Anpo, M. (2004). "Efficient adsorption and photocatalytic degradation of organic pollutants diluted in water using fluoride-modified hydrophobic mesoporous silica." *Applied Surface Science*, 237(1-4), 393-397.

94. Yang, S., Chen, Y., Zheng, J., and Cui, Y. (2007). "Enhanced photocatalytic activity of TiO_2 by surface fluorination in degradation of organic cationic compound." *Journal of Environmental Sciences*, 19(1), 86-89.

95. Yu, J., Wang, W., Cheng, B., and Su, B.-L. (2009). "Enhancement of photocatalytic activity of mesporous TiO_2 powders by hydrothermal surface fluorination treatment." *The Journal of Physical Chemistry C*, 113(16), 6743-6750.

96. Yu, J. C., Ho, W., Yu, J., Yip, H., Wong, P. K., and Zhao, J. (2005). "Efficient Visible-Light-Induced Photocatalytic Disinfection on Sulfur-Doped Nanocrystalline Titania." *Environmental Science & Technology*, 39(4), 1175-1179.

97. Yu, J. C., Yu, J., Ho, W., Jiang, Z., and Zhang, L. (2002). "Effects of F- doping on the photocatalytic activity and microstructures of nanocrystalline TiO_2 powders." *Chemistry of Materials*, 14(9), 3808-3816.

98. Yu, J. C., Zhang, L., Zheng, Z., and Zhao, J. (2003). "Synthesis and Characterization of Phosphated Mesoporous Titanium Dioxide with High Photocatalytic Activity." *Chemistry of Materials*, 15(11), 2280-2286.

99. Yupeng, Z., and Chunxu, P. (2011). "TiO_2/graphene composite from thermal reaction of graphene oxide and its photocatalytic activity in visible light." *Journal of Materials Science*, 46(8), 2622-2626.

100. Zallen, R., and Moret, M. P. (2006). "The optical absorption edge of brookite TiO_2." *Solid State Communications*, 137(3), 154-157.

101. Zhang, J., Hu, Y., Matsuoka, M., Yamashita, H., Minagawa, M., Hidaka, H., and Anpo, M. (2001). "Relationship between the local structures of titanium oxide photocatalysts and their reactivities in the decomposition of NO." *The Journal of Physical Chemistry B*, 105(35), 8395-8398.

102. Zhang, J., Minagawa, M., Ayusawa, T., Natarajan, S., Yamashita, H., Matsuoka, M., and Anpo, M. (2000). "In Situ Investigation of the Photocatalytic Decomposition of NO on the Ti-HMS under Flow and Closed Reaction Systems." *The Journal of Physical Chemistry B*, 104(48), 11501-11505.

103. Zhang, L., Anderson, W. A., Sawell, S., and Moralejo, C. (2007). "Mechanistic analysis on the influence of humidity on photocatalytic decomposition of gas-phase chlorobenzene." *Chemosphere*, 68(3), 546-553.

104. Zhao, J., Zhang, R., Misawa, K., and Shibuya, K. (2005). "Experimental product study of the OH-initiated oxidation of m-xylene." *Journal of Photochemistry and Photobiology A: Chemistry*, 176(1-3), 199-207.

105. Zhong, J., Wang, J., Tao, L., Gong, M., Zhimin, L., and Chen, Y. (2007). "Photocatalytic degradation of gaseous benzene over TiO_2/Sr_2CeO_4: Kinetic model and degradation mechanisms." *Journal of Hazardous Materials*, 139(2), 323-331.

106. Zhou, J., You, Y., Bai, Z., Hu, Y., Zhang, J., and Zhang, N. (2011). "Health risk assessment of personal inhalation exposure to volatile organic compounds in Tianjin, China." *Science of The Total Environment*, 409(3), 452-459.

BIOGRAPHICAL INFORMATION

Sulak Sumitsawan received his Bachelor and Master of Engineering in Environmental Engineering from Chiangmai University (Chiangmai, Thailand) in 1998 and 2002, respectively. He worked as an environmental engineer at Consultant of Technology Ltd., Bangkok, Thailand during 2002 to 2003. From 2003 to 2006, he had worked as a lecturer in the department of civil engineering at University of Phayao (Phayao, Thailand). Sulak joined the Department of Civil Engineering at the University of Texas at Arlington in 2006. He worked in many projects, including school bus emission testing, database of coating facilities in the state of Texas, under the supervision of Dr. Melanie L. Sattler. He joined Dr. Richard B. Timmons' laboratory and began to work on RF pulsed plasma modification of titanium dioxide for air pollutant photocatalysis under the supervision of Dr. Richard B. Timmons and Dr. Melanie L. Sattler. He received PhD in Civil Engineering in 2011.